

# **USE OF A BCD FOR COMPACTION CONTROL**

A Dissertation

by

**YANFENG LI**

Submitted to the Office of Graduate Studies of  
Texas A&M University  
in partial fulfillment of the requirements for the degree of

**DOCTOR OF PHILOSOPHY**

August 2004

Major Subject: Civil Engineering

# USE OF A BCD FOR COMPACTION CONTROL

A Dissertation

by

YANFENG LI

Submitted to Texas A&M University  
in partial fulfillment of the requirements  
for the degree of

DOCTOR OF PHILOSOPHY

Approved as to style and content by:

---

Jean-Louis Briaud  
(Chair of Committee)

---

James D. Murff  
(Member)

---

Harry L. Jones  
(Member)

---

Christopher C. Mathewson  
(Member)

---

Paul Roschke  
(Head of Department)

August 2004

Major Subject: Civil Engineering

## **ABSTRACT**

Use of a BCD for Compaction Control.

(August 2004)

Yanfeng LI, B.S., Xi'an University of Architecture & Technology, China;

M.S., Xi'an University of Architecture & Technology, China

Chair of Advisory Committee: Dr. Jean-Louis Briaud

Compaction of soil is essential in the construction of highways, airports, buildings, and bridges. Typically compaction is controlled by measuring the dry density and the water content of the compacted soil and checking that target values have been achieved. There is a current trend towards measuring the soil modulus instead or in addition to density. The reasons are that the density measurements are made using nuclear density meter, an undesirable tool in today's political environment and that pavement design uses moduli as an input parameter. Although there are many apparatus available to measure soil modulus in the field such as Falling Weight Deflectometer, Dynamic Cone Penetrometer and Seismic Pavement Analyzer, a light weight and easy to use device which can measure the soil modulus fast and accurately is in great need.

Briaud Compaction Device (BCD) is a portable device which can measure a soil modulus in several seconds. The principle of the BCD is to use the bending of a plate resting on the ground surface as an indicator of the modulus of the soil below. Numerical simulations show that within a certain range, the soil modulus is simply related to the plate

bending. Strain gauges are glued on the top of the plate of BCD and a double half Wheatstone bridge is used to measure the strain. BCD tests were done in parallel with plate tests of the same size. A good correlation was found between the ratio of the plate pressure over the bending strain measured with a BCD and the reload soil modulus obtained from the plate test. This correlation can be incorporated into the BCD processor to display the soil modulus directly.

To transit from dry density based compaction control to modulus based compaction control, BCD tests were also performed in the laboratory on top of a soil sample compacted inside the Proctor mold followed by plate tests. That way, a soil modulus versus water content curve is developed which parallels the approach for the dry density versus water content. The soil modulus versus water content curve can be used to provide the target values for compaction control in the field.

## ACKNOWLEDGEMENTS

I would like to express my cordial gratitude to Dr. Jean-Louis Briaud, the chair of the committee, for his invaluable guidance, discussions and financial support throughout my graduate study at Texas A&M University. My Ph.D study and this dissertation would not be possible without his supervision and support.

I would like to extend my thanks to Dr. Don Murff for his help and suggestions during my graduate study. I also wish to thank Dr. Harry Jones and Dr. C.C. Mathewson for serving on my committee and for giving me helpful advice during my Ph.D program.

Matt Potter, Andrew Fawcett and Sammy Pirano from TMRF were very helpful for building the BCD prototype.

I would like to thank Keunyoung Rhee, Nick Jaynes, Patrick Briaud and Kim Knesek for their help in doing field testing and laboratory testing for this research.

And last but not least, I am indebted to my family for their enduring support, encouragement, and assistance. A special word of thanks is due to my parents and my wife.

## TABLE OF CONTENTS

	Page
ABSTRACT .....	iii
ACKNOWLEDGEMENTS .....	v
TABLE OF CONTENTS .....	vi
LIST OF FIGURES.....	viii
LIST OF TABLES .....	xiv
<b>CHAPTER</b>	
<b>I    INTRODUCTION.....</b>	<b>1</b>
1.1    Soil Compaction.....	1
1.2    Current Soil Compaction Control Apparatus .....	2
1.3    Current Status of Soil Compaction Control .....	7
1.4    Research Objective.....	7
1.5    Dissertation Organization.....	8
<b>II    LITERATURE REVIEW .....</b>	<b>9</b>
2.1    Density or Modulus? .....	9
2.2    Introduction to Soil Modulus .....	12
2.3    Soil Modulus Measurement Apparatus .....	25
2.4    Comparison of Moduli from Different Apparatus .....	40
2.5    Conclusion.....	56
<b>III    BRIAUD COMPACTION DEVICE-BCD.....</b>	<b>58</b>
3.1    Idea of BCD .....	58
3.2    Strain Gauge.....	60
3.3    Wheatstone Bridge .....	73
3.4    Components of BCD .....	80
<b>IV    PLATE THEORY AND NUMERICAL SIMULATION OF BCD.....</b>	<b>90</b>
4.1    Plate Theory .....	90
4.2    Plate on Winkler Foundation.....	98
4.3    Numerical Simulation of BCD.....	102

CHAPTER	Page
4.4	Comparison between Plate Theory and Numerical Simulation ..... 106
4.5	Dimensional Analysis of BCD ..... 114
4.6	Depth of Influence of BCD ..... 117
4.7	Upper and Lower Limit of BCD ..... 119
4.8	BCD on Two-Layer System ..... 122
V	FIELD TEST AND CALIBRATION OF BCD ..... 130
5.1	Plate Test-Theory, Apparatus and Procedure ..... 130
5.2	BCD-Procedure ..... 138
5.3	Correlations between Plate Test and BCD Test Results ..... 140
5.4	Field Test Results vs. Numerical Simulation Results ..... 148
5.5	Influence of Rough Surface on BCD Test Results ..... 149
5.6	Influence of Sand Cushion on BCD Results ..... 154
5.7	Repeatability of BCD ..... 157
5.8	Calibration of BCD ..... 158
VI	LAB TEST OF BCD ..... 165
6.1	Introduction ..... 165
6.2	Lab Test of BCD ..... 167
6.3	BCD Lab Test Result ..... 176
VII	CONCLUSIONS AND RECOMMENDATIONS ..... 190
7.1	Conclusions ..... 190
7.2	Recommendations ..... 193
	REFERENCES ..... 194
	APPENDIX A ..... 198
	APPENDIX B ..... 199
	VITA ..... 217

## LIST OF FIGURES

FIGURE	Page
1.1 Field Unit Weight Determined by Sand Cone Method .....	5
1.2 Schematic Drawing of Calibrated Vessel Used with Rubber Balloon.....	6
1.3 Nuclear Density Meter .....	6
2.1 Stress-Strain Curve of Triaxial Test .....	14
2.2 Different Soil Moduli .....	16
2.3 Loading Factors for Soil Moduli .....	21
2.4 The Cross-Section of Geogauge from Humboldt.....	26
2.5 Geogauge in the Field .....	27
2.6 Dynamic Cone Penetrometer .....	31
2.7 Standard Clegg Impact Soil Tester.....	34
2.8 Falling Weight Deflectometer .....	36
2.9 LFWD in the Field .....	39
2.10 Relationship between Quasi-Static Plate Load Modulus and Geogauge Modulus.....	41
2.11 Modulus Comparison to FWD .....	43
2.12 Geogauge vs. FWD .....	45
2.13 Geogauge vs. GPLT .....	46
2.14 Small Load FWD vs. GPLT .....	47
2.15 Large Load FWD vs. GPLT .....	48
2.16 US 171 Site A Comparison Test .....	54



FIGURE	Page
2.17 US 171 Site B Comparison Test .....	55
2.18 Unconfined Compression Test Modulus vs. Geogauge Stiffness .....	57
2.19 Geogauge Stiffness vs. Water Content for Four Compaction Energies .....	57
3.1 The Conceptual Design of BCD.....	59
3.2 Plan View of BCD Plate.....	60
3.3 Definition of Stress.....	61
3.4 Definition of Strain.....	62
3.5 Hooke's Law. ....	63
3.6 Plot of Strain Gauge. ....	65
3.7 Strain Gage in Use.....	66
3.8 Variation of Thermal Output with Temperature for Variety of Strain Gage Alloys Bonded to Steel.....	69
3.9 Typical Thermal Output Variation with Temperature for Self-Temperature-Compensated Constantan (A-alloy) and Modified Karma (K-alloy) Strain Gages.....	71
3.10 Quarter Bridge Circuit .....	73
3.11 Half Wheatstone Bridge .....	76
3.12 Full Bridge Wheatstone Bridge.....	78
3.13 Dimensions of Gauge.....	82
3.14 Data Curve of Self-Temperature Compensation.....	83
3.15 Double Half Bridge for Strain Gauges in Radial Direction .....	84
3.16 Double Half Bridge for Strain Gauges in Hoop Direction.....	85
3.17 Diagram of MH-C777PLUS-II Universal Charger .....	87

FIGURE	Page
4.1 Bending Moment of Circular Plate in Polar Coordinate.....	95
4.2 Shearing Force of Circular Plate in Polar Coordinate.....	95
4.3 Part of Mesh of BCD in ABAQUS Simulation.....	103
4.4 Separation between Plate and Soil. ....	105
4.5 Example Plot of Plate on Elastic Foundation.....	107
4.6 Comparison of Settlement of Plate between ABAQUS Simulation and Plate Theory .....	111
4.7 Comparison of Bending Moment between ABAQUS Simulation and Plate Theory .....	112
4.8 Winkler Foundation with 11 Springs. ....	113
4.9 Winkler Foundation with 31 Springs .....	113
4.10 Dimensional Analysis of BCD.....	114
4.11 Depth of Influence of BCD .....	118
4.12 Typical Stress- Strain Curve of EPP Model.....	119
4.13 Empirical Relationship between Soil Modulus and Undrained Shear Strength.....	120
4.14 Upper and Lower limit of BCD.....	121
4.15 BCD on Two Layer System (10 MPa-20 MPa). ....	123
4.16 BCD on Two Layer System (20 MPa-10 MPa) .....	123
4.17 BCD on Two Layer System (10 MPa-100 MPa) .....	124
4.18 BCD on Two Layer System (100 MPa-10 MPa). ....	124
4.19 Correlations to Calculate Soil Modulus from BCD Result. ....	125
4.20 Predicted BCD Modulus from Radial Strain for 10 MPa-20 MPa System.....	126

FIGURE	Page
4.21 Predicted BCD Modulus from Hoop Strain for 10 MPa-20 MPa System .....	126
4.22 Predicted BCD Modulus from Radial Strain for 20 MPa-10 MPa System.....	127
4.23 Predicted BCD Modulus from Hoop Strain for 20 MPa-10 MPa System. ....	127
4.24 Predicted BCD Modulus from Radial Strain for 10 MPa-100 MPa System.....	128
4.25 Predicted BCD Modulus from Hoop Strain for 10 MPa-100 MPa System. ....	128
4.26 Predicted BCD Modulus from Radial Strain for 100 MPa-10 MPa System.....	129
4.27 Predicted BCD Modulus from Hoop Strain for 100 MPa-10 MPa System. ....	129
5.1 Top View of Plate Tester with Dimensions. ....	131
5.2 Mesh of ABAQUS Simulation of Plate Test.....	132
5.3 Mesh of ABAQUS Simulation of Plate Test (after loading).....	133
5.4 Plate Settlement from ABAQUS Simulation. ....	133
5.5.a Plate Test in the Field. ....	136
5.5.b Plate Test in the Field (loading). ....	136
5.6 A Typical Plate Test Curve. ....	137
5.7 BCD on the Ground.....	139
5.8 Zero Out the Display .....	139
5.9 Correlation between Plate Test and BCD Test.....	140
5.10 Bending of Plate When Soil Modulus is Very Small.....	142
5.11 The Intercept Changing with the Thickness of the Plate .....	142
5.12 Bending of Plate When Soil Modulus $E=1\text{MPa}$ .....	143
5.13 Bending of Plate When Soil Modulus $E=10\text{MPa}$ .....	144

FIGURE	Page
5.14 Correlation between Plate Test and BCD in Radial Strain (4mm Plate) .....	145
5.15 Distribution of Strain on Top of Plate (Soil Modulus=20 MPa).....	147
5.16 Comparison between Numerical Simulation and Field Tests .....	148
5.17 Three Locations of Gravel.....	152
5.18 Dent at Center of BCD. ....	153
5.19 Sand Cushion with Gravel on the Ground .....	155
5.20 Repeatability Test of BCD at Location #1 .....	157
5.21 Repeatability Test of BCD at Location #2 .....	158
5.22 Calibration of BCD. ....	160
6.1 Compacted Soil in Mold. ....	168
6.2 Plate Test on Compaction Mold.....	169
6.3 BCD Test on Compaction Mold.....	170
6.4 Mesh of BCD on Proctor Mold. ....	171
6.5 BCD on Proctor Mold after Loading (Fixed Boundary). ....	172
6.6 Mesh of Plate on Proctor Mold. ....	172
6.7 Plate on Proctor Mold after Loading (Fixed Boundary). ....	173
6.8 Mesh of Mold and Material under Compaction Mold. ....	175
6.9 Mesh of Mold and Material under Compaction Mold after Loading.....	176
6.10 Sieve Analysis of NGES Sand. ....	178
6.11 Compaction Curve for NGES Sand. ....	180

FIGURE	Page
6.12	Compaction Curve and Plate Modulus vs. Water Content Curve (Mold #5). ... 181
6.13	Compaction Curve and Plate Modulus vs. Water Content Curve (Mold #6). ... 181
6.14	Relationship between Plate Modulus and Pressure/Hoop Strain (Mold #5)..... 182
6.15	Relationship between Plate Modulus and Pressure/Hoop Strain (Mold #6)..... 182
6.16	Sieve Analysis of Mixture of NGES Sand and Porcelain Clay..... 183
6.17	Compaction Curve for Mixture of NGES Sand and Porcelain Clay..... 185
6.18	Plate Modulus and Dry Unit Weight Change with Water Content (Mold #5).....186
6.19	Plate Modulus and Dry Unit Weight Change with Water Content (Mold #6).....186
6.20	Relationship between Plate Modulus and Pressure/Hoop Strain (Mold #5)..... 187
6.21	Relationship between Plate Modulus and Pressure/Hoop Strain (Mold #6)..... 187
6.22	Relationship between Plate Modulus and Pressure/Hoop Strain (Mold #5)..... 188
6.23	Relationship between Plate Modulus and Pressure/Hoop Strain (Mold #6)..... 189

## LIST OF TABLES

TABLE	Page
2.1 Technical Specification of the Geogauge.....	29
2.2 Comparison of FWD and Plate Test at Riverside Campus .....	49
2.3 Comparison of FWD, Clegg Impact Tester and Plate Tester at Riverside Campus. ....	50
2.4 US 171 Site A Test Results. ....	52
2.5 US 171 Site B Test Results .....	53
3.1 General Information of CEA-06-125UW-350 Strain Gauges.....	81
3.2 Dimensions of CEA-06-125UW-350 Gauge. ....	82
3.3 Specification of S-350-01 Resistors .....	86
3.4 Specification of MH-C777 PLUS-II Charger .....	88
4.1 Thickness of Plate and Corresponding Moduli when Plate and Soil Separates.....	105
5.1 BCD Test for Bump at Different Locations (Gravel Size 2 mm×6 mm) .....	150
5.2 BCD Test for Bump at Different Locations (Gravel Size 12 mm×7 mm) .....	151
5.3 ABAQUS Simulation Results with Dent at Three Locations .....	154
5.4 BCD Test for Bump at Different Locations with Sand Cushion.....	156
5.5 BCD Test Result on Rubber Pad 1 .....	161
5.6 BCD Test Result on Rubber Pad 2.....	161
5.7 BCD Test Result on Rubber Pad 1 above Pad 2 .....	162
5.8 BCD Test Result on Rubber Pad 2 above Pad 1 .....	162
5.9 Test Result of Rubber Pad on 1” Thick Wooden Plate .....	163
5.10 Test Result of Rubber Pad on Concrete Floor.....	164

TABLE	Page
5.11 Test Result of Rubber Pad on Soil. ....	164
6.1 Sieves No. for Sieve Analysis of NGES Sand .....	178

# CHAPTER I

## INTRODUCTION

### 1.1 Soil Compaction

The general meaning of the verb compact is "to press closely together." In soil mechanics, it means to press the soil particles tightly together by expelling air from the void space. Compaction is normally produced deliberately and proceeds rapidly during construction, often by heavy compaction rollers (Liu and Evett, 2001).

Compaction of soil increases its density and produces three important effects: (1) increase in the soil's shear strength, (2) decrease in future settlement of the soil, and (3) decrease in soil's permeability. Compaction is actually a rather cheap and effective way to improve the properties of a given soil.

Compacted soil is an essential element in the construction of highways, airports, buildings, sewers, and bridges. Even though soil density is not the most desired engineering property, it is used almost exclusively by the transportation industry to specify, estimate, measure, and control soil compaction. This practice was adopted many years ago because soil density can be easily determined via weight and volume measurements.

---

This dissertation follows the style and format of *Journal of Geotechnical and Geoenvironmental Engineering*.



## 1.2 Current Soil Compaction Control Apparatus

Soil placed as engineering fill (embankments, foundation pads, and road base) is compacted to obtain satisfactory engineering properties such as shear strength, compressibility and permeability. Also, foundation soils are often compacted to improve their engineering properties. Laboratory compaction tests provide the basis for determining the percent compaction and water content needed to achieve the required engineering properties, and for controlling the construction to assure that the required compaction and water content are achieved.

Currently, it is common practice to first determine the optimum water content  $w_o$  and the maximum dry unit weight  $\gamma_{d\max}$  by means of a laboratory compaction test.

In most specifications for earthwork, the contractor is required to achieve a compacted field dry unit weight of 90 to 95% of the maximum dry unit weight determined in the laboratory by either the standard or modified Proctor test. This is a specification for relative compaction, R, which can be expressed as:

$$R (\%) = \frac{\gamma_{d(\text{field})}}{\gamma_{d(\text{max-lab})}} \times 100 \quad (1.1)$$

The apparatus currently used for determining the field unit weight of compaction include sand cone method, rubber balloon method and nuclear density meter.

### 1.2.1 Sand Cone Method (ASTM D-1556)

The sand cone device consists of a glass or plastic jar with a metal cone attached at its top. The jar is filled with uniform dry Ottawa sand. The combined weight of the jar, the cone, and the sand filling the jar is determined ( $W_1$ ). In the field, a small hole is excavated in the area where the soil has been compacted. If the weight of the moist soil excavated from the hole ( $W_2$ ) is determined and the moisture content of the excavated soil is known, the dry weight of the soil ( $W_3$ ) can be obtained as follows:

$$W_3 = \frac{W_2}{1 + \frac{w(\%)}{100}} \quad (1.2)$$

where  $w$  = moisture content.

After excavation of the hole, the cone with the sand-filled jar attached to it is inverted and placed over the hole (Fig.1.1). Sand is allowed to flow out of the jar to fill the hole and the cone. After that, the combined weight of the jar, the cone, and the remaining sand in the jar is determined ( $W_4$ ), so

$$W_5 = W_1 - W_4 \quad (1.3)$$

where  $W_5$  = weight of sand to fill the hole and cone.

The volume of the excavated hole can then be determined as follows:

$$V = \frac{W_5 - W_c}{\gamma_{d(sand)}} \quad (1.4)$$

where  $W_c$  = weight of sand to fill the cone only

$\gamma_{d(sand)}$  = dry unit weight of Ottawa sand used

The values of  $W_c$  and  $\gamma_{d(sand)}$  are determined from the calibration done in the laboratory. The dry unit weight of compaction made in the field can then be determined as follows:

$$\gamma_d = \frac{W_3}{V} \quad (1.5)$$

### 1.2.2 Rubber Balloon Method (ASTM D-2167)

The procedure for the rubber balloon method is similar to that for the sand cone method. A test hole is made and the moist weight of soil removed from the hole and its moisture content are determined. However, the volume of the hole is determined by introducing into it a rubber balloon filled with water from a calibrated vessel, from which the volume can be read directly. The dry unit weight of the compacted soil can be determined by using Eq.1.5. Fig. 1.2 shows a calibrated vessel that would be used with a rubber balloon.

### 1.2.3 Nuclear Density Meter

Nuclear density meter is often used for determining the compacted dry unit weight of soil. The density meter operates either in drilled holes or from the ground surface. The instrument measures the weight of wet soil per unit volume and weight of water present in a unit volume of soil. The dry unit weight of compacted soil can be determined by subtracting the weight of water from the moist unit weight of soil. The water content of the compacted soil can also be determined. Fig.1.3 shows the nuclear density meter measuring dry density and water content in the field.

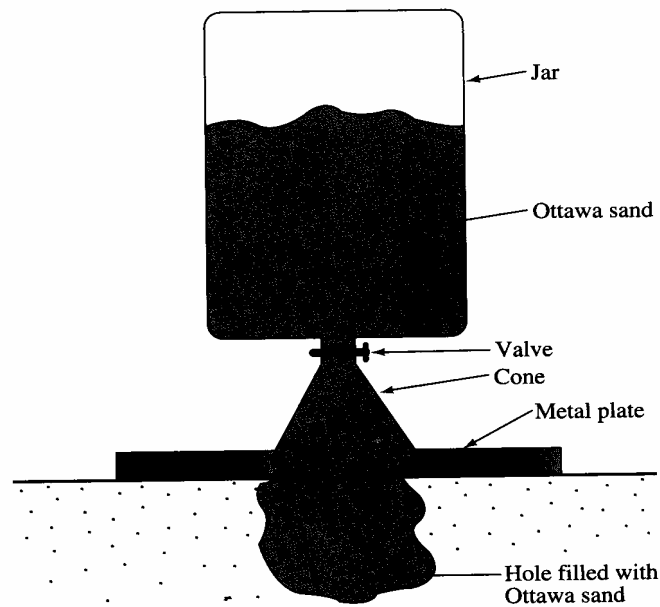


Fig.1.1. Field Unit Weight Determined by Sand Cone Method (Das, 1998)

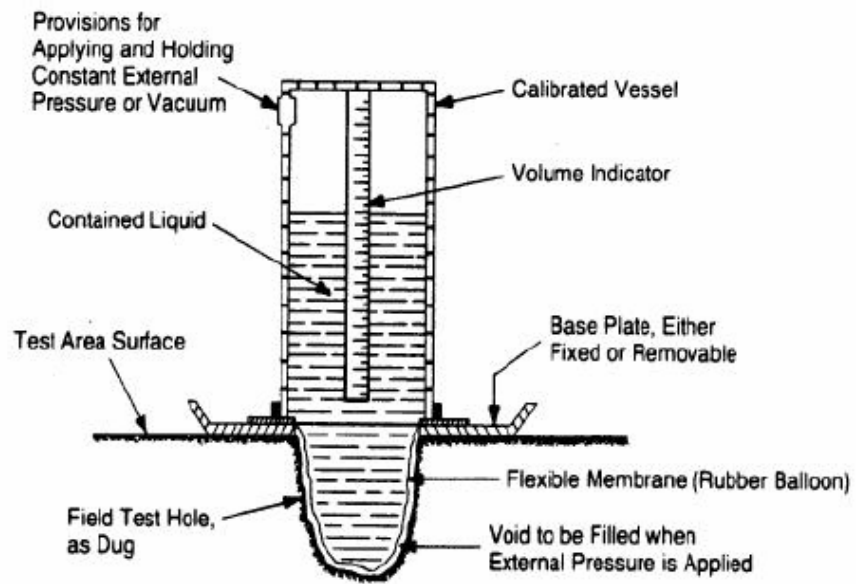


Fig.1.2. Schematic Drawing of Calibrated Vessel Used with Rubber Balloon  
(After Nebraska DOR)



Fig.1.3. Nuclear Density Meter

### **1.3 Current Status of Soil Compaction Control**

State departments of transportation and contractors suggest that the present methods for measuring density are slow, labor-intensive, sometimes dangerous, and of uncertain accuracy. Hence, construction sites are often undersampled, causing inadequate compaction to go undetected or feedback to be provided too late for the cost-effective correction of problems. Sometimes, the opposite is true. Designers are encouraged to overspecify to allow for the significant variability of the finished product, and contractors are encouraged to overcompact to ensure acceptance and avoid rework. All of which means add cost to the owner. To eliminate overspecification and overcompaction, improved quality control of soil compaction would be a welcome addition to civil works projects.

### **1.4 Research Objective**

Compaction of soil is essential in the construction of highways, airports, buildings, and bridges. Typically compaction is controlled by measuring the dry density and the water content of the compacted soil and checking that a target value has been achieved. There is a very strong trend towards measuring the soil modulus instead or in addition to density because the density measurements are made using Nuclear Density Meter, an undesirable tool in today's political environment. The objectives of this research are as follows:

1. Study the principles and mechanisms of currently used apparatus for modulus based compaction control.
2. Design and build a new device to measure the soil modulus fast and accurately.
3. Use plate theory and numerical simulations to study the new device.
4. Run field tests and laboratory tests to validate the design.
5. Develop a procedure to calibrate the device.

## **1.5 Dissertation Organization**

The introduction and theoretical background of currently used modulus measurement apparatus such as CBR, FWD, SPA and Geogauge will be presented in Chapter II. Some available field comparison tests between these apparatus are also included into this chapter. The principle and components of BCD will be presented in Chapter III. Chapter IV includes plate theory and numerical simulation of BCD under different conditions. Field test procedures and correlations between plate test and BCD test will be presented in Chapter V. The influence of testing surface and calibration of BCD are also included into this chapter. In Chapter VI, the apparatus, procedure and results of validating BCD in the lab will be presented. The last chapter summarizes the conclusions of this dissertation and gives recommendations on the BCD.

## **CHAPTER II**

### **LITERATURE REVIEW**

Holtz and Kovacs (1981) state "Since the objective of compaction is to stabilize soils and improve their engineering properties, it is important to keep in mind the desired engineering properties of the fill, not just its dry density and water content. This point is often lost in earthwork construction control."

#### **2.1 Density or Modulus?**

Controlling compaction by measuring dry density and water content has been done for many years. Recently, there is a strong trend towards using the soil modulus rather than the dry density to control compaction. So the question is should we use density or modulus to control compaction?

The answer to this question is not simple for the following reason. It is possible to have a high modulus without having particles which are close together. A high modulus may exist if a very soft clay dries out. The particles may be relatively far apart (un-compacted structure) yet the clay may be quite strong because the suction which develops between the particles upon drying generates high compression stresses between the particles. This apparent stiffness is destroyed as soon as the clay gets wet again. This is why it is not possible to control compaction on the basis of modulus measurements alone.



On the other hand, density gives the compactness of the soil because the density is directly related to how many particles are within a given volume. However, there is no solid evidence to show that the soil density is directly correlated to the soil modulus. Also, one can obtain the same density for at least two different water content (either side of the Proctor compaction curve). This is why it is not possible to control compaction on the basis of the dry density alone.

The best way to control compaction is to ensure that the dry density is within tolerance from a target value, that the modulus is within tolerance from a target value, and that the water content is within tolerance of a target value. It is possible to achieve reasonable control of compaction by ensuring that two of those three parameters are within tolerance of their target values. In this respect it is possible to control compaction by ensuring that the soil modulus and the water content are within tolerance of their target value. Using the modulus for compaction control is essential but it cannot be used alone. The modulus has not been used in the past but it should be used in the future because it responds to a basic need for the engineer to check that his or her modulus design assumption is verified in the field.

When soil is compacted for pavements, pipe bedding and backfill, and foundations, the desired engineering properties are the soil modulus or soil stiffness. Briaud (2001) pointed out that the main reason why the modulus is a better parameter than the density is that the performance goal for the structure is to limit deformations. Indeed, deformations are directly tied to the modulus and not directly tied to density. In

pavement design, the resilient modulus is used, in embankment design the modulus of the fill can be used to address issues such as the general settlement and the bump at the end of the bridge, in retaining wall design again the modulus can be used to calculate the vertical compression of the backfill under its own weight. The drawback of measuring the modulus is that it is a new approach and that some issues still need to be resolved such as the choice of a target value for the specifications and the modulus-water content relationship.

Target values for compaction control are routinely obtained in the laboratory for density and water content. This is the Proctor test and the modified Proctor test. The target values are the maximum dry density and the optimum water content. There is no target value yet established for the soil modulus. Yet in many cases the design of the geotechnical structure (pavement, embankment for example) is based on the assumption that the soil has a target modulus value. It would make sense to use that target value and achieve compaction control by ensuring that such a modulus exist in the field after the compaction process.

This is not easily achieved because often the modulus used in the design is derived from a laboratory test which has no equivalent in the field; for example the resilient modulus used in pavement design has no field equivalent and it is often not possible to obtain an undisturbed sample in the field to bring it back to the lab and check that the modulus of this field sample is equal to or higher than the one used in the design. Even if that was possible the test is very time consuming and such control could only be very limited in scope.

There is a need for a tool which could provide verification of the modulus value at a speed consistent with modern construction apparatus and the building pace of the construction industry. This tool should provide a quick measurement of the modulus and of the water content of the soil tested. There is also a need for the target value to be established prior to beginning the compaction process. In other words there is a need for a lab test which would be to the soil modulus and water content what the Proctor test is to the soil density and water content.

## 2.2 Introduction to Soil Modulus

Soil moduli vary significantly. The range of soil moduli is highlighted below by quoting the modulus of other materials.

- Steel: 200,000 MPa
- Concrete: 20,000 MPa
- Wood, Plastic: ~ 13,000 MPa
- Rock: 2,000 MPa to 30,000 MPa
- Soil: 5 MPa to 1000 MPa
- Mayonnaise: ~ 0.5 MPa

### 2.2.1 How to Get Soil Modulus from Stress Strain Curve?

The modulus of a soil is one of the most difficult soil parameters to estimate because it depends on so many factors (Briaud, 2001). We usually obtain soil modulus from the stress strain curve obtained in a triaxial test. In a triaxial test, the cylindrical soil sample is wrapped in an impermeable membrane and confined by a hydrostatic pressure. Then the vertical stress is increased gradually and the non linear stress strain curve is obtained (Fig. 2.1). According to the theory of elasticity, the strains experienced by an elastic material are linearly related to the stresses applied. The equations of elasticity for axi-symmetrical loading relating the stresses and the strains in the three directions are given in Eqs.2.1 to 2.5. Because of the axi-symmetry, Eqs.2.1 and 2.2 are identical. In Eqs.2.1 and 2.3, there are two unknowns: the soil's Young's modulus  $E$  and the Poisson's ratio  $\nu$ . In the triaxial test, it is necessary to measure the stresses applied in both directions as well as the strains induced in both directions in order to calculate the modulus of the soil. Indeed one needs two simultaneous equations to solve for  $E$  and  $\nu$ . Note that the modulus is not the slope of the stress strain curve. An exception to this statement is the case where the confining stress is zero as it is for a typical concrete cylinder test or an unconfined compression test on clay.

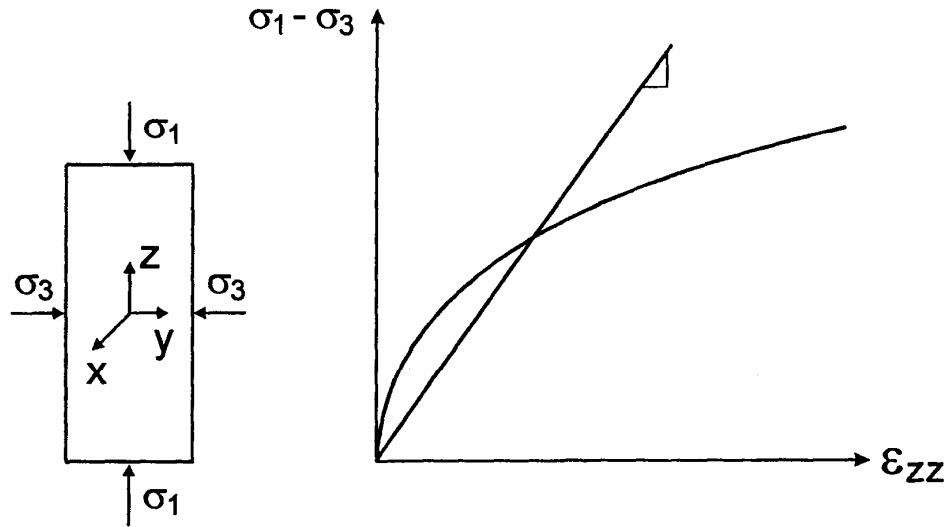


Fig.2.1 Stress-Strain Curve of Triaxial Test

$$\varepsilon_{xx} = \frac{1}{E}(\sigma_{xx} - \nu(\sigma_{yy} + \sigma_{zz})) = \frac{1}{E}(\sigma_3 - \nu(\sigma_1 + \sigma_3)) \quad (2.1)$$

$$\varepsilon_{yy} = \frac{1}{E}(\sigma_{yy} - \nu(\sigma_{xx} + \sigma_{zz})) = \frac{1}{E}(\sigma_3 - \nu(\sigma_1 + \sigma_3)) \quad (2.2)$$

$$\varepsilon_{zz} = \frac{1}{E}(\sigma_{zz} - \nu(\sigma_{xx} + \sigma_{yy})) = \frac{1}{E}(\sigma_1 - \nu(\sigma_3 + \sigma_3)) \quad (2.3)$$

$$E = \frac{\sigma_1 - 2\nu\sigma_3}{\varepsilon_{zz}} \quad (2.4)$$

$$\nu = \frac{\varepsilon_{xx}}{\varepsilon_{zz}} = \frac{\sigma_3 - \nu(\sigma_1 + \sigma_3)}{\sigma_1 - 2\nu\sigma_3} \quad (2.5)$$

### 2.2.2 Which Modulus Should We Use?

In Fig.2.1, it was pointed out that the slope of the stress strain curve is not necessarily the Young's modulus of the soil. However the slope of the curve is related to the modulus and it is convenient to associate the slope of the stress-strain curve to a modulus. Indeed this gives a simple image tied to the modulus value; note however that in Fig.2.2 the slope is not labeled as Young's modulus  $E$  but rather as slope  $S$ . There are five moduli shown in Fig.2.2.

1. Secant Modulus: if the slope is drawn from the origin to a point on the curve (O to A on Fig.2.2), the secant slope  $S_s$  is obtained and the secant modulus  $E_s$  is calculated from it. Secant modulus can be used to predict the movement due to the first application of a load as in the case of a spread footing.

2. Tangent Modulus: if the slope is drawn as the tangent to the point considered on the stress strain curve then the tangent slope  $S_t$  is obtained and the tangent modulus  $E_t$  is calculated from it. Tangent modulus can be used to calculate the incremental movement due to an incremental load as in the case of the movement due to one more story in a high-rise building.

3. Unloading Modulus: if the slope is drawn as the line which joins points A and B on Fig.2.2, then the unloading slope  $S_u$  is obtained and the unloading modulus  $E_u$  is calculated from it. Unloading modulus is often used when calculating the heave at the bottom of an excavation or the rebound of a pavement after the loading by a truck tire (resilient modulus).

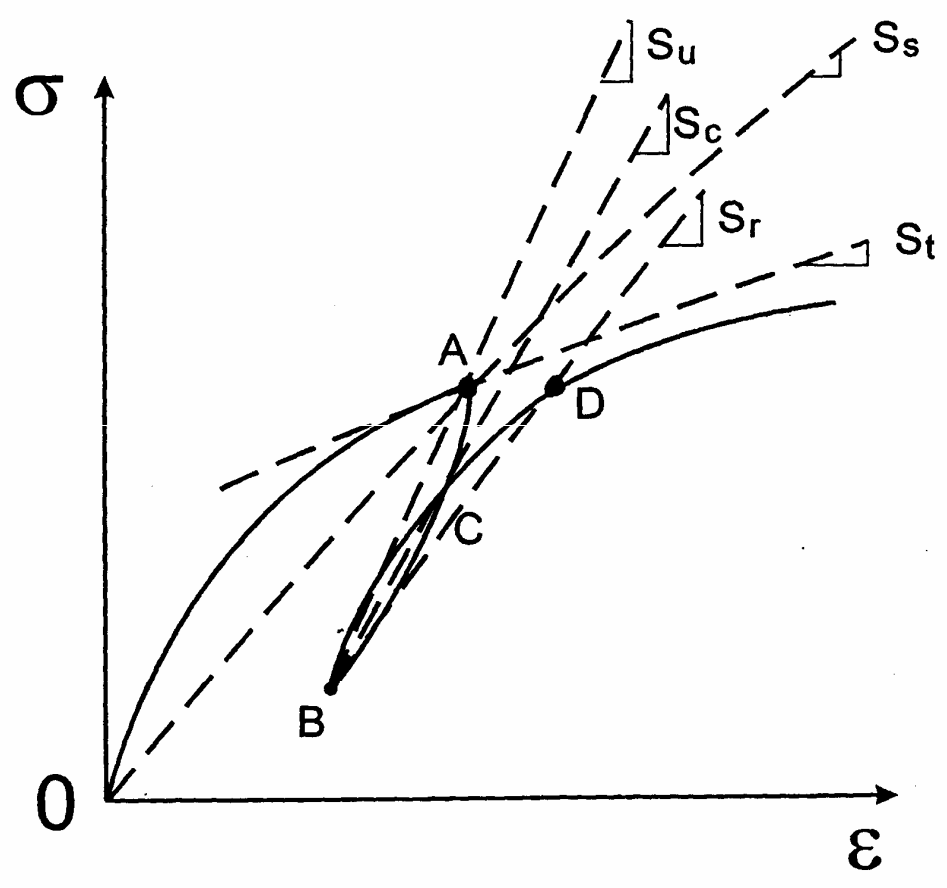


Fig.2.2 Different Soil Moduli

4. Reloading Modulus: if the slope is drawn from point B to point D on Fig.2.2, then the reloading slope  $S_r$  is obtained and the reload modulus  $E_r$  is calculated from it. Reloading modulus should be used to estimate the movement at the bottom of an excavation if the excavated soil or a building of equal weight was placed back in the excavation or to calculate the movement of the pavement under reloading by the same truck tire.

5. Cyclic Modulus: if the slope is drawn from point B to point C on Fig.2.2, then the cyclic slope  $S_c$  is obtained and the cyclic modulus  $E_c$  is calculated from it. Cyclic modulus and its evolution as a function of the number of cycles for the movement of a pile foundation subjected to repeated wave loading.

### **2.2.3 Parameters Influencing Soil Moduli**

Whichever one of these moduli is defined and considered, the state in which the soil is at a given time will affect that modulus. Some of the main state parameters influencing soil moduli are listed below:

1. Dry Density. If soil is closely packed, the modulus tends to be high. This is measured by the dry density (ratio of the weight of solids over the total volume of the wet sample) of the soil. It can also be measured by the porosity (ratio of the volume of voids over the total volume of the wet sample).



2. How are the particles organized? This refers to the structure of the soil. For example a coarse grained soil can have a loose or dense structure and a fine grain soil can have a dispersed or flocculated structure. Note that two soil samples can have the same dry density yet different structures and therefore different soil moduli. This is why taking a disturbed sample of a coarse grain soil in the field and reconstituting it to the same dry density and water content in the laboratory can lead to laboratory and field moduli which are different.

3. Water content. Water content has a major impact because at low water contents the water binds the particles (especially for fine grained soils) and increases the effective stress between the particles through the suction and tensile skin of water phenomenon. Therefore in this case low water contents lead to high soil moduli. This is why clay shrinks and becomes very stiff when it dries. At the same time at low water contents the compaction of coarse grain soils is not as efficient as it is at higher water contents because the lubrication effect of water is not there. Therefore in this case low water contents lead to low moduli. As the water content increases, the water occupies more and more room and gets to the point where it pushes the particles apart thereby increasing compressibility and reducing the modulus.

4. Stress history. If the soil has been prestressed in the past, it is called overconsolidated. If the soil has not been prestressed in the past, in other words, if the current stress is the highest stress experienced by the soil and if the soil is at equilibrium under this stress, the soil is normally consolidated. An over-consolidated (OC) soil will generally have higher modulus than the same normally consolidated (NC) soil because

the OC soil is on the reload part of the stress strain curve while the NC soil is on the first loading part. Some soils are still in the process of consolidating under their own weight. These are called underconsolidated soils such as the clays deposited offshore the Mississippi Delta where the deposition rate is more rapid than the rate which would allow the pore water pressures induced by deposition to dissipate. These clays have very low moduli.

5. Cementation. Cementation refers to the "glue" which can exist at the contacts between particles. As discussed above, low water contents in fine grained soils can generate suction in the water strong enough to simulate a significant "glue effect" between particles. This effect is temporary as an increase in water content will destroy it. Another glue effect is due to the chemical cementation which can develop at the contacts. This cementation can be due to the deposition of calcium at the particle to particle contacts for example. Such cementation can lead to a significant increase in modulus.

#### **2.2.4 Loading Factors Influencing Soil Moduli**

If we assume that the state factors for the soil considered are fixed. The loading factors also have influences on the soil moduli.

1. Mean stress level. The loading process induces stresses in the soil. These stresses can be shear stresses or normal stresses or a combination of both. At one point and at any given time in a soil mass there is a set of three principal normal stresses. The

mean of these three stresses has a significant influence on the soil modulus. This is also called the confinement effect. Fig.2.3 (a) shows an example of two stress strain curves at two different confinement levels. As common sense would indicate, the higher the confinement, the higher the soil modulus will be. A common model for quantifying the influence of the confinement on the soil modulus is given on Fig.2.3 (a) and is usually attributed to the work of Janbu (1963). According to this model, the modulus is proportional to a power law of the confinement stress. The modulus  $E_0$  is the modulus obtained when the confinement stress is equal to the atmospheric pressure  $P_a$ . A common value for the power exponent  $a$  in Fig.2.3 (a) is 0.5.

2. Strain level in the soil. The loading process induces strains in the soil mass. Because soils are nonlinear materials, the secant modulus depends on the mean strain level in the zone of influence. In most cases the secant modulus will decrease as the strain level increases because the stress strain curve has a downward curvature. Note that an exception to this downward curvature occurs when the results of a consolidation test is plotted as a stress strain curve on arithmetic scales for both axes. Indeed in this case the stress strain curve exhibits an upward curvature because the increase in confinement brought about by the steel ring is more influential than the decrease in modulus due to the increase in strain in the soil. In the triaxial test, the stress strain curve can be fitted with a hyperbola and the associated model for the modulus is shown on Fig.2.3.(b).

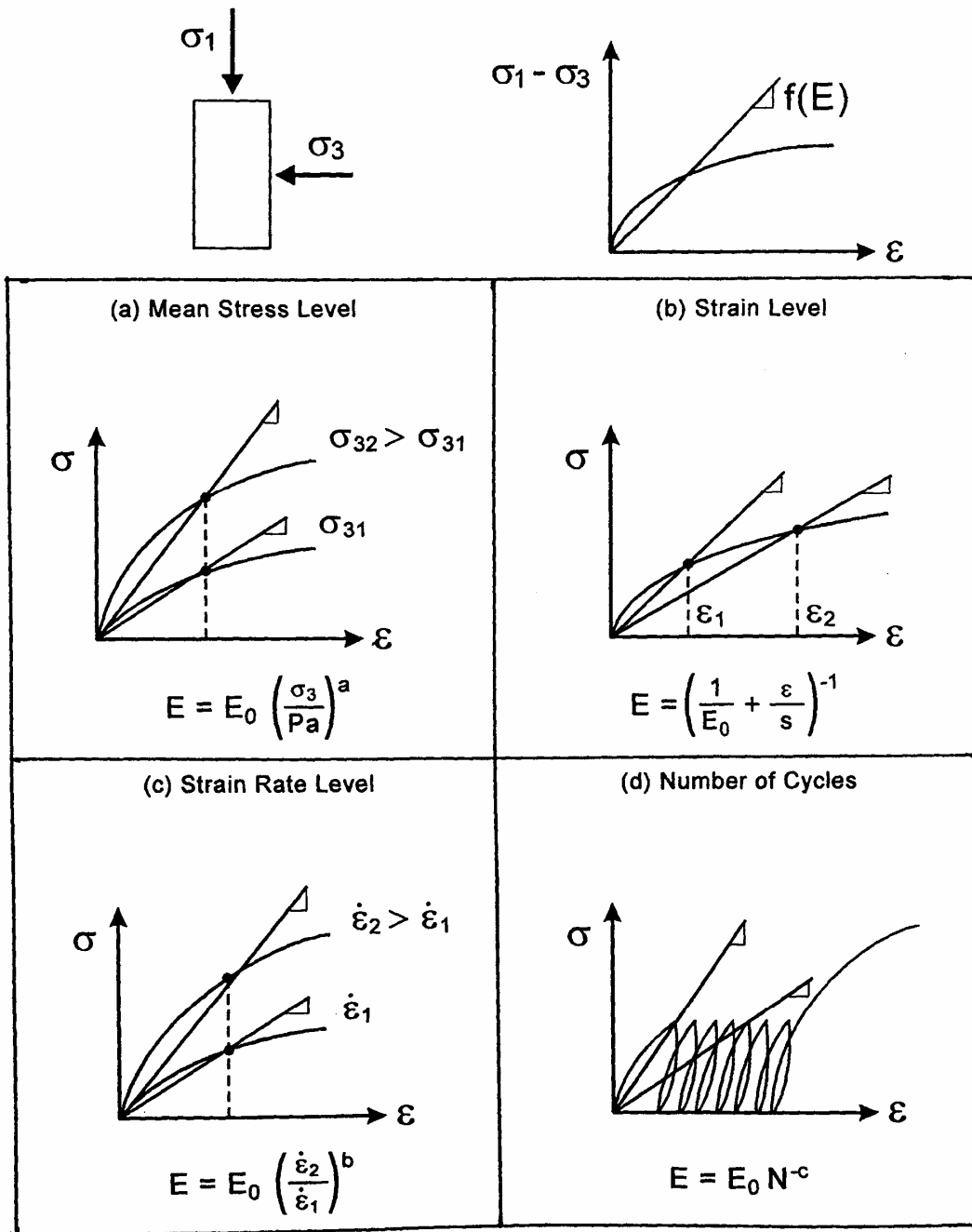


Fig.2.3 Loading Factors for Soil Moduli

This hyperbolic model is usually attributed to the work of Duncan and Chang (1970). In this model (Fig.2.3 (b)),  $E_0$  is the initial tangent modulus also equal to the secant modulus for a strain of zero. The parameter  $s$  is the asymptotic value of the stress for a strain equal to infinity. In that sense it is related to the strength of the soil.

3. Strain rate in the soil. Soils like many other materials are viscous. This means that the faster a soil is loaded, the stiffer it is and therefore the higher the modulus is. In some instances the reverse behavior is observed. Fig.2.3 (c) shows an example of two stress strain curves obtained by loading the soil at two drastically different strain rates. The strain rate is defined as the strain accumulated per unit of time. The modulus usually varies as a straight line on a log-log plot of modulus versus strain rate. The slope of that line is the exponent  $b$  in Fig.2.3 (c). In clays, common values of this exponent vary from 0.02 for stiff clays to 0.1 for very soft clays. In sands, common values of  $b$  vary from 0.01 to 0.03. The modulus  $E_0$  is the modulus obtained at a reference strain rate. Much of the work on this model has been done at Texas A&M University.

4. Number of loading cycles experienced by the soil. If the loading process is repeated a number of times, the number of cycles applied will influence the soil modulus. Again referring to the secant modulus, the larger the number of cycles the smaller the modulus becomes. This is consistent with the accumulation of movement with an increasing number of cycles. The model used to describe this phenomenon is shown on Fig.2.3 (d). The exponent  $c$  in the model is negative and varies significantly. The most common values are of the order of -0.1 to -0.3. Much of the work on this model has been done at Texas A&M University.

5. Drainage during loading. Two extreme cases can occur: drained or undrained loading. The undrained case may occur if the drainage valve is closed during a laboratory test or if the test is run sufficiently fast in the field. The time required to maintain an undrained behavior or to ensure that complete drainage takes place depends mainly on the soil type. For example a 10 minutes test in a highly plastic clay is probably undrained while a 10 minutes test in a clean sand is probably a drained test. The Poisson's ratio is sensitive to whether or not drainage takes place. For example if no drainage takes place during loading in a clay it is common to assume a Poisson's ratio equal to 0.5. On the other hand if complete drainage takes place (excess pore pressures are kept equal to zero), then a Poisson's ratio value of 0.35 may be reasonable. The difference between the two calculated moduli is the difference between the undrained modulus and the drained modulus.

### **2.2.5 Why Modulus is Better than Stiffness and Coefficient of Subgrade Reaction?**

The modulus  $E$  has been defined in Fig.2.1. It has units of force per unit area ( $kN/m^2$ ). The stiffness  $K$  is defined here as the ratio of the force applied on a boundary through a loading area divided by the displacement experienced by the loaded area. It has units of force per unit length ( $kN/m$ ). The loaded area is typically a plate which can be square or circular or in the shape of a ring. There is a relationship between the modulus and the stiffness. For the case of a circular plate having a diameter  $B$ , the relationship is of the form:

$$E = f(K / B) \quad (2.6)$$

The coefficient of subgrade reaction  $k$  is defined here as the ratio of the pressure applied to the boundary through a loading area divided by the displacement experienced by the loaded area. It has units of force per unit volume ( $kN / m^3$ ). The loaded area can be a footing (coefficient of vertical subgrade reaction) or a horizontally loaded pile (coefficient of horizontal subgrade reaction). There is a relationship between the modulus and the coefficient of subgrade reaction. For the footing and the pile cases mentioned, that relationship is of the form:

$$E = g(k \times B) \quad (2.7)$$

Eqs.2.6 and 2.7 show that, if the modulus is a soil property, the stiffness and coefficient of subgrade reaction are not soil property and depend on the size of the loaded area. Therefore, for an elastic material, the stiffness and coefficient of subgrade reaction measured with one test will be different from the stiffness and coefficient of subgrade reaction measured with another test if the loading areas are different. Yet, for the same elastic material, the modulus obtained from both tests would be the same. In that sense the use of the stiffness or coefficient of subgrade reaction is not as convenient as the modulus and the use of the modulus is preferred.

## **2.3 Soil Modulus Measurement Apparatus**

Currently, there are many devices to measure the soil modulus/stiffness in field. They are listed as follows:

### **2.3.1 The California Bearing Ratio-CBR Test (ASTM D 1883-99)**

The California Bearing Ratio (CBR) was developed by The California State Highways Department. It is in essence a simple penetration test developed to evaluate the strength of road subgrades.

CBR consists of causing a plunger of standard area to penetrate a soil sample, (this can be in the laboratory or on site). The force required to cause the penetration is plotted against measured penetration, the readings noted at regular time intervals.

This information is plotted on a standard graph, and the plot of the test data will establish the CBR result of the soil tested.

### **2.3.2 The Geogauge (ASTM D 6758-02)**

The Geogauge is a portable instrument manufactured by Humboldt Manufacturing Company (Fig.2.4). It was developed to provide a simple and rapid means of measuring the stiffness of compacted subgrade, subbase and base course layers in earthen construction. The steps to use the Geogauge are very simple. First, the user must ensure that there is adequate seating for the Geogauge. In order to ensure good



seating, Humboldt suggests that 60 percent of the Geogauge footprint be clearly visible after removing the Geogauge following a test on natural material. In the case of very rough surfaces, a moist fine sand layer may be placed as a coupling between the Geogauge foot and the soil. After placing the sand layer, the Geogauge is put on the sand layer and turned one quarter to one half of the way around without downward force. The user then presses the MEAS button on the Geogauge display. The Geogauge will first measure the background noise as a function of frequency followed by a measurement of stiffness as a function of frequency. After approximately 70 seconds, the Geogauge will display the signal to noise ratio (SNR), the standard deviation of stiffness measurements at all 25 frequencies and the stiffness or Young's modulus, depending on what is selected by the user.

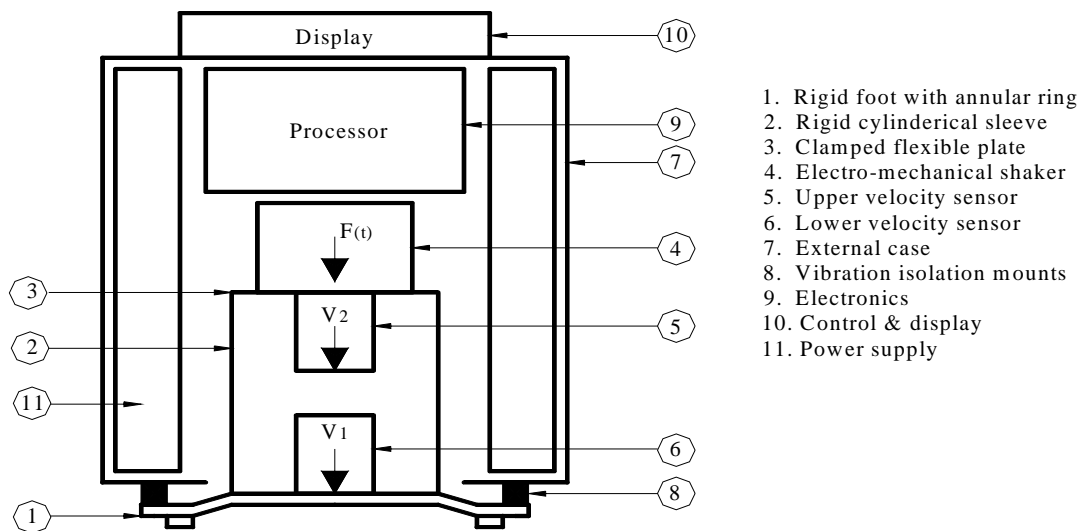


Fig. 2.4 The Cross-Section of Geogauge from Humboldt



Fig. 2.5 Geogauge in the Field

As Figs.2.4 and 2.5 indicate, the Geogauge consists of a computer and display, an electro-mechanical shaker on top of a flexible plate that is attached to a rigid cylinder, two geophones, a rigid foot with annular ring, vibration isolation mounts, and a power supply. During the measurement, the Geogauge begins to impart very small vertical vibration displacements ( $<0.0013$  mm) to the soil through a harmonic electromechanical shaker, which operates over a frequency range between 100 to 200 Hertz. Two geophones located inside the Geogauge measure velocity between the rigid foot and a flexible plate below the shaker. A computer inside the Geogauge then integrates the velocities into displacements and the stiffness of the soil is determined at 25 different frequencies. Each measurement takes about 70 seconds. The stiffness that is output on

the Geogauge screen is the average of the stiffnesses at the 25 different frequencies between 100 and 200 Hertz. The Geogauge is able to store 500 stiffness values and the first 20 stored results will include stiffness versus frequency details. That data can be downloaded from the Geogauge via an infrared connector that hooks to the serial port of a computer where it can then be converted into a Microsoft Excel spreadsheet and evaluated. The technical specification of the Geogauge is listed in Table 2.1.

### **2.3.3 The Seismic Pavement Analyzer-SPA**

The SPA is a small trailer equipped with eight transducers and two pneumatic hammers. The trailer is towed to the test site, and the hammers and transducers are lowered to the pavement surface. The hammers then strike the pavement, producing vibrations that are picked up by the transducers, which relay the data to a computer onboard the vehicle towing the SPA. The test is almost fully automated and only takes about 1 minute. The data are analyzed by a computer software program, which then generates a report describing the condition, thickness, and stiffness of the pavement; any defects in the pavement subgrade; and other properties that are directly related to pavement performance.

SPA could be used to pinpoint the location of problems in the pavement or subgrade. It could also reveal the severity of a problem, which would help engineers then select the best maintenance or repair method. In addition, it could be used to test how well a repair or maintenance treatment is working.

Table 2.1 Technical Specification of the Geogauge (After Humboldt 2000c)

<b>Soil Measurement Range</b>	
Stiffness	3MN/m(17klbf/in) to 70 MN/m(399klbf/in)
Young's Modulus	26.2 MPa (3.8 ksi) to 610 MPa (89 ksi)
Measurement Accuracy	(typical, % of absolute) $< \pm 5\%$
<b>Depth of Measurement from Surface</b>	220 mm (9in)
<b>Calibration</b>	Laboratory
Accuracy (% of actual mass)	$< \pm 1\%$
Range (effective)	4MN/m (22.8 lb/in) to 16 MN/m (91.4 lb/in)
<b>Electrical</b>	
Power Source	6 D size disposable cells
Battery Life	Sufficient for 500 to 1,500 measurements
<b>Mechanical</b>	
External Materials	Aluminum case & foot, rubber isolators & seal
Vibration	$< 0.00005$ in. @ 125 Hz
Level re Vertical	$\pm 5^\circ$
Operating Temperature	$0^\circ C$ to $38^\circ C$ (ambient)
Storage Temperature	$-20^\circ C$ to $50^\circ C$
Humidity	98%, without condensation
Gauge Dimension (w/o handle)	280 mm (11 in) diameter 255 mm (10 in) height
Weight	Net 10 kg (22 lbs) Shipping, with case 16.8 kg (37 lbs)
<b>Standard Accessories</b>	Transit case, 6 'D' batteries, user guide
<b>Optional Accessories</b>	Verifier Mass Infrared (IR) com serial interface adapter cable with software template (3.5" floppy, PC)

### 2.3.4 The Dynamic Cone Penetrometer-DCP

The Dynamic Cone Penetrometer (DCP) is a hand held instrument designed for the rapid in-situ measurements of the strength and variability of existing pavement layers and subgrades. The device consists of two 0.63 in. (16 mm) diameter rods, with the lower rod containing an anvil, a replaceable 60° pointed tip, and depth markings every 0.2 inches (5.1 mm). The upper rod contains a 17.6 lbs. (8 kg) drop hammer with a 22.6 inch (575 mm) drop distance, an end plug for connection to the lower rod, and a top grab handle (Fig.2.6). All materials (except the drop hammer) are stainless steel for corrosion resistance.

Operation of the DCP requires two persons, one to drop the hammer and the other to record the depth of penetration. The test begins with the operator "seating" the cone tip by dropping the hammer until the widest part of the cone is just below the testing surface. At this point the other person records this initial penetration as "Blow 0". The operator then lifts and drops the hammer either one or more times depending upon the strength of the soil at that test location. Following each sequence of hammer drops, a penetration reading is taken. This process continues until the desired depth of testing is reached, or the full length of the lower rod is buried. At that time, a specially adapted jack is used to extract the device.

Data from a DCP test is processed to produce a penetration index (PI), which is simply the distance the cone penetrates with each drop of the hammer. The PI is expressed in terms of inches per blow or millimeters per blow. The penetration index can be plotted on a layer strength diagram or directly correlated with a number of common

pavement design parameters. The average PI can be used to estimate the California Bearing Ratio, and the Elastic Modulus,  $E$ , using available correlations.



Fig.2.6 Dynamic Cone Penetrometer

### **2.3.5 The Clegg Impact Soil Tester (ASTM D5874-02)**

The Clegg Impact Soil Tester was developed by Dr. Baden Clegg in the Department of Civil Engineering at the University of Western Australia in the 1970s. The Clegg Impact Soil Tester, also known as the Clegg Hammer, is a simple to use device consisting of two basic components: a flat-ended cylindrical mass and a guide tube. The mass is a hammer which is manually dropped from a predetermined height. Four basic hammer masses are available: 4.5 kg (the "Standard Clegg Hammer"), 2.25 kg (the "Medium Clegg Hammer"), 0.5 kg (the "Light Clegg Hammer") and 20 kg (the "Heavy Clegg Hammer"). The set height of drop for the Standard and Medium Hammers is 45 cm whilst it is 30 cm for the Light and Heavy Hammers. The 4.5 kg Clegg Impact Standard Test (CIST) is the "general purpose" Hammer for roadworks, earthworks, airstrips, etc. The two lighter Hammers are used primarily for turf or sand testing. The Heavy Hammer is for testing through a larger zone or on top of the running course of flexible pavements. Because of its larger size and weight, the guide tube is set on wheels with a pull handle to ease movement on site.

The 4.5 kg "Standard" Clegg Impact Soil Tester (Fig.2.7) was initially conceived for basecourse testing but has turned out to be the "general purpose" Clegg hammer. It is based on the instrumentation of a "modified proctor" laboratory compaction hammer. The Hammer mass is 5 cm in diameter at 4.5 kg and is dropped from a set height of 45 cm. The weight of the guide tube and meter is approximately 1.6 kg. Instrument height is 70 cm and the guide tube is 15 cm in diameter. The output of the standard Hammer

when dropped from its standard height is known as the Clegg Impact Value (CIV). The impact of the hammer causes an electronic output to a digital display. The output is based on the peak deceleration of the hammer's impact with the surface in units of tens of gravities. Four successive blows of the hammer on the same spot constitute one test, called a Clegg Impact Test (CIT). The CIT provides a soil strength/stiffness or "hardness" parameter known commonly as Clegg Impact Value (CIV), also known as Impact Value (IV) (ASTM Standard D 5874) and notation is as CIV, CIV/M, CIV/L, and CIV/H for the "Standard", "Medium", "Light" and "Heavy" Hammers.

The following is the major use of the Standard 4.5 kg Clegg Hammer:

1. Pavement Design. CIV is similar in concept to the California Bearing Ratio (CBR). CIV may be used as an alternative to CBR in both laboratory and field on unsoaked samples. CIV may be converted to a Clegg Hammer Modulus (CHM), analogous to an elastic modulus.
2. Construction. CIV provides a means of process control by monitoring the effect of roller passes and checking variability. Percent compaction may be estimated by determining the CIV (termed an "As Compact Target CIV") needed to achieve the desired density level for the given material and field moisture content.
3. Evaluation. CIV may be used to ensure adequate basecourse strength before sealing or proceeding with subsequent layers. It may also be used to monitor the effect of environmental changes and to investigate pavement failures.





Fig.2.7 Standard Clegg Impact Soil Tester

### 2.3.6 The Falling Weight Deflectometer-FWD

The Falling Weight Deflectometer is mounted on a trailer (Fig.2.8). The control/recording system is housed in the towing vehicle. The weight and drop height can be adjusted to give the desired impact loading. Typically, a 250 kg weight is used, producing an impact load of 25-30 msec duration and giving a peak stress of approximately 50 kN. The weight is dropped onto a rubber-cushioned circular loading plate of 300mm diameter. The vertical displacement is measured by a series of geophones at distances of 0, 300, 600, 900, 1200, 1500 and 2100 mm from the center of the loading plate. The load and resultant peak deflections are recorded on computer disk. In routine surveys, the tests are carried out at a spacing of 20-50 meters along the road, normally in the left-hand wheelpath. When doing the test, lane closures may be necessary. Pavement temperature is measured at a depth of 40mm.

The Falling Weight Deflectometer is used to establish elastic modulus values for the pavement layers. From these values, the residual life and overlay requirements can be determined; also there will be an indication of which of the layers will reach a critical condition first. The principle of the test is the measurement of the deflection bowl produced by dropping a weight onto the pavement. The analysis involves establishing a set of moduli values which would produce deflections to match the displacements recorded.

The first stage of the analysis is the calculation of the modulus of each layer. This involves the Method of Equivalent Thickness, using the Boussinesq equations to

calculate deflections and, using an iterative procedure, calculating moduli which will result in deflections close to the observed values. The pavement can be modeled as a two, three, or four layer system. The second stage of the analysis is the calculation of the residual life of the pavement. This is achieved by analyzing the stresses and strains in the individual layers to predict the time at which critical stress or strain conditions (leading to cracks in bituminous layers and cement-bound layers, or unacceptable rutting in unbound layers) will be reached. Finally, an estimate is made of the thickness of overlay required to delay the onset of critical conditions for a specified period (usually 20 years).



Fig. 2.8 Falling Weight Deflectometer

### **2.3.7 The Light (Portable) Falling Weight Deflectometer-LFWD (PFWD)**

The LFWD is a device used to determine the bearing capacity of soils and to evaluate the strength of flexible pavement systems. The device has different versions due to different manufacturers and different countries of origin, but they are very similar in principle. Prima 100, which is developed by Carl Bro Pavement Consultants (Denmark). The device is easy to handle and is an alternative to plate load tests, enabling rapid measurements without disturbing the soil. It weighs 26 kg in total with a 10 kg falling mass that falls on the bearing plate via four rubber buffers (Fig. 2.9). It can be used on all construction sites and materials.

There are other portable falling weight deflectometers available in the market. The devices that have the same principle and similar impact energy as the Prima LFWD are the German Dynamic Plate Test (GDPT), also known in the UK as the Lightweight Drop Tester and the Loadman, which was originated in Finland.

There is very limited literature about the Prima LFWD. Most of the previous work on small-scale dynamic devices was conducted with the Loadman and GDPT. Although the mechanisms and impact loads are similar to each other, results obtained with alternative portable falling weight deflectometers shows significant variability even for the same field conditions. Fleming (2000) evaluated the Loadman, German Plate Bearing Test and TRL Foundation Tester (TFT), which was not commercially available. After laboratory investigations and reviewing field results, it was shown that the different buffer materials and different mass of bearing plates has effect on the

contrasting results. Also the technology used by different manufacturers is not the same. For example the Prima LFWD has a load cell for measuring the impact force whereas GDPT and the Loadman do not have a load cell. Instead an approximation is used with these devices to estimate the impact force from deflection. Carl Bro states that they used the same technology as the full scale FWD, load cell, geophones etc. for developing Prima LFWD.

The measuring principle of LFWD is explained as follows: in LFWD, a center geophone sensor measures the deflection caused by dropping a 10 kg hammer freely onto the loading plate. The falling mass impacts the plate and produces a load pulse of 15-20 milliseconds. The diameter of the loading plate is 200 mm. Alternatively 100 mm and 300 mm plates are also available. The load range of the LFWD is 1 to 15 kN. It measures both force and deflection. The measured deflection of the ground is combined with the applied load to calculate the stiffness using conventional Boussinesq static analysis. The measured center deflection is used to estimate the dynamic deformation modulus as follows:

$$E_{LFWD} = \frac{K \cdot (1 - \nu^2) \cdot P \cdot r}{\delta_c} \quad (2.8)$$

Where:

$E_{LFWD}$  = LFWD dynamic modulus

$K = \pi/2$  and 2 for rigid and flexible plates, respectively.

$\delta_c$  = Center deflection

$\nu$  = Poisson Ratio of soil

P = Applied Stress

r = Radius of the plate



Fig.2.9 LFWD in the Field

## **2.4 Comparison of Moduli from Different Apparatus**

Since there are so many apparatus to measure soil modulus/stiffness in the field, people need to know which one can give the consistent and good results. Many comparison tests between these apparatus have been done in the field and the correlations between them were also given.

### **2.4.1 Petersen et al. Comparison Tests**

Petersen et al. (2002) did comparison tests between quasi-static plate test and Geogauge. He reported that the unloading, reloading and initial modulus values have different correlations with the geogauge modulus values. Geogauge test results show a relatively good correlation ( $R^2=0.66$ ) with the first load moduli obtained by the quasi-static plate load tester. However the geogauge modulus was nearly 7 times larger than the initial loading modulus. There was a very low to non-existent correlation between the Geogauge test results and the unload ( $R^2=0.27$ ) and reload moduli ( $R^2=0.23$ ) obtained by the quasi-static plate load tester (Fig.2.10).

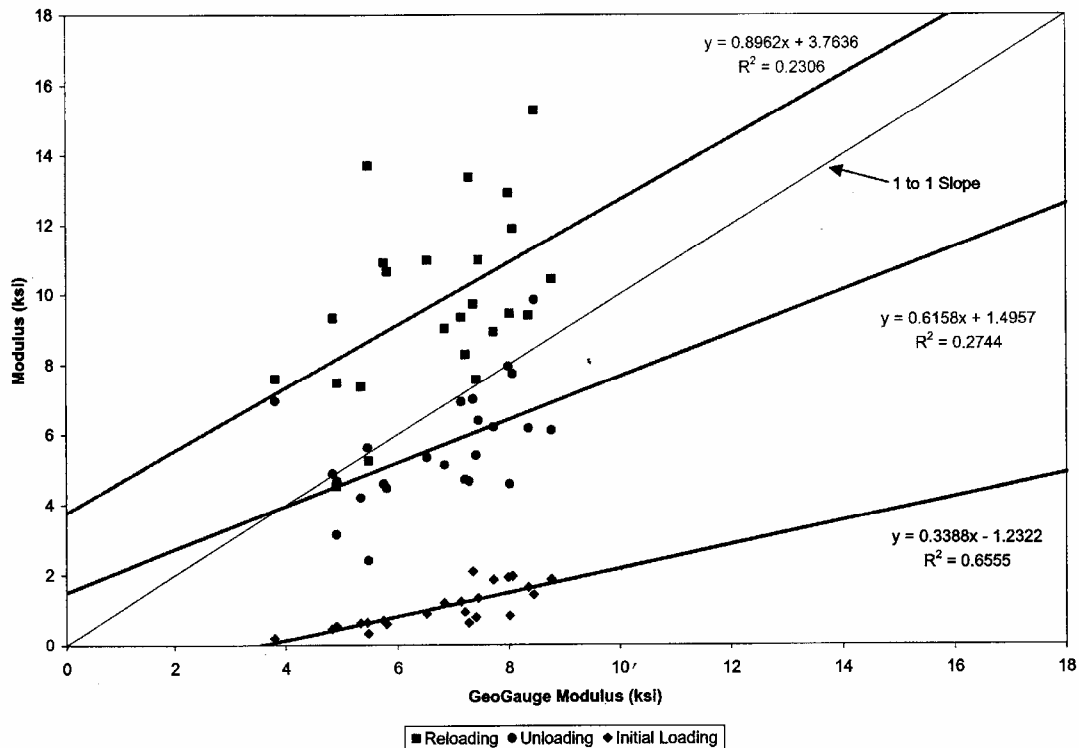


Fig.2.10 Relationship between Quasi-Static Plate Load Modulus and Geogauge Modulus (After Petersen et al. 2002)

#### 2.4.2 Chen & Bilyeu Comparison Tests

Chen & Bilyeu (1999) compared the results from the SPA, the P-SPA, the FWD, the MDD, laboratory ultrasonic, triaxial, free resonant column, resilient modulus and the Geogauge tests at 8 locations on top of a pavement. The pavement consisted of a 0.18 m (7.25 inch) thick layer of asphalt placed on top of a 0.38 m (15 inch) thick base layer, which was placed on top of the natural subgrade. A summary of the results on the subgrade are as follows:



- Humboldt Geogauge:  $E(GG)=106$  MPa (COV=19.2%);
- Falling Weight Deflectometer (FWD):  $E(FWD)=37$  MPa (COV=11.6%);
- MultiDepth Deflectometer (MDD):  $E(MDD)=57$  MPa;
- Seismic Pavement Analyzer (SPA):  $E(SPA)=289$  MPa (COV=25%);
- Portable Seismic Pavement Analyzer (P-SPA):  $E(P-SPA)=304$  MPa (COV=38.3%);
- Laboratory Resonant Column Test:  $E(RC)=244$  MPa;
- Laboratory Resilient Modulus:  $E(RM)=100$  MPa.

All the apparatus gave different soil moduli except that the Geogauge modulus (106 MPa) is similar to the laboratory resilient modulus, which was 100 MPa.

### **2.4.3 McKane Comparison Test**

McKane (2000) performed tests on the subgrade at five different road test sections in Minnesota. The testing devices that were used were the PFWD, the FWD, the Geogauge and the DCP. The subgrade that was tested was classified as a sandy lean clay according to the USCS classification system.

Because the FWD has been around the longest and is recognized as a standard by many road authorities, the results from all the measuring devices were compared to the FWD results by best-fit curves. All devices measured higher moduli than the FWD. The PFWD had the strongest correlation with the FWD indicating a 2 to 1 ratio with the FWD and an  $R^2$  value of 0.70. The DCP results showed a 3 to 1 ratio with the FWD

results and have an offset of 62 MPa. That is, when the FWD is reading a modulus of zero, the DCP is reading a modulus of around 62 MPa. Geogauge modulus results show a 1 to 1 correspondence with the FWD measurements but the offset is around 67 MPa. Both the DCP and Geogauge relationships show an  $R^2$  value of 0.60. These correlations can be found in Fig.2.11.

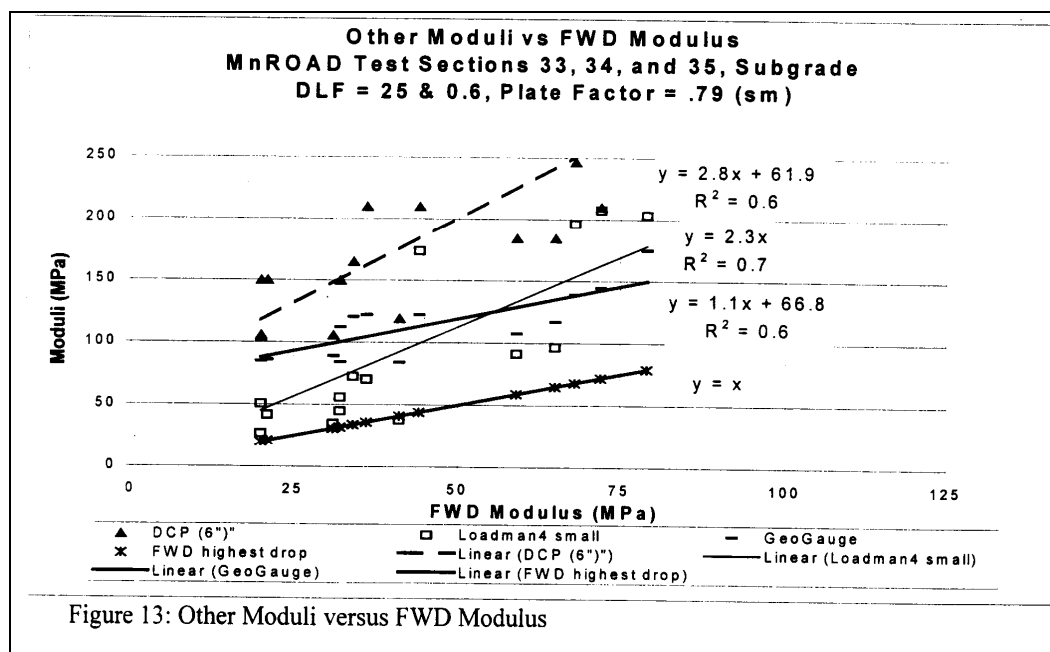


Fig.2.11 Modulus Comparison to FWD (from McKane, 2000)

#### 2.4.4 Sargand, et al. Comparison Tests

Sargand, Edwards & Salimath (2001) reported a test on a 2,000 foot long section of new construction on a silty clay subgrade material. The purpose of the project was to measure the structural characteristics of the subgrade and base material of the test

section with various non-destructive testing devices. The testing devices that were used included the nuclear density meter, the Geogauge, the German plate load tester, the FWD and the DCP. A small load FWD (3,500 to 4,500 pound load) test and a large load FWD (6,500 to 9,000 pound) test were conducted at each test location. The German plate load tester consisted of statically loading the soil through a pressure application device on a load plate. The results of the test showed that the Geogauge and German plate load tester gave lower stiffness values than the FWD. For subgrade material, the resilient modulus from the laboratory was 26 percent lower than the Geogauge modulus from the field. For the base material, the resilient modulus from the laboratory was 40 percent lower than the Geogauge modulus from the field. A relationship between the Geogauge modulus and the small load FWD on subgrade material was not provided by the author of this reference. However, using the data provided by the authors, the Texas A&M research team created a plot that shows a relatively good correlation with a  $R^2$  value of 0.61. The plot also indicates that when the small load FWD modulus is zero, the Geogauge modulus is around 102 MPa (Fig.2.12).

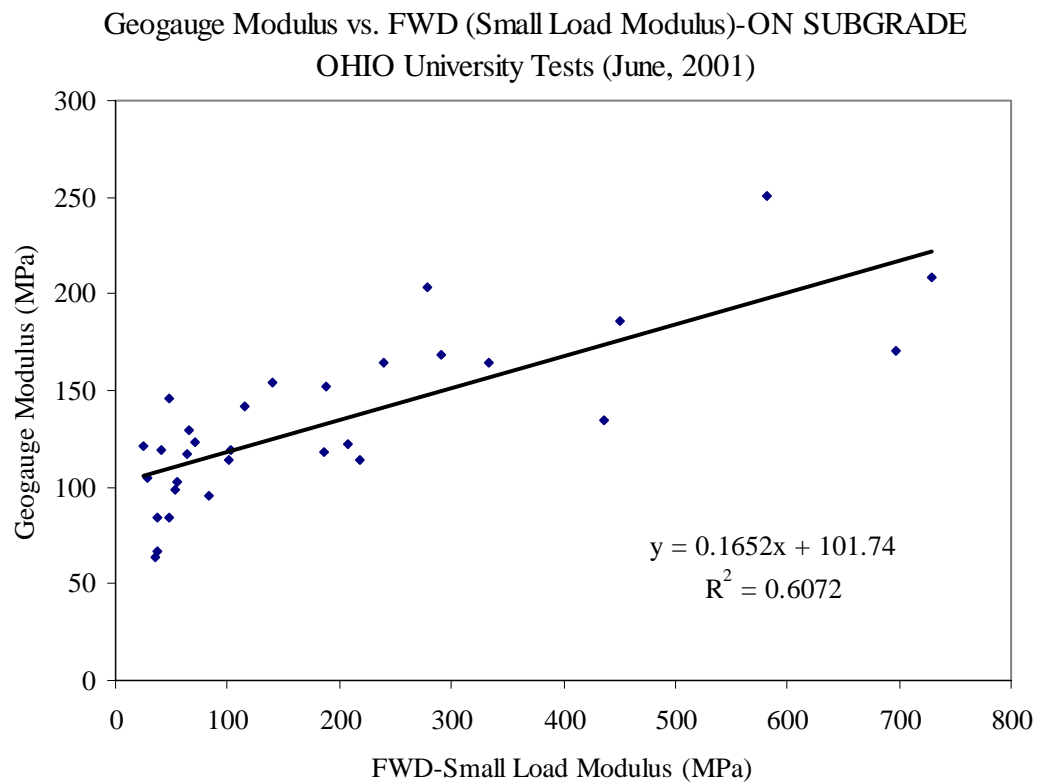


Fig.2.12 Geogauge vs. FWD (data from Sargand et al. 2001)

A plot was also created by the Texas A&M research team that shows a fair correlation ( $R^2=0.47$ ) between the Geogauge modulus and the German plate load tester modulus on subgrade material. The plot also indicates that when the German plate load tester modulus is zero, the Geogauge modulus is around 13 MPa (Fig.2.13).

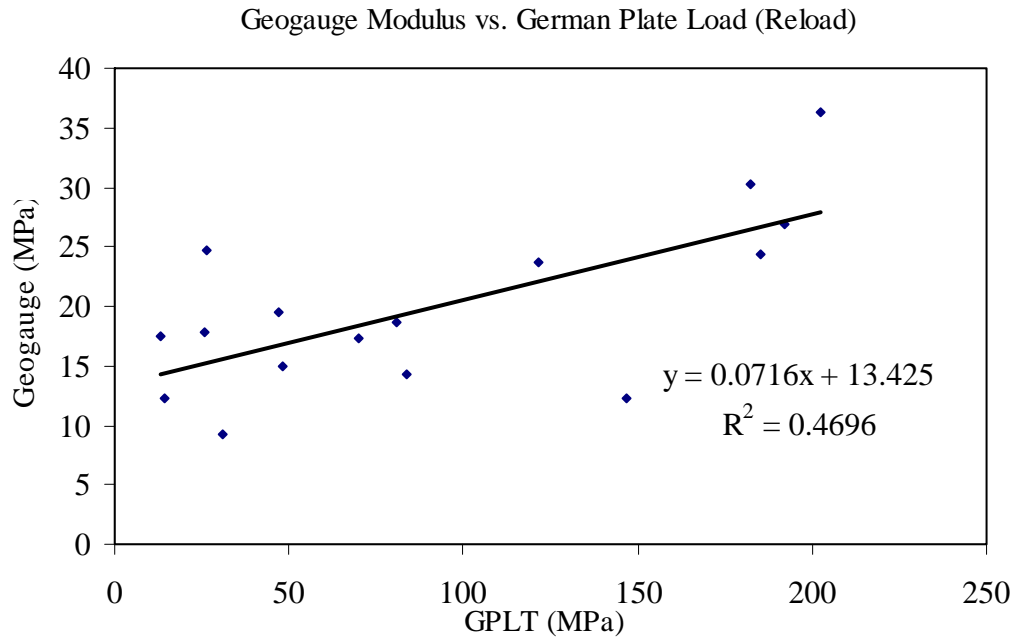


Fig.2.13 Geogauge vs. GPLT (data from Sargand, et al. 2001)

A correlation plot between the small load FWD modulus and the German plate reload test modulus had an average intercept of around 27 MPa (Fig.2.14) and a correlation plot between the large load FWD modulus and the German plate load test modulus had an average intercept around 15 MPa (Fig.2.15).

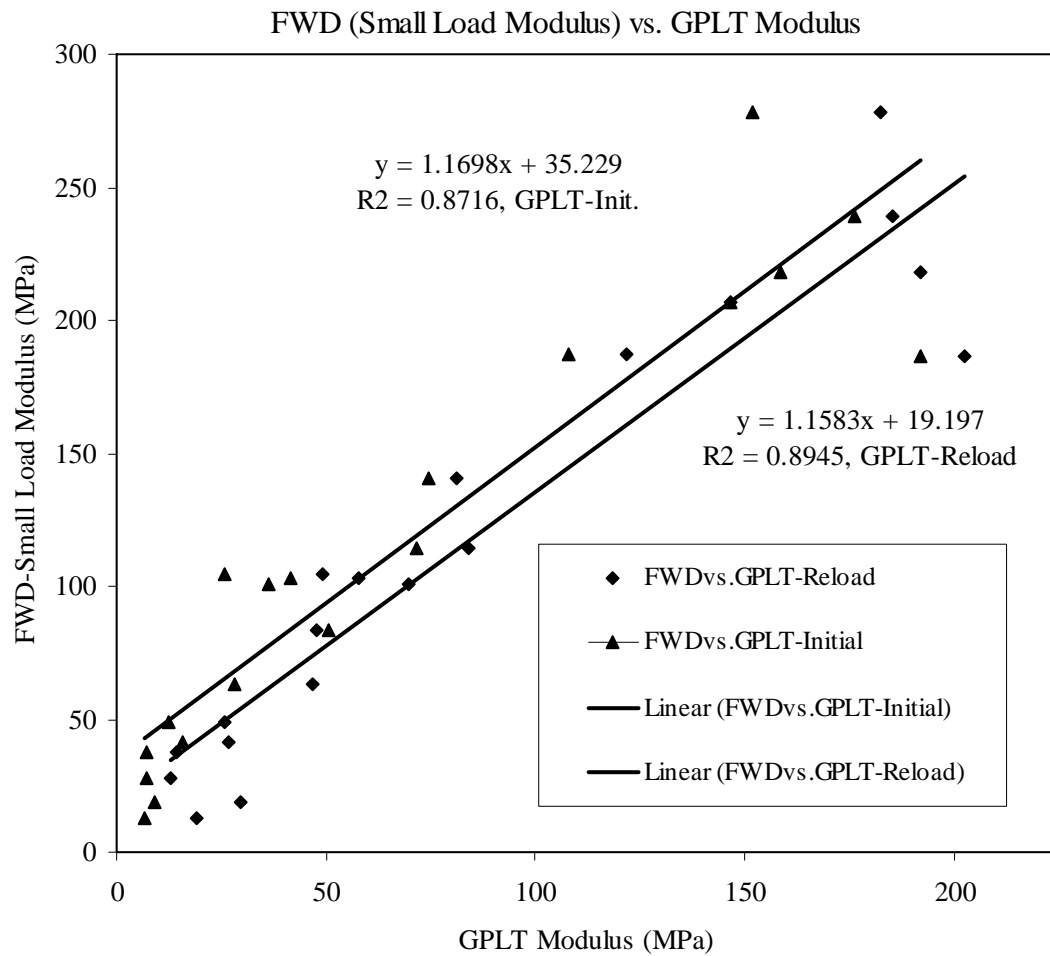


Fig.2.14 Small Load FWD vs. GPLT (data from Sargand, et al. 2001)

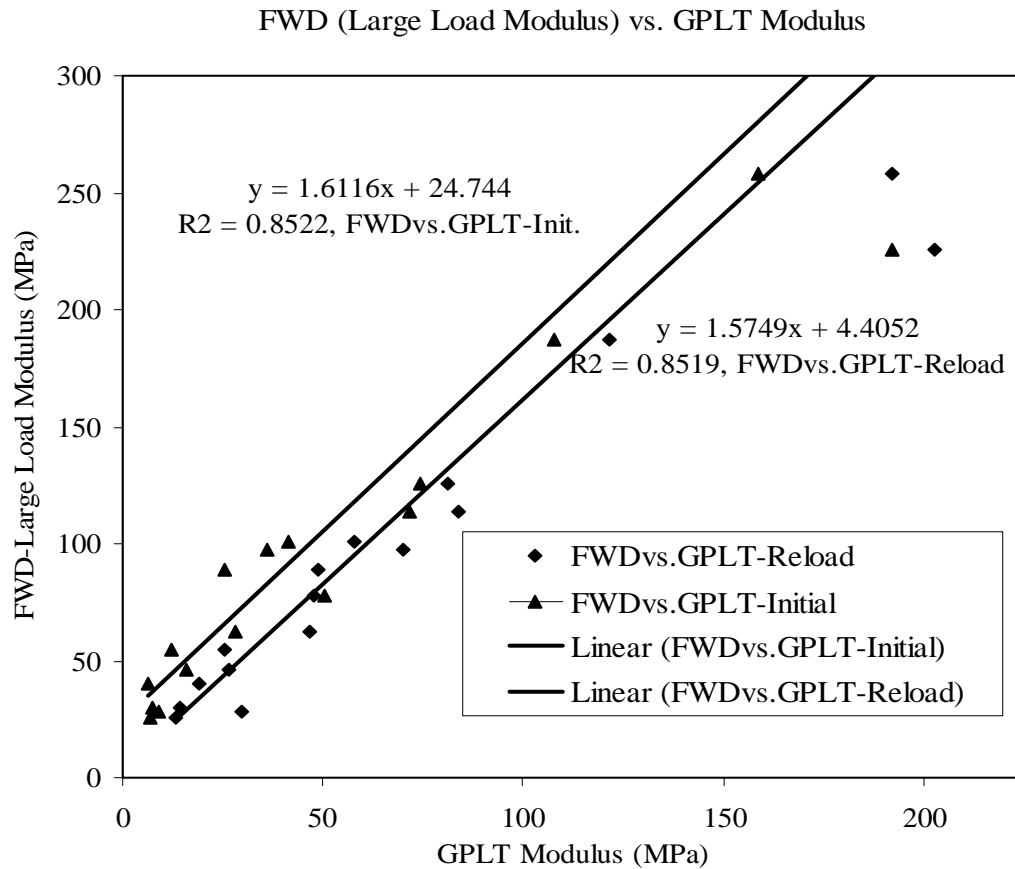


Fig.2.15 Large Load FWD vs. GPLT (data from Sargand, et al. 2001)

As Fig.2.14 and Fig.2.15 show, the correlation between the FWD and GPLT (average  $R^2=0.87$ ) was substantially stronger than the Geogauge vs. FWD ( $R^2=0.61$ ) and Geogauge vs. GPLT correlation ( $R^2=0.47$ ).

#### 2.4.5 TAMU Riverside Campus Lime Treated Road Comparison Test

In September 08, 2003, the author and Stephen Sebesta from Texas Transportation Institute (TTI) did a comparison test at riverside campus. Three locations on a new lime treated road were chosen to do the comparison test. Falling Weight Deflectometer (FWD) and Clegg Impact Tester were run by Stephen Sebesta. Rigid plate tester was run by the author. The test results are shown in Table 2.2.

Table 2.2 Comparison of FWD and Plate Test at Riverside Campus

Test Location	FWD Result (MPa)	Plate Test Result (MPa)
#1	358.28	48.25
#2	330.72	85.78
#3	626.00	58.11

Unfortunately, the FWD tests at location #1 and #2 appear to be no good because errors in back calculations are very high. For location #1, absolute error/sensor=15.1. For location #2, error/sensor=15.2. For location #3, error/sensor=1.2. Typically for FWD, good data will have error/sensor below 5, definitely below 10. So FWD results from locations #1 and #2 should be used with cautions. Plate test result seems more consistent than FWD although it is much smaller than FWD results.



The only site tested with the Clegg Impact Tester, FWD and Plate Tester is location 3. Two types of Clegg Impact Tester were used at location #3. One is the standard Clegg Impact Tester with 4.5 kg hammer, the other is the heavy Clegg Impact Tester with 20 kg hammer. The test result is shown in Table 2.3.

Table 2.3 Comparison of FWD, Clegg Impact Tester and Plate Tester at Riverside Campus

Testing Apparatus	Soil Modulus (MPa)
FWD	626
Standard Clegg Impact Tester	82.6
Heavy Clegg Impact Tester	36.8
Plate Tester	58.11

From Table 2.3, we found that different types of Clegg Impact Tester can give different results. The Clegg Impact Tester's result is comparable to Plate tester's result. The author thinks the big difference between FWD result and Plate test result is because FWD is measuring the dynamic modulus while plate test is measuring the static modulus.

#### **2.4.6 US 171, Ragley-Longville, LA Comparison Test**

On August 8, 2003, a field comparison test was done at a construction site of US 171, Ragley-Longville, LA. During this test, Falling Weight Deflectometer (FWD), Light Falling Weight Deflectometer (LFWD), Geogauge, Ring Plate Tester were used to measure the soil moduli at two sections A and B after different roller passing. Limestone was used in the compaction of road base. Water was applied to the ground after each passing during the compaction. The LFWD, Geogauge and Ring Plate Test results were collected and listed in Table 2.4 and Table 2.5.

Table 2.4 US 171 Site A Test Results

Roller Passing	2	4	6
Water Content (%)	6.6	9.8	10.5
Dry Density (pcf)	118	122.5	123.3
Geogauge Modulus (MPa)	75.78	59.47	39.85
LFWD Modulus (MPa)	70.82	68.36	58.16
Ring Plate Load Modulus (MPa)	5.93	8.79	12.41
Ring Plate Reload Modulus (MPa)	22.43	36.42	33.96

Table 2.5 US 171 Site B Test Results

Roller Passing	2	4	6	10	15
Water Content (%)	8	8.4	8.7	12.3	15
Dry Density (pcf)	115.9	117.2	117.9	121.7	119.4
Geogauge Modulus (MPa)	36.39	48.32	47.27	42.53	54.25
LFWD Modulus (MPa)	55.21	62.51	59.09	50.34	58.89
Ring Plate Load Modulus (MPa)	7.16	7.53	7.07	4.97	8.25
Ring Plate Reload Modulus (MPa)	28.14	19.65	24.11	18.62	27.02

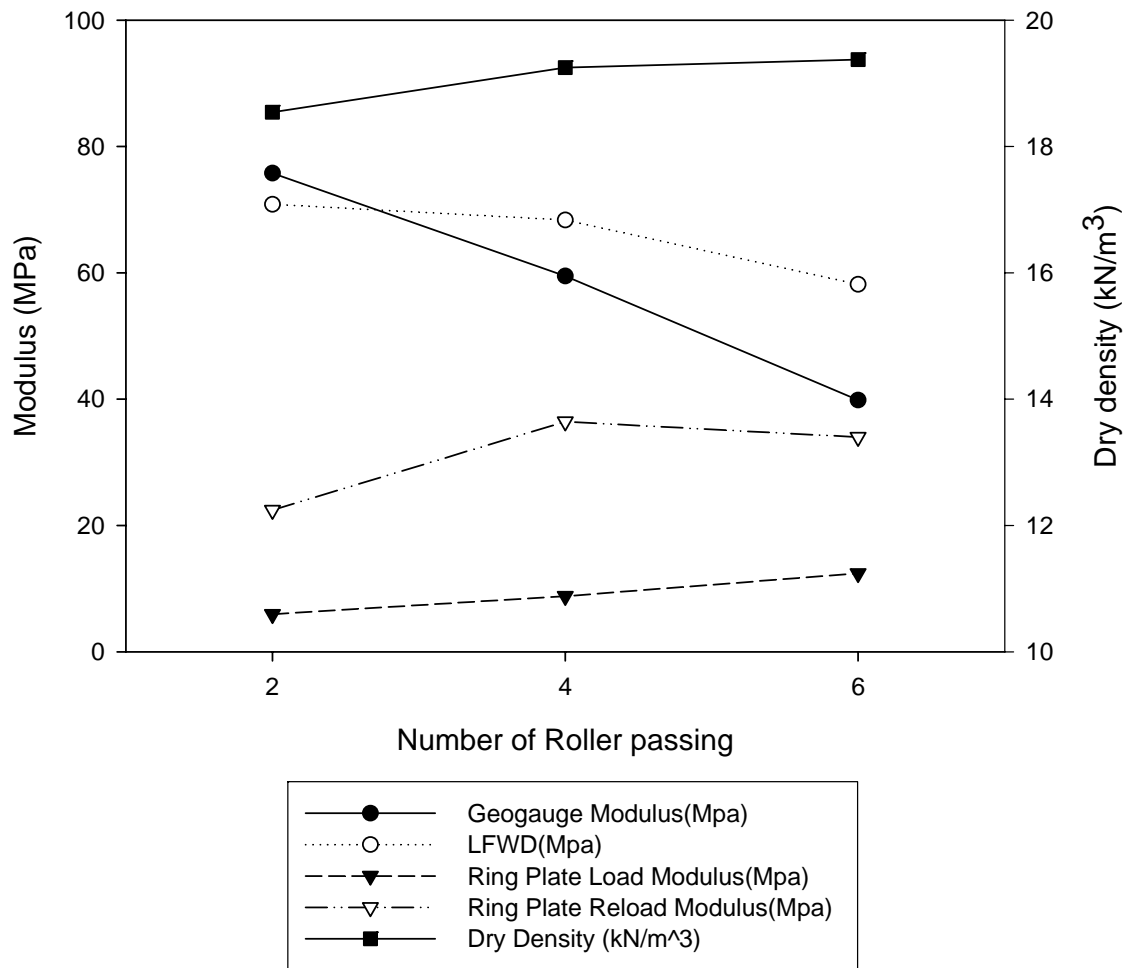


Fig.2.16 US 171 Site A Comparison Test

The test results at section A are shown in Fig.2.16. We found that at section A, ring plate load and reload moduli have the same trend as dry density and increase with the number of roller passing. But the moduli from LFWD and Geogauge decrease with the number of passing.

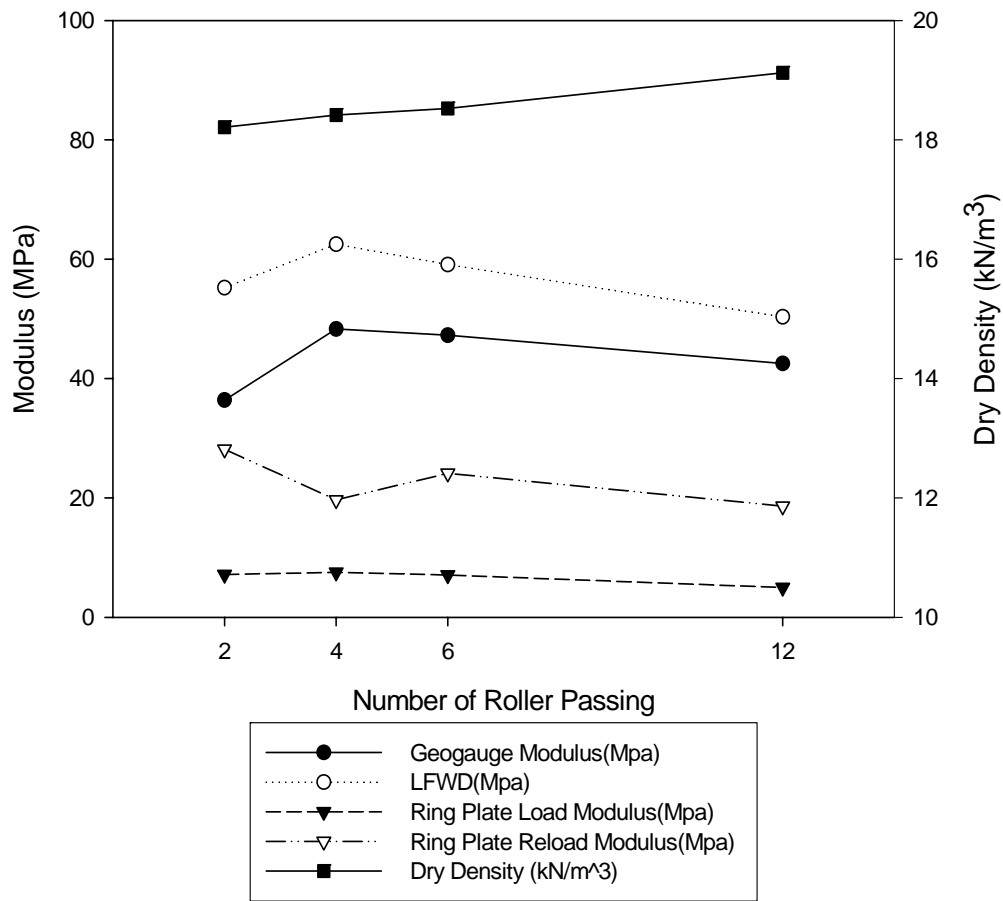


Fig.2.17 US 171 Site B Comparison Test

The test results at section B are shown in Fig.2.17. We found that at section B, dry density increases with the number of passing until it reaches the peak after 10 passing. Moduli from LFWD, Geogauge and ring plate test don't have the same or even reverse trend with the number of passing.

## 2.5 Conclusion

Among all the apparatus listed above, only Geogauge and Clegg Impact Tester are light and portable devices. Clegg Impact Tester can't tell us the soil modulus right at the field and some people argue this is a strength testing apparatus and does not necessarily indicate compaction or density. Although it is relatively easy to use, it must be used on each compacted layer of material. Only using it on the last layer of material to be backfilled into the trench will not give an accurate reflection of the compaction of the full depth of the trench.

Geogauge is the only apparatus which can measure the soil modulus in the field easy and fast. Unfortunately, according to report (Briaud et al. 2003), although there is a relatively good correlation between Geogauge and ring plate test in the field, many unexplained phenomena were found in the laboratory Geogauge study. The correlation between unconfined compression test modulus and Geogauge stiffness of the compacted soil sample is very poor with  $R^2 = 0.3627$  (Fig.2.18). Currently the best way to transition from dry density based compaction control to modulus based compaction control is to find a way to obtain a modulus versus water content curve similar to the dry density curve in the laboratory test. After the modulus versus water content curve was obtained, the target value can be given for modulus and water content in the Geogauge field test. The Geogauge stiffness versus water content for four compaction energies is shown in Fig.2.19. For standard compaction effort, it is difficult to define the target values of modulus and water content and this will greatly limit the use of Geogauge.

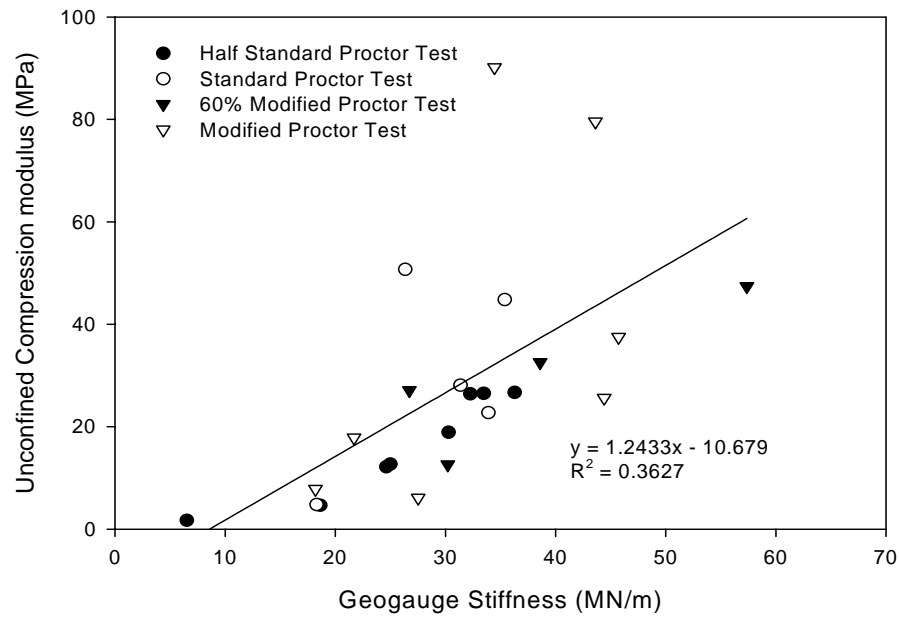


Fig.2.18 Unconfined Compression Test Modulus vs. Geogauge Stiffness (After Briaud, et al., 2003)

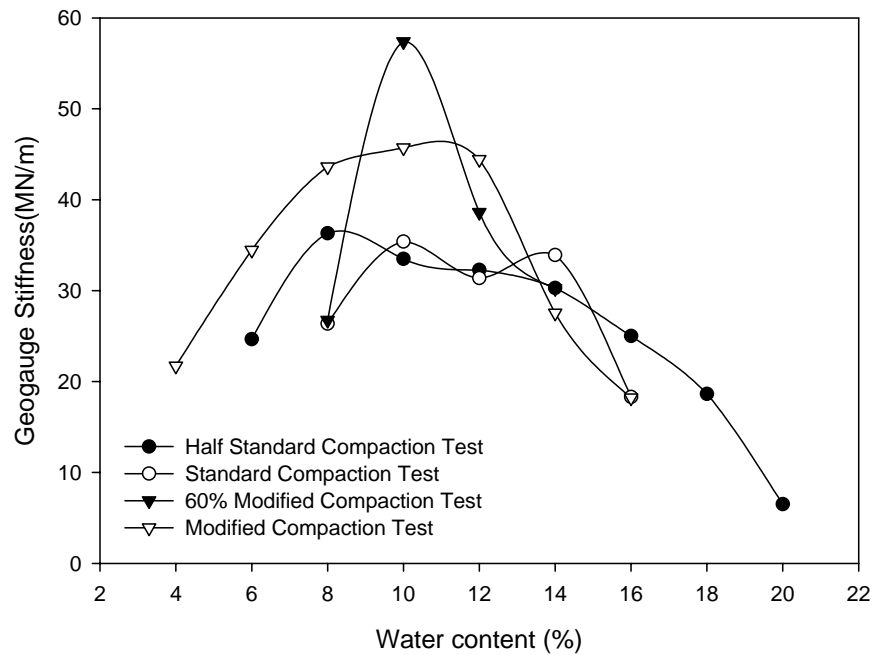


Fig. 2.19 Geogauge Stiffness vs. Water Content for Four Compaction Energies (After Briaud, et al., 2003)



## **CHAPTER III**

### **BRIAUD COMPACTION DEVICE (BCD)**

In response to the need for a fast, inexpensive and more accurate compaction testing device, Briaud Compaction Device-BCD, a portable, lightweight and safe prototype model of instrument was developed by Dr. J.L. Briaud at Texas A&M University to measure the modulus in the field fast and accurately.

#### **3.1 Idea of BCD**

The idea of BCD is to use the bending of a plate resting on the ground surface as an indicator of the modulus of the soil below (Fig.3.1). If the soil is stiff, the plate does not bend much. If the soil is soft the plate bends a lot. If the soil is very soft, the plate simply punches through the soil. Within the range of soil stiffness where the plate bending is proportional to the soil modulus, the correlation between the bending strain (hoop and radial) measured with strain gauges glued to the top of the plate is used to obtain the modulus. The location of strain gauges in radial and hoop directions is given in Fig.3.2.

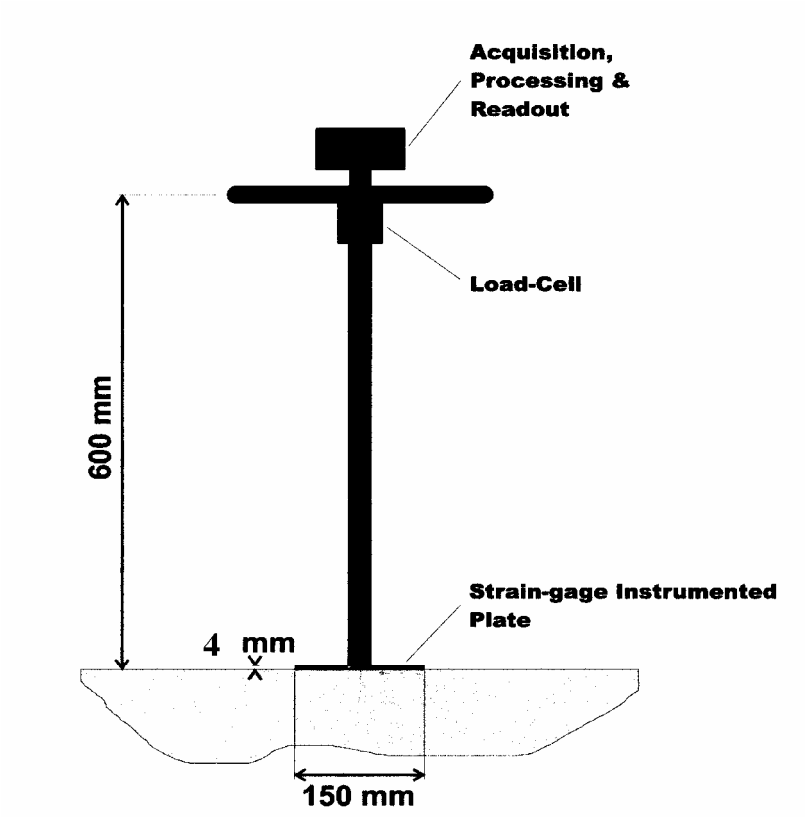
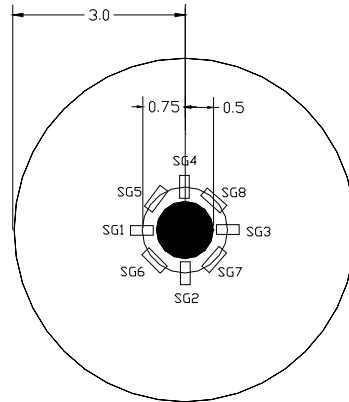


Fig. 3.1 The Conceptual Design of BCD



- 1: SG1, SG2, SG3, SG4 are radial direction strain gauges on the circle of radius of 0.75 inch.
- 2: SG5, SG6, SG7, SG8 are the hoop direction strain gauges on the circle of radius of 0.75 inch.

Fig.3.2 Plan View of BCD Plate

### 3.2 Strain Gauge

The strain gauge is one of the most important components of BCD. To better understand how a strain gage works, several basic principles such as stress, strain and resistance are discussed below.

### 3.2.1 Stress

When a material is loaded with a force, stress at some location in the material is defined as force per unit area. For example, consider a wire anchored at the top, and hanging down. Some force  $F$  pulls at the bottom, as Fig.3.3.

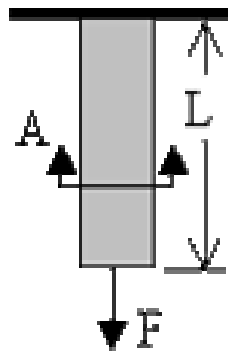


Fig.3.3 Definition of Stress

$A$  is the original cross-sectional area of the wire, and  $L$  is the original wire length. In this situation, the material will experience a stress, called an axial stress  $\sigma_a$ .

$$\sigma_a = \frac{F}{A} \quad (3.1)$$

The dimension of stress is the same as that of pressure, i.e. force per unit area.

### 3.2.2 Strain

In Fig.3.3, the wire will stretch vertically as a result of the force. Strain is defined as the ratio of increase in length to original length. Specifically, when force is applied to the wire, its length  $L$  increases, while its cross-sectional area  $A$  decreases (Fig.3.4).

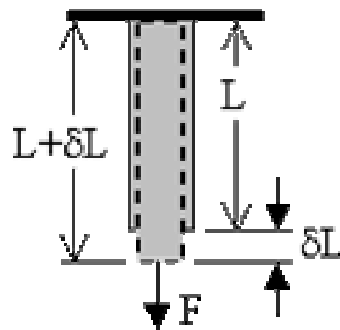


Fig.3.4 Definition of Strain

The axial strain is:

$$\varepsilon_a = \frac{\delta L}{L} \quad (3.2)$$

The dimensions of strain are unity, i.e. strain is non dimensional.

### 3.2.3 Hooke's Law

For elastic materials, stress is linearly proportional to strain. Mathematically, this is expressed by Hooke's law, which states:

$$\sigma_a = E\varepsilon_a \quad (3.3)$$

where  $E$  = Young's modulus, also called the modulus of elasticity. Young's modulus is assumed to be constant for a given material. On a typical stress-strain diagram (Fig.3.5), Hooke's law applies only in the elastic stress region, in which the loading is reversible. Beyond the elastic limit (or proportional limit), the material starts to behave irreversibly in the plastic deformation region, in which the stress vs. strain curve deviates from linear, and Hooke's law no longer holds.

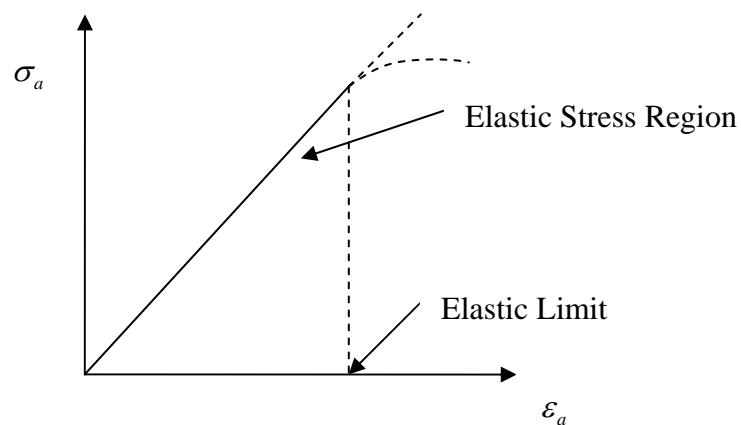


Fig.3.5 Hooke's Law

### 3.2.4 Wire Resistance

The electrical resistance  $R$  of a wire of length  $L$  and cross-sectional area  $A$  is given by:

$$R = \frac{\rho L}{A} \quad (3.4)$$

where  $\rho$  is the resistivity of the wire material.

From Eq.3.4, we can see the electrical resistance of a wire changes with strain. As strain increases, the wire length  $L$  increases, which increases  $R$ . As strain increases, the wire cross-sectional area  $A$  decreases, which increases  $R$ . For most materials, as strain increases, the wire resistivity  $\rho$  also increases, which further increases  $R$ .

The bottom line is that wire resistance increases with strain. In fact, it turns out that at constant temperature, wire resistance increases linearly with strain. Mathematically

$$\frac{dR}{R} = S \varepsilon_a \quad (3.5)$$

where  $S$  is the strain gage factor, defined from the Eq. 3.5.

$$S = \frac{dR/R}{\varepsilon_a} \quad (3.6)$$

S is typically around 2.0 for commercially available strain gages. S is dimensionless.

### 3.2.5 Strain Gage

A strain gage consists of a small diameter wire, usually an etched metal foil, which is attached to a backing plastic material. The wire is looped back and forth several times to create an effectively longer wire. The longer the wire is, the larger the resistance, and the larger the change in resistance with strain.

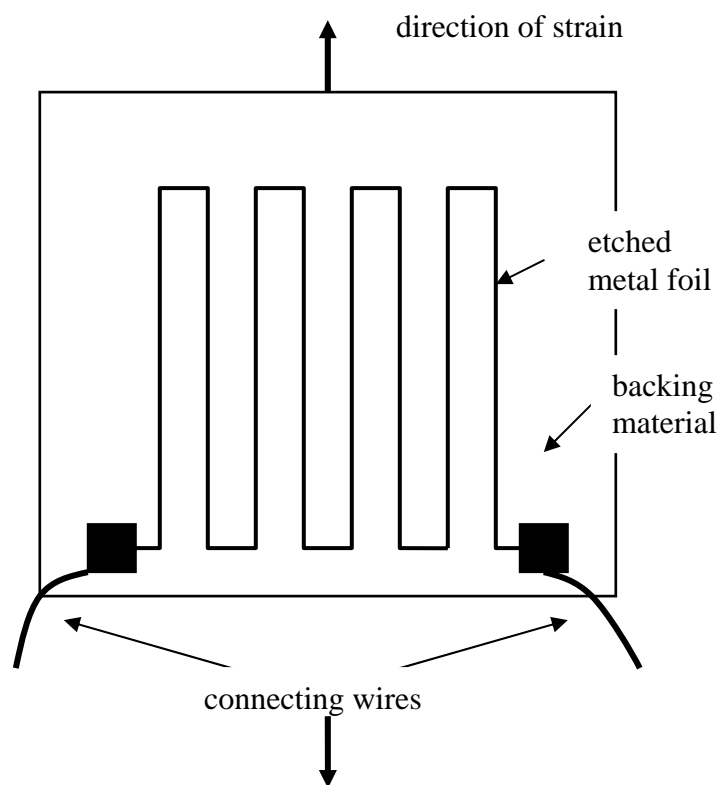


Fig.3.6 Plot of Strain Gauge



On Fig.3.6, four loops of metal foil are shown, providing an effective total foil length  $L$  eight times greater than if a single wire, rather than a looping pattern, was used.

Actual commercially available strain gauges have even more loops than this. The direction of the applied strain is indicated in Fig.3.6. The connecting wires go to an electronic circuit which measures the change in resistance.

### 3.2.6 How to Use Strain Gauge

Consider a beam undergoing axial strain (Fig.3.7). A strain gauge is glued to the surface of the beam, with the long sections of the etched metal foil aligned with the applied axial strain.

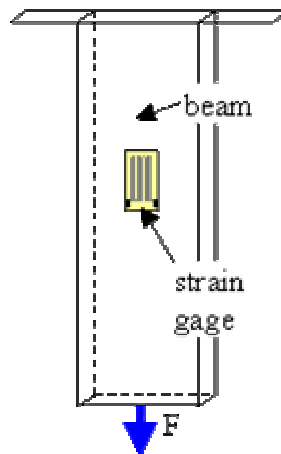


Fig.3.7 Strain Gage in Use

As the surface stretches, the strain gage stretches along with it. The resistance of the strain gage therefore increases with applied strain. If the change in resistance can be measured, the strain gauge provides a method for measuring strain.

### **3.2.7 Strain Gage Thermal Output and Gage Factor Variation with Temperature**

Ideally, a strain gage bonded to a test part would respond only to the applied strain in the part, and be unaffected by other variables in the environment. Unfortunately, the resistance strain gage, in common with all other sensors, is somewhat less than perfect. The electrical resistance of the strain gage varies not only with strain, but with temperature as well. In addition, the relationship between strain and resistance change, the gage factor, itself varies with temperature. Once an installed strain gage is connected to a strain indicator and the instrument balanced, a subsequent change in the temperature of the gage installation will normally produce a resistance change in the gage. This temperature-induced resistance change is independent of, and unrelated to, the stress-induced strain in the test object to which the strain gage is bonded. It is purely due to temperature change, and is thus called the thermal output of the gage.

Thermal output is potentially the most serious error source in the practice of static strain measurement with strain gages. In fact, when measuring strains at temperatures remote from room temperature or from the initial balance temperature of the gage circuit, the error due to thermal output, if not controlled, can be much greater than the magnitude of the strain to be measured. At any temperature, or in any temperature range, this error source requires careful consideration, and it is usually

necessary to either provide compensation for thermal output or correct the strain measurements for its presence.

Thermal output is caused by two concurrent and algebraically additive effects in the strain gage installation. First, the electrical resistivity of the grid conductor is somewhat temperature dependent; and, as a result, the gage resistance varies with temperature. The second contribution to thermal output is due to the differential thermal expansion between the grid conductor and the test part or substrate material to which the gage is bonded. With temperature change, the substrate expands or contracts; and, since the strain gage is firmly bonded to the substrate, the gage grid is forced to undergo the same expansion or contraction. To the extent that the thermal expansion coefficient of the grid differs from that of the substrate, the grid is mechanically strained in conforming to the free expansion or contraction of the substrate. Because the grid is, by design, strain sensitive, the gage exhibits a resistance change proportional to the differential expansion.

Fig.3.8 shows the variation of thermal output with temperature for a variety of strain gage alloys bonded to steel.

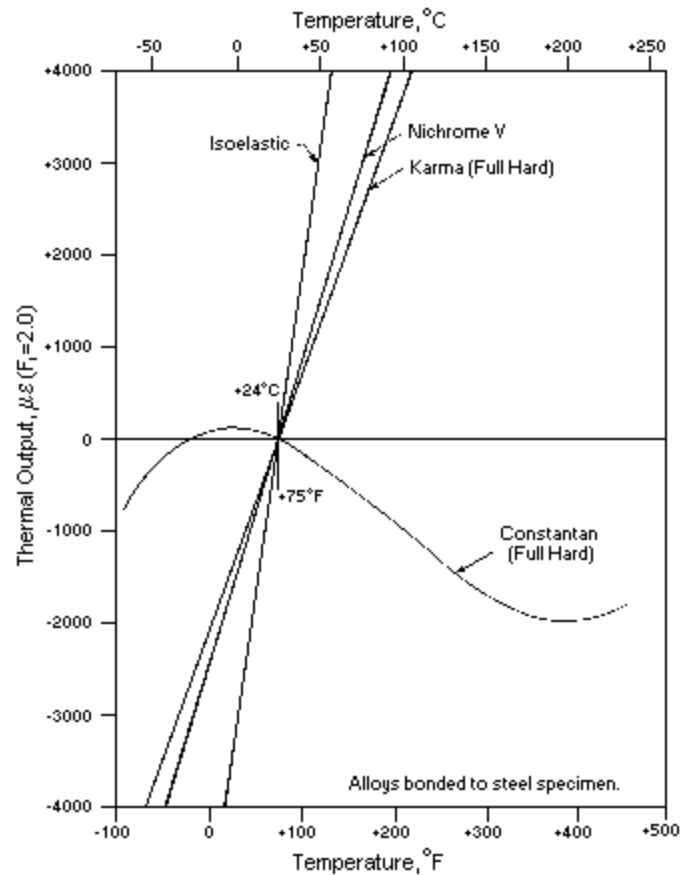


Fig.3.8 Variation of Thermal Output with Temperature for Variety of Strain Gage Alloys Bonded to Steel

As indicated by the Fig.3.8, the errors due to thermal output can become extremely large as temperatures deviate from the arbitrary reference temperature (ordinarily, room temperature) with respect to which the thermal output is measured. The illustration shows distinctly the necessity for compensation or correction if accurate static strain measurements are to be made in an environment involving temperature changes.

The metallurgical properties of certain strain gage alloys like constantan and modified Karma (Micro-Measurements A- and K- alloys, respectively) are such that these alloys can be processed to minimize the thermal output over a wide temperature range when bonded to test materials with thermal expansion coefficients for which they are intended. Strain gages employing these specially processed alloys are referred to as self-temperature-compensated.

Fig.3.9 illustrates the thermal output characteristics of typical A- and K- alloy self-temperature-compensated strain gages. As demonstrated by Fig.3.9, the gages are designed to minimize the thermal output over the temperature range from about 0° to +400° F (-20° to +205° C). When the self-temperature-compensated strain gage is bonded to a material having the thermal expansion coefficient for which the gage is intended, and when operated within the temperature range of effective compensation, strain measurements can often be made without the necessity of correcting for thermal output.

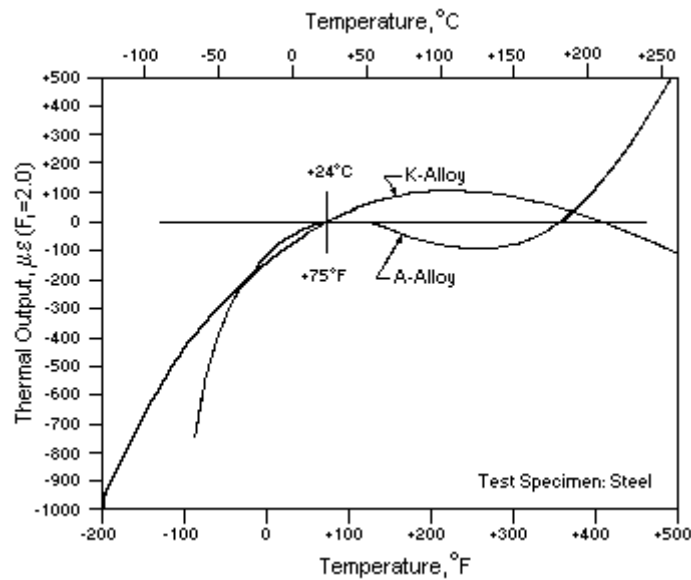


Fig.3.9 Typical Thermal Output Variation with Temperature for Self-Temperature-Compensated Constantan (A-alloy) and Modified Karma (K-alloy) Strain Gages

Depending upon the test temperature and the degree of accuracy required in the strain measurement, it will sometimes be necessary to make corrections for thermal output, even though self-temperature-compensated gages are used. In any case, when making strain measurements at a temperature different from the instrument balance temperature, the indicated strain is equal to the sum of the stress-induced strain in the test object and the thermal output of the gage (plus the strain equivalent of any other resistance changes in the gage circuit). With the thermal output expressed in strain units, correction for this effect is made by simply subtracting the thermal output from the indicated strain.

### 3.2.8 Typical Strain Gauge Values

For strain gauges, there are typical values for resistance, strain gauge factor, and strain, along with the predicted values of change in resistance.

The electrical resistance,  $R$ , of a strain gauge is typically either  $120\Omega$  or  $350\Omega$ . The most widely used commercially available strain gauges are  $120\Omega$ . The strain gauge factor,  $S$ , of the metal foil used in strain gauges is typically around 2.0. In typical engineering applications with metal beams, axial strain  $\varepsilon_a$  is in the range of  $10^{-6}$  to  $10^{-3}$ .

For a typical  $120\Omega$  strain gauge, the change in resistance expressed as a ratio with  $R$  is  $dR/R = 2 \times 10^{-6}$  to  $2 \times 10^{-3}$ .

The main problem when working with strain gauges is one cannot simply stick in an ohm meter to measure the change in resistance, because  $dR/R$  is so small. Most ohm meters do not have sufficient resolution to measure changes in resistance that are 3 to 6 orders of magnitude smaller than the resistance itself.

### 3.3 Wheatstone Bridge

Wheatstone bridge is the circuit to measure very small changes in resistance. Based on the number of strain gauges in the circuit, Wheatstone bridge can be classified into quarter bridge, half bridge and full bridge.

#### 3.3.1 Quarter Bridge

In circuit showed in Fig.3.10, to measure strain, one of the resistors  $R_3$  is replaced by the strain gage. With only one out of the four available resistors substituted by a strain gage, the circuit is called a quarter bridge circuit.

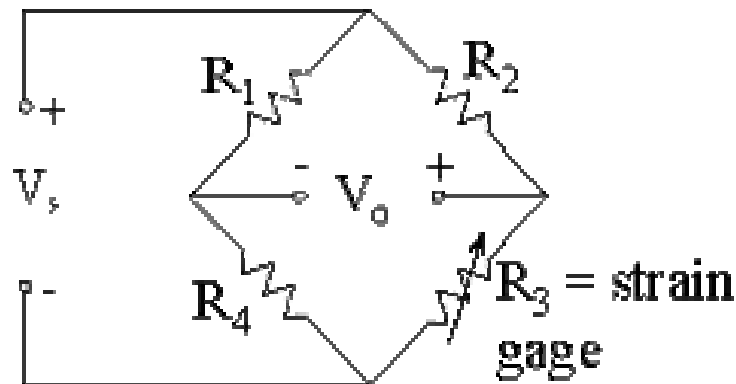


Fig.3.10 Quarter Bridge Circuit

The output voltage  $V_o$  can be calculated from Ohm's law and expressed as Eq.3.7.



$$V_o = V_s \frac{R_3 R_1 - R_4 R_2}{(R_2 + R_3)(R_1 + R_4)} \quad (3.7)$$

In normal operation, the Wheatstone bridge is initially balanced. Suppose strain is applied to the strain gage, such that its resistance changes by some small amount  $dR_3$ , i.e.  $R_3$  changes from  $R_{3i}$  to  $R_{3i} + dR_3$ . Under this condition the bridge is unbalanced, and the resulting output voltage  $V_o$  will not be zero, but can be calculated as follows:

$$V_o = V_s \frac{(R_{3i} + dR_3)R_1 - R_4 R_2}{(R_2 + R_{3i} + dR_3)(R_1 + R_4)} \approx \frac{dR_3 R_1}{(R_2 + R_{3i})(R_1 + R_4)} V_s \quad (3.8)$$

The numerator is simplified by invoking the initial conditions  $R_{3i}R_1 - R_4R_2 = 0$ . The denominator is simplified by recognizing that the resistance of a strain gage changes very little as strain is added, i.e.  $dR_3 \ll R_{3i}$ .

From Eq.3.6, we can find that change in resistance of a strain gage is a function of axial strain, resistance, and strain gage factor. So we can get

$$dR_3 = S \varepsilon_a R_{3i} \quad (3.9)$$

Note that  $R_{3i}$  is the initial resistance of the strain gage. After applying Eq.3.9 to Eq.3.8, after some algebra, we can get:

$$\varepsilon_a = \frac{V_o}{V_s} \frac{1}{S} \frac{(R_2 + R_{3i})^2}{R_2 R_{3i}} \quad (3.10)$$

Furthermore, if  $R_2 = R_{3i}$ , the above equation can be reduced to

$$\varepsilon_a = 4 \frac{V_o}{V_s} \frac{1}{S} \quad (3.11)$$

The significance of the above result is: if supply voltage  $V_s$  and strain gage factor  $S$  are constants, axial strain at the location of the strain gage is a linear function of the output voltage from the Wheatstone bridge circuit. Even more significantly, for known values of  $S$  and  $V_s$ , the actual value of the strain can be calculated from the above equation after measurement of output voltage  $V_o$ .

### 3.3.2 Half Bridge

If two strain gages are put into the Wheatstone bridge circuit, as in Fig.3.11, since half of the four available resistors in the bridge are strain gages, this is called a half bridge circuit.

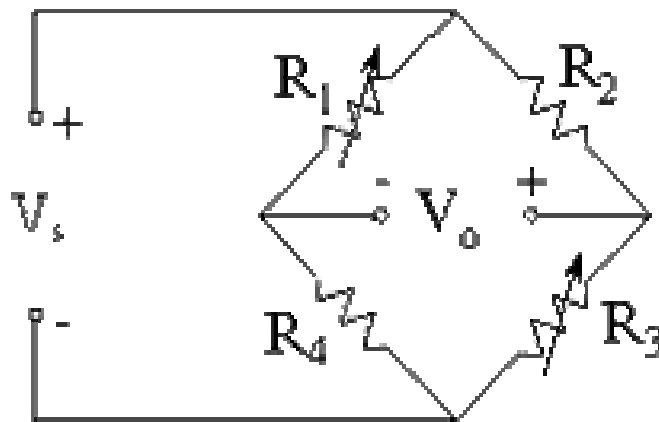


Fig.3.11 Half Wheatstone Bridge

After some algebra, assuming that both strain gage resistances change identically as the strain is applied, it can be shown that

$$\varepsilon_a = \frac{V_o}{V_s} \frac{1}{2S} \frac{(R_{2i} + R_{3i})^2}{R_{2i}R_{3i}} \quad (3.12)$$

If all the resistors are initially the same, this reduces to

$$\varepsilon_a = 2 \frac{V_o}{V_s} \frac{1}{S} \quad (3.13)$$

In general, for any system, sensitivity is defined as the ratio of output to input. In this case, the output is the voltage  $V_o$ , and the input is the axial strain being measured. Compared to the quarter bridge circuit, the half bridge circuit yields twice the output voltage for a given strain.

One can say, alternately, that the sensitivity of the circuit has improved by a factor of two. One might ask why  $R_1$ , rather than  $R_2$  or  $R_4$  was chosen as the resistor to replace the second strain gage. The reason why only  $R_1$  can be used for the second strain gage is because its strain is of the same sign as that of  $R_3$ .

To prove the above statement, suppose all four resistors are strain gages with initial values  $R_{1i}$ ,  $R_{2i}$ , etc. The corresponding changes in resistance due to applied strain are  $dR_1$ ,  $dR_2$ , etc. Through application of Ohm's law, it can be shown that the output voltage varies as follows:

$$\frac{V_o}{V_s} = \frac{R_{2i}R_{3i}}{(R_{2i} + R_{3i})^2} \left( \frac{dR_1}{R_{1i}} - \frac{dR_2}{R_{2i}} + \frac{dR_3}{R_{3i}} - \frac{dR_4}{R_{4i}} \right) \quad (3.14)$$

As can be seen from Eq.3.14, the terms with  $dR_1$  and  $dR_3$  are of positive sign, and therefore contribute to a positive output voltage as strain is increased. However, the terms with  $dR_2$  and  $dR_4$  are of negative sign, and therefore contribute to a negative output voltage as strain is increased.

If both strain gages in half Wheatstone bridge measure strain of the same sign, it is appropriate to choose only  $R_1$  for the second strain gage. If  $R_2$  or  $R_4$  had been chosen instead, the output voltage would not change at all as strain was increased, because of the change in resistance of the two strain gages would cancel each other out.

### 3.3.3 Full Bridge

One can actually substitute strain gages for all four resistors in a Wheatstone bridge. The result is called a full bridge Wheatstone bridge. As shown in Fig.3.12.

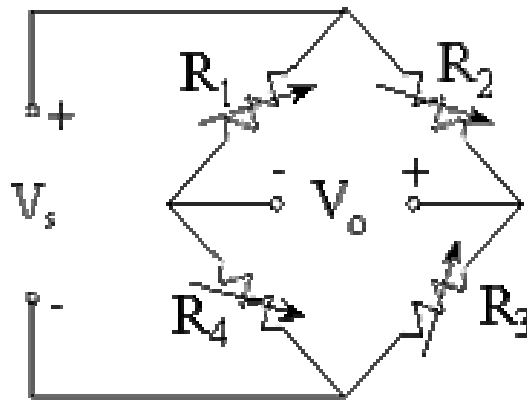


Fig.3.12 Full Bridge Wheatstone Bridge

If the wiring is done properly (e.g.  $R_1$  and  $R_3$  have positive strain, while  $R_2$  and  $R_4$  have negative strain), the sensitivity of the full bridge circuit is four times that of a quarter bridge circuit,

$$\varepsilon_a = \frac{V_o}{V_s} \frac{1}{S} \quad (3.15)$$

In general, if  $n$  is defined as the number of active gages in the Wheatstone bridge, then the strain can be generalized to:

$$\varepsilon_a = \frac{V_o}{V_s} \frac{4}{n} \frac{1}{S} \quad (3.16)$$

It is not always necessary to initially balance the bridge. In other words, suppose there is some initial non-zero value of bridge output voltage, namely  $V_{oref}$ . This voltage represents the reference output voltage at some initial conditions of the experiment, which may not necessarily even be zero strain. One can still calculate the strain by using the output voltage difference rather than the output voltage itself, as follows:

$$\varepsilon_a = \frac{(V_o - V_{oref})}{V_s} \frac{4}{n} \frac{1}{S} \quad (3.17)$$

### **3.4 Components of BCD**

BCD consists of many components. The most important components are listed as below.

#### **3.4.1 Strain Gauge**

The strain gauges glued on top of BCD are CEA-06-125UW-350 gauges manufactured by Micro-Measurements division of Measurements Group, Inc. The CEA-06-125UW-350 gauge is a general-purpose constantan strain gauges widely used in experimental stress analysis. The gauge is supplied with a fully encapsulated grid and exposed copper-coated integral solder tabs. The general information of the strain gauges on BCD is listed in Table 3.1 ([www.vishay.com](http://www.vishay.com)). The dimensions of the strain gauges are shown in Fig.3.13 and Table 3.2.

Table 3.1 General Information of CEA-06-125UW-350 Strain Gauges

Temperature Range	-100° to +350° F (-75° to +175° C) for continuous use in static measurements
Strain Limits	Approximately 5%
Fatigue Life	10 <sup>5</sup> cycles at $\pm 1500 \mu m / m$
Cements	Micro-Measurements M-Bond AE-10/15, M-Bond GA-2, M-Bond 600 and M-Bond 610 are excellent
Solder	M-Line solder 361A (63-37) tin-lead solder when temperature not exceeds +300° F (+150° C). M-Line solder (95-5) tin-antimony is satisfactory to +400° F (+205° C).



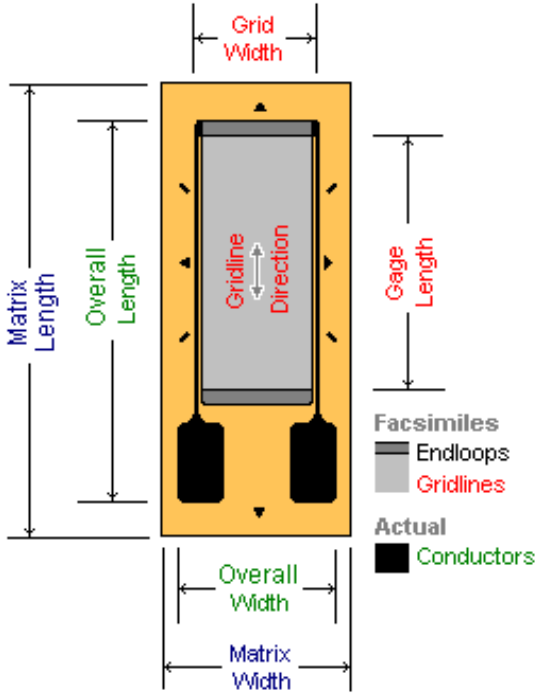


Fig.3.13 Dimensions of Gauge

Table 3.2 Dimensions of CEA-06-125UW-350 Gauge

Dimensions	in	mm
Gage Length	0.125	3.18
Overall Length	0.325	8.26
Grid Width	0.180	4.57
Overall Width	0.180	4.57
Matrix Length	0.42	10.7
Matrix Width	0.27	6.9

As an aid to the user in correcting for temperature dependent properties, the technical data sheet in each package of Micro-Measurements A- and K- alloy strain gages includes a graph showing the thermal output and gage-factor variation with temperature. Fig.3.14 is the graph supplied with the gages. In addition to plots of thermal output and gage factor variation, polynomial equations are provided in both Fahrenheit and Celsius units for the thermal output curve. Also given on the graph are two other important items of information: (1) the lot number of the strain gages, and (2) the test material used in measuring the thermal output characteristics. It should be noted that the thermal output data are specifically applicable to only gages of the designated lot number and applied to the same test material.

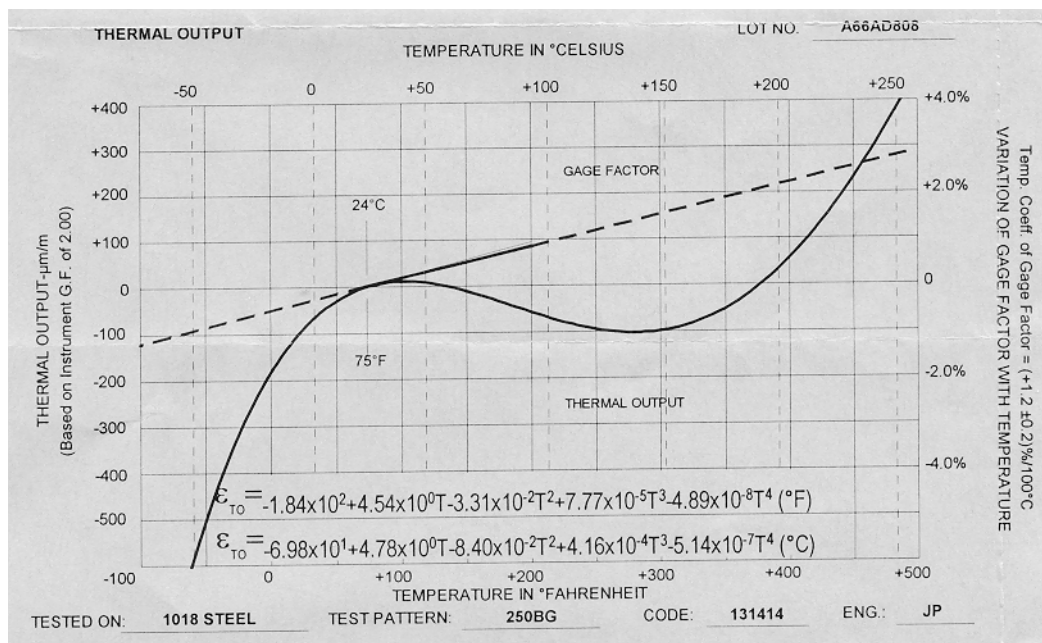


Fig.3.14 Data Curve of Self-Temperature Compensation

### 3.4.2 Wheatstone Bridge in BCD

The Wheatstone bridge in BCD is the so-called “Double Half Bridge” because four strain gauges are put into two arms of the circuit. Four resistors are also put into the other two arms to constitute the bridge. The output of the bridge will be the sum of all the strains happened on the four strain gauges. There are two such bridges in BCD. One is to measure the radial strain on top of plate (Fig.3.15). The other is to measure the hoop strain on the plate (Fig.3.16).

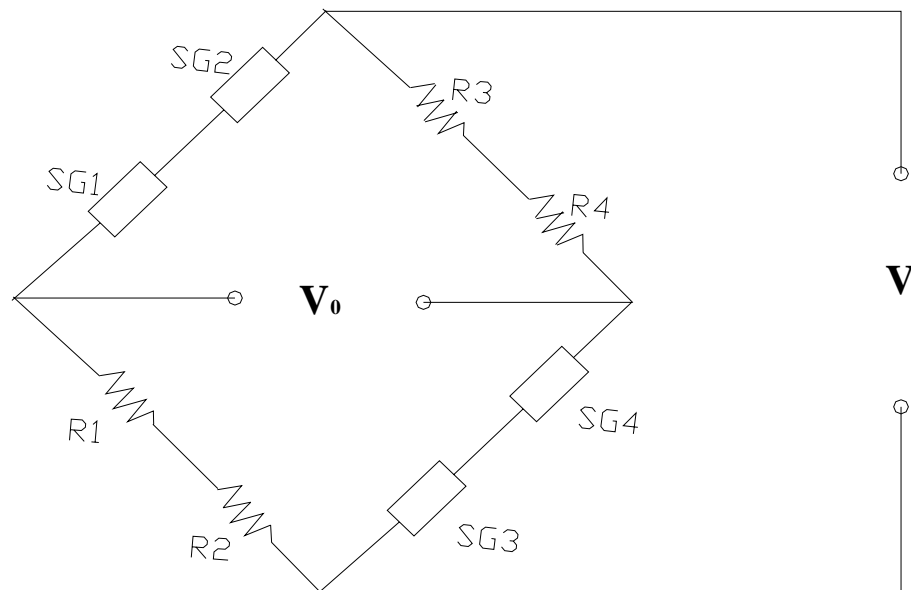


Fig.3.15 Double Half Bridge for Strain Gauges in Radial Direction

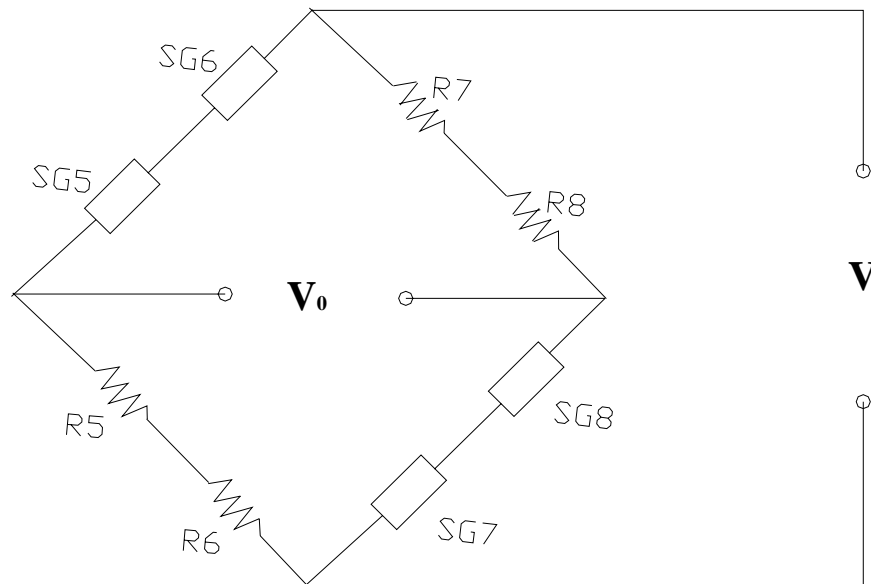


Fig.3.16 Double Half Bridge for Strain Gauges in Hoop Direction

### 3.4.3 Bridge-Completion Resistors

There are eight bridge-completion resistors in the Wheatstone bridge of BCD. Their order code is S-350-01. Each one has 350.0 ohms resistance with 0.01% tolerance. The specification of S-350-01 resistor is in Table 3.3 ([www.vishay.com](http://www.vishay.com)).

Table 3.3 Specification of S-350-01 Resistors

Size	0.295×0.320×0.10 in (7.5×8.1×2.5mm)
Temperature Coefficient	±0.6 ppm/°F ; 32° to 140° F (±1 ppm/°C ; 0° to 60° C)
Stability	25 ppm/year maximum drift
Wattage	0.3 at 75° F (24° C)
Leadwires	22 AWG-tinned copper

#### 3.4.4 Battery

The power of the BCD is from 10 Dantona D-4400 high capacity rechargeable batteries. The voltage for each Ni-cad battery is 1.2V and the capacity is 4400mAh. The total voltage is 12 V and a DC-DC converter inside BCD converts the voltage for various electrical components. The battery is 34mm in diameter and 61mm in height. More details about the battery can get from Dantona's website (<http://www.dantona.com/handbook.htm>).

### 3.4.5 Charger

The Maha MH-C777PLUS-II universal charger and analyzer from POWEREX company is used to charge the battery in BCD. The diagram of the charger is shown in Fig.3.17. The specification for MH-C777 PLUS-II universal charger is listed in Table 3.4.

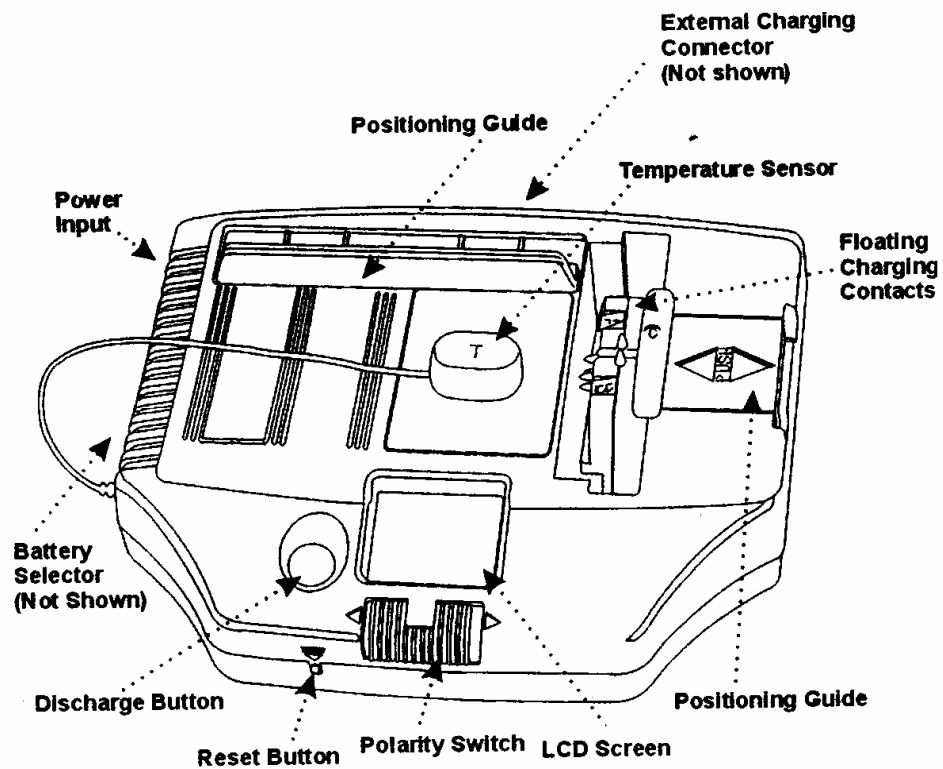


Fig.3.17 Diagram of MH-C777PLUS-II Universal Charger

Table 3.4 Specification of MH-C777 PLUS-II Charger  
(from User's Manual of Powerex Company)

Detection	Negative Delta V, Zero Delta V, and Max. Temperature
Chemistry Supported	Lithium Ion, Nickel Metal Hydride, Nickel Cadmium
Voltage Supported	1.2V to 14.4V (1 to 12 cells) for NiMH & NiCD 3.6V to 14.4V (1 to 4 cells) for Lithium Ion
Rapid Charge Current	800 mAh +/-50mAh for NiMH & NiCD 400 mAh max for Lithium Ion
Trickle Charge Current	70 mA
Discharge Current	300mA +/-50mA
Safety Timer	13 hours
Included Adapter	Switching adapter 80V-240V AC Autoswitch to 24 VDC 0.83A
Capacity Accuracy	+/- 5%
Voltage Accuracy	+/-0.3V

When using MH-C777PLUS-II Universal Charger to charge the BCD, just simply connect the BCD to the charger and a brief beep will be heard. The charger is a microprocessor driven unit that will automatically terminate rapid charging and enter a gentle slow trickle charging when the battery pack becomes fully charged. The charger has a built-in safety timer that will terminate the charging process automatically after 13 hours of charging regardless of battery condition. Based on previous experiences, after one full charge, the BCD can work properly at least for three months.

#### **3.4.6 Load Cell**

A load cell is instrumented in BCD to measure the applied load. The load cell is a tension and compression load cell manufactured by Lebow Associates, Inc. The full capacity of the load cell is 500 lbs.



## CHAPTER IV

### PLATE THEORY AND NUMERICAL SIMULATION OF BCD

#### 4.1 Plate Theory

Elastic plates are widely used in the engineering field. The word “plate” refers to solid bodies that are bounded by two parallel planes whose lateral dimensions are large compared with the separation between them. When a plate is subjected to forces applied in a direction normal to its own plane, the plate bends and is said to be in a state of flexure.

There are two plate theories. One is classical plate theory which is an extension of the Euler-Bernouli beam theory to plate, and is known as the Kirchhoff plate theory. The other is first-order shear deformation theory which is an extension of the Timoshenko beam theory, and is known as the Henchy-Mindlin plate theory.

The classical plate theory is one which the displacement field is selected so as to satisfy the following three assumptions:

- 1 Straight lines perpendicular to the mid-surface before deformation remain straight after deformation.
- 2 The transverse normals do not experience elongation.
- 3 The transverse normals rotate such that they remain perpendicular to the mid-surface after deformation.

Assumptions 1 and 2 imply that the thickness normal strain is zero and the third assumption results in zero transverse shear strains.

The Mindlin plate theory has the same assumptions as the classical plate theory except that the transverse normals to the mid-surface before deformation remain straight but not necessarily normal to the mid-surface after deformation. This assumption results in a constant state of transverse shear strains through thickness and zero transverse normal strains. The most significant difference between these two theories is the effect of including transverse shear deformation on the predicted deflections. Therefore, the transverse shear strains are not zero.

#### **4.1.1 Plate Classification**

A plate resists vertical load by means of bending. According to Eduard and Theodor's *Thin Plates and Shells* (2001), plate can be classified into three groups according to the ratio  $a/h$ , where  $a$  is the typical dimension of plate in a plane and  $h$  is the plate thickness. These groups are:

##### 1. Thick plate

When  $a/h \leq 8 \dots 10$ , plate is classified as thick plate. The analysis of such bodies includes all the components of stresses, strains and displacements as for solid bodies using the general equations of three-dimensional elasticity.

## 2. Membrane

When  $a/h \geq 80 \dots 100$ , plate is referred to as membrane and it is devoid of flexural rigidity. Membranes carry the lateral loads by axial tensile forces  $N$  (and shear forces) acting in the plate middle surface. These forces are called membrane forces. They produce projection on a vertical axis and thus balance a lateral load applied to the plate.

## 3. Thin plate

The most extensive group represents an intermediate type of plate, so-called thin plate with  $8 \dots 10 \leq a/h \leq 80 \dots 100$ . Depending on the value of the ratio  $w/h$ , the ratio of the maximum deflection of the plate to its thickness, the part of flexural and membrane forces here may be different. Therefore, this group, in turn, may also be subdivided into two different classes.

### a. Stiff plate.

A plate can be classified as a stiff plate if  $w/h \leq 0.2$ . Stiff plates are flexurally rigid thin plates. They carry loads two dimensionally, mostly by internal bending and twisting moments and by transverse shear forces. The middle plane deformations and the membrane forces are negligible. In engineering practice, the term plate is understood to mean a stiff plate, unless otherwise specified. The concept of stiff plates introduces serious simplifications. The fundamental feature of stiff plates is that the equations of static equilibrium for a plate element may be set up for an original (undeformed) configuration of the plate.

b. Flexible plate.

If the plate deflections are beyond a certain level,  $w/h \geq 0.3$ , then, the lateral deflections will be accompanied by stretching of the middle surface. Such plates are referred to as flexible plates. These plates represent a combination of stiff plates and membranes and carry external loads by the combined action of internal moments, shear forces, and membrane (axial) forces. Such plates, because of their favorable weight-to-load ratio, are widely used by the aerospace industry. When the magnitude of the maximum deflection is considerably greater than the plate thickness, the membrane action predominates. If  $w/h \geq 5$ , the flexural stress can be neglected compared with the membrane stress. Consequently, the load-carrying mechanism of such plates becomes of the membrane type, i.e., the stress is uniformly distributed over the plate thickness.

In BCD, we measure the strain both in radial and hoop directions at the top of the steel plate. So we need to study the plate theory and get the formulas to calculate bending moment, stress and strain on the plate. For circular plate, it is convenient to express the moment and stress in polar coordinates. Fig.4.1 (a) shows the geometrical relations between Cartesian coordinates and polar coordinates. Fig.4.1 (b) gives the bending moments in radial and hoop directions. From Eduard and Theodor's *Thin Plates and Shells* (2001), the bending moment and stress on the circular plate is expressed in the following equations:

$$M_r = -D \left[ \frac{\partial^2 w}{\partial r^2} + \nu \left( \frac{1}{r} \frac{\partial w}{\partial r} + \frac{1}{r^2} \frac{\partial^2 w}{\partial \phi^2} \right) \right] = -D \left( \frac{d^2 w}{dr^2} + \frac{\nu}{r} \frac{dw}{dr} \right) \quad (4.1)$$

$$M_t = -D \left[ \frac{1}{r} \frac{\partial w}{\partial r} + \frac{1}{r^2} \frac{\partial^2 w}{\partial \phi^2} + \nu \frac{\partial^2 w}{\partial r^2} \right] = -D \left( \frac{1}{r} \frac{dw}{dr} + \nu \frac{d^2 w}{dr^2} \right) \quad (4.2)$$

$$M_{rt} = M_{tr} = -D(1-\nu) \left[ \frac{1}{r} \frac{\partial^2 w}{\partial r \partial \phi} - \frac{1}{r^2} \frac{\partial w}{\partial \phi} \right] = 0 \quad (4.3)$$

$M_r$ -Moment per unit length in radial direction

$M_t$ -Moment per unit length in hoop direction

$M_{rt}$ -Twisting moment

w- Settlement of plate

h- Thickness of plate

$\nu$  - Poisson's ratio of plate

E- Elastic modulus of plate

$$D = \frac{Eh^3}{12(1-\nu^2)} = \text{flexural rigidity of plate}$$

The formulas for the stress components are in the following forms:

$$\sigma_r = \frac{12M_r}{h^3} z, \quad \sigma_t = \frac{12M_t}{h^3} z \quad (4.4)$$

z- the distance of the surface of plate to the midplane.

The maximum stresses and maximum strain take place on the surfaces  $z = \pm h/2$ .

$$\varepsilon_{r(\max)} = \pm \frac{6M_r}{Eh^2}, \quad \varepsilon_{t(\max)} = \pm \frac{6M_t}{Eh^2} \tag{4.5}$$

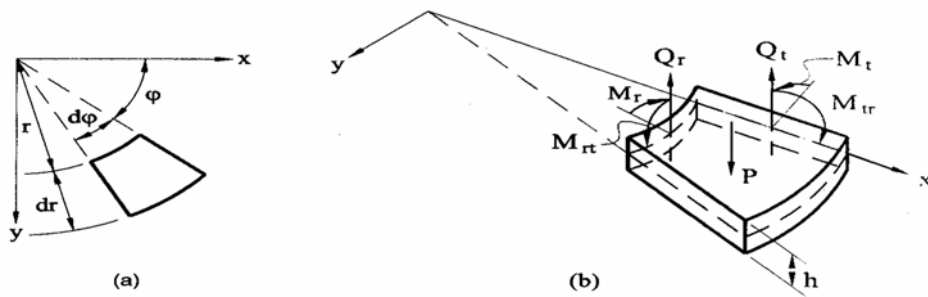


Fig.4.1 Bending Moment of Circular Plate in Polar Coordinate

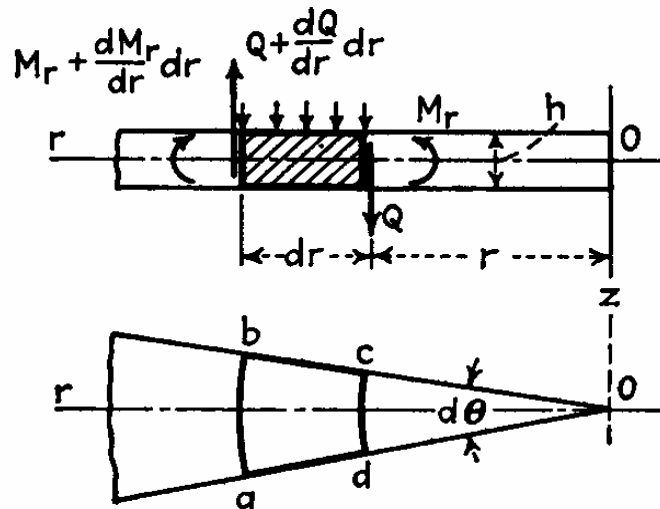


Fig.4.2 Shearing Force of Circular Plate in Polar Coordinate

In Fig.4.2, an element of the plate abcd is cut out from the plate by two cylindrical sections ab and cd and by two diametrical sections ad and bc. The moment acting on the side of cd of the element is  $M_r r d\theta$ , the corresponding moment on the side of ab is  $\left(M_r + \frac{dM_r}{dr} dr\right)(r + dr)d\theta$ . The moments acting on the sides of ad and bc of the element are each  $M_t dr$ , and they give a resultant moment in the plane  $roz$  equal to  $M_t dr d\theta$ .

From symmetry it can be concluded that the shearing forces that may act on bc and ad must vanish but they are usually present on cylindrical sections such as sides cd and ab of the element. Denoting by  $Q$  the shearing force per unit length of the cylindrical section of radius  $r$ , the total shearing force acting on the side cd of the element is  $Qrd\theta$ , and the corresponding force on the side ab is  $\left[Q + \left(\frac{dQ}{dr}\right)dr\right](r + dr)d\theta$ .

Neglecting the small difference between the shearing forces on the two opposite sides of the element, we can state that these forces give a couple in the  $rz$  plane equal to  $Qrd\theta dr$ .

Summing up the all the four moments with proper signs and neglecting the moment due to the external load on the element as a small quantity of higher order, we obtain the following equation of equilibrium of the element abcd:

$$\left(M_r + \frac{dM_r}{dr} dr\right)(r + dr)d\theta - M_r r d\theta - M_t dr d\theta + Qrd\theta dr = 0 \quad (4.6)$$

from which we find, by neglecting a small quantity of higher order,

$$M_r + \frac{dM_r}{dr} r - M_t + Qr = 0 \quad (4.7)$$

Substituting Eqs.4.1 and 4.2 for  $M_r$  and  $M_t$ , Eq.4.7 becomes:

$$\frac{d^3 w}{dr^3} + \frac{1}{r} \frac{d^2 w}{dr^2} - \frac{1}{r^2} \frac{dw}{dr} = \frac{Q}{D} \quad (4.8)$$

In any particular case of a symmetrically loaded circular plate the shearing force  $Q$  can easily be calculated by dividing the load distributed within the circle of radius  $r$  by  $2\pi r$ . The integration of Eq.4.8 is simplified if we put it in the following forms:

$$\frac{d}{dr} \left[ \frac{1}{r} \frac{d}{dr} \left( r \frac{dw}{dr} \right) \right] = \frac{Q}{D} \quad (4.9)$$

If  $Q$  is represented by a function of  $r$ , these equations can be integrated without any difficulty in each particular case.

If the load is represented by distributed load  $q$  over the plate, then

$$Q2\pi r = \int_0^r q2\pi r dr \quad (4.10)$$

Plug Eq.4.10 into Eq.4.9, we obtain:

$$r \frac{d}{dr} \left[ \frac{1}{r} \frac{d}{dr} \left( r \frac{dw}{dr} \right) \right] = \frac{1}{D} \int_0^r q r dr \quad (4.11)$$



Differentiating both sides of Eq.4.11 with respect to  $r$  and dividing by  $r$ , we finally obtain:

$$\frac{1}{r} \frac{d}{dr} \left\{ r \frac{d}{dr} \left[ \frac{1}{r} \frac{d}{dr} \left( r \frac{dw}{dr} \right) \right] \right\} = \frac{q}{D} \quad (4.12)$$

This equation can easily be integrated if the intensity of the load is given as a function of  $r$ .

#### 4.2 Plate on Winkler Foundation

Because the plate of BCD is placed on soil, for simplicity, we can consider circular plates loaded symmetrically with respect to their center and resting on a Winkler-type foundation. The foundation reaction,  $p(r)$ , can be described by

$$p(r) = k \cdot w(r) \quad (4.13)$$

where  $k$  is the subgrade reaction of foundation which is related to soil modulus,

$w$  is the settlement of the plate.

From Timoshenko's *Theory of Plates and Shells* (1987), the governing differential equation of bending of circular plates resting on a Winkler-type foundation is:

$$\left(\frac{d^2}{dr^2} + \frac{1}{r} \frac{d}{dr}\right) \left(\frac{d^2 w}{dr^2} + \frac{1}{r} \frac{dw}{dr}\right) = \frac{1}{D}(q - kw) \quad (4.14)$$

In the particular case of a plate loaded at the center with a load P, introducing the notation:

$$l = \sqrt[4]{\frac{D}{k}} \quad \frac{w}{l} = z \quad \frac{r}{l} = x \quad (4.15)$$

Eq.4.14 becomes:

$$\left(\frac{d^2}{dx^2} + \frac{1}{x} \frac{d}{dx}\right) \left(\frac{d^2 z}{dx^2} + \frac{1}{x} \frac{dz}{dx}\right) + z = 0 \quad (4.16)$$

Using the symbol  $\Delta = \left(\frac{d^2}{dx^2} + \frac{1}{x} \frac{d}{dx}\right)$ , we can write:

$$\Delta \Delta z + z = 0 \quad (4.17)$$

This is a linear differential equation of the fourth order, the general solution of which can be represented in the following form:

$$z = A_1 X_1(x) + A_2 X_2(x) + A_3 X_3(x) + A_4 X_4(x) \quad (4.18)$$

The solution can be expressed in the form of power series as following:

$$\begin{aligned}
z = & A_1 \left( 1 - \frac{x^4}{2^2 \cdot 4^2} + \frac{x^8}{2^2 \cdot 4^2 \cdot 6^2 \cdot 8^2} - \dots \right) + A_2 \left( x^2 - \frac{x^6}{4^2 \cdot 6^2} + \frac{x^{10}}{4^2 \cdot 6^2 \cdot 8^2 \cdot 10^2} - \dots \right) + \\
& A_3 \left[ \left( 1 - \frac{x^4}{2^2 \cdot 4^2} + \frac{x^8}{2^2 \cdot 4^2 \cdot 6^2 \cdot 8^2} - \dots \right) \log x + \frac{3}{128} x^4 - \frac{25}{1,769,472} x^8 + \dots \right] \\
& + A_4 \left[ \left( x^2 - \frac{x^6}{4^2 \cdot 6^2} + \frac{x^{10}}{4^2 \cdot 6^2 \cdot 8^2 \cdot 10^2} - \dots \right) \log x + \frac{5}{3,456} x^6 - \frac{1,540 \cdot 10^{-4}}{442,368} x^{10} + \dots \right]
\end{aligned} \tag{4.19}$$

$A_1, A_2, A_3, A_4$  are constants which can be determined by boundary conditions.

When the edge of a circular plate of radius  $a$  is entirely free, from Eq.4.1 for the radial moments and Eq.4.9 for the radial shear force  $Q_r$ , we can write the boundary condition as:

$$\left( \frac{d^2 w}{dr^2} + \frac{\nu}{r} \frac{dw}{dr} \right)_{r=a} = 0 \tag{4.20}$$

$$\frac{d}{dr} \left( \frac{d^2 w}{dr^2} + \frac{1}{r} \frac{dw}{dr} \right)_{r=a} = 0 \tag{4.21}$$

In addition to these two conditions we have two more conditions that hold at the center of the plate: (1) the deflection at the center of the plate must be finite, (2) the sum of the shearing forces distributed over the lateral surface of an infinitesimal circular cylinder cut out of the plate at its center must balance the concentrated force  $P$ .

From the first of these two conditions, at the center of the plate,  $x=0$ , in Eq.4.19,  $\log(x)$  will be infinite, the constant  $A_3$  must be 0 to keep the deflection be finite.

The second condition gives:

$$\left( \int_0^{2\pi} Q_r r d\theta \right)_{r=\varepsilon} + P = 0 \quad (4.22)$$

By using Eq.4.15,

$$-kl^4 \frac{d}{dr} \left( \frac{d^2 w}{dr^2} + \frac{1}{r} \frac{dw}{dr} \right)_{r=\varepsilon} 2\pi\varepsilon + P = 0 \quad (4.23)$$

where  $\varepsilon$  is the radius of the infinitesimal cylinder. Substituting  $l_z$  for  $w$  in this equation and using expression for  $z$  Eq.4.19, we find that for an infinitely small value of  $x$  equal to  $\varepsilon/l$ , the Eq.4.23 reduces to:

$$-kl^4 \frac{4A_4}{l\varepsilon} 2\pi\varepsilon + P = 0 \quad (4.24)$$

From which we can get:

$$A_4 = \frac{P}{8\pi kl^3} \quad (4.25)$$

Having the values of the constants  $A_3$  and  $A_4$ , the remaining two constants  $A_1$  and  $A_2$  can be found from Eq.4.20. and 4.21. For given dimensions of the plate and given moduli of the plate and of the foundation these equations furnish two linear equations about  $A_1$  and  $A_2$ .  $A_1$  and  $A_2$  can be solved through these two linear equations.

### 4.3 Numerical Simulation of BCD

ABAQUS will be the software chosen for the study because it is a very great three-dimensional package with a wide range of capabilities. To simulate the behavior of BCD, we have used the general finite element program ABAQUS V6.2 installed on the supercomputer at Texas A&M University. The dimensions and parameters of the simulated BCD are shown in Figs. 3.1 and 3.2. The mesh used is shown in Fig. 4.3.

Because of the axisymmetric properties of BCD, in the ABAQUS input file, 4-node axisymmetrical element CAX4 was used to simulate the soil under BCD and the rod above BCD. The plate of BCD is simulated by two-node shell element SAX1. A contact surface is formed between bottom of the plate and top of the soil. The friction coefficient between plate and soil is also determined along this surface. An elastic soil model is used as a first step. Elastic plastic soil model is also used.

After running ABAQUS, we can output the strains, bending moments and curvatures in both radial and hoop directions on top of plate.

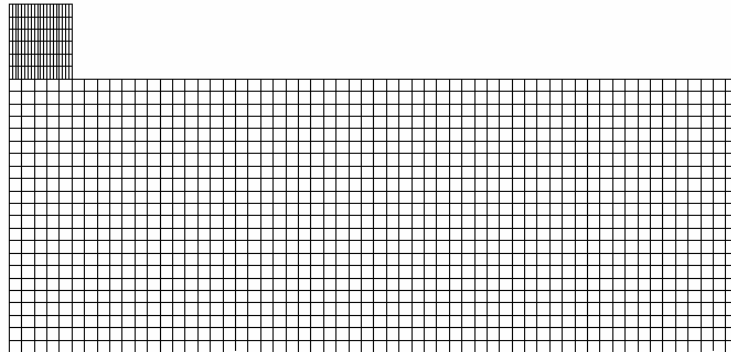


Fig.4.3 Part of Mesh of BCD in ABAQUS Simulation

Many engineering problems involve contact between two or more components. In these problems a force normal to the contacting surfaces acts on the two bodies when they touch each other. If there is friction between the surfaces, shear forces may be created that resist the tangential motion (sliding) of the bodies. The general aim of contact simulations is to identify the areas on the surfaces that are in contact and to calculate the contact pressures generated.

In a finite element analysis contact conditions are a special class of discontinuous constraint, allowing forces to be transmitted from one part of the model to another. The constraint is discontinuous because it is applied only when the two surfaces are in contact. When the two surfaces separate, no constraint is applied. The analysis has to be able to detect when two surfaces are in contact and apply the contact constraints

accordingly. Similarly, the analysis must be able to detect when two surfaces separate and remove the contact constraints.

In an ABAQUS contact simulation, the first step in defining contact between two structures in ABAQUS is to create surfaces using the “SURFACE” option. Next, pairs of surfaces that may contact each other are created using the “CONTACT PAIR” option. Each contact pair refers to a surface interaction definition, which is created with the “SURFACE INTERACTION” option.

ABAQUS uses a pure master-slave contact algorithm: nodes on one surface (the slave) cannot penetrate the segments that make up the other surface (the master). The algorithm places no restriction on the master surface; it can penetrate the slave surface between slave nodes. The order of the two surfaces given on the “CONTACT PAIR” option is important because it determines which surface is the master surface and which is the slave surface. The first surface is taken to be the slave surface, and the second is the master surface. In BCD simulation, the surface of bottom of plate is the master surface, and the surface of top of soil is slave surface.

Finally, the constitutive models governing the interactions between the various surfaces must be defined. These surface interaction definitions include behavior such as friction.

A separation between plate and soil was detected after using contact element (Fig.4.4). The relationship between plate thickness and soil modulus when soil and plate start separating is listed in Table 4.1.

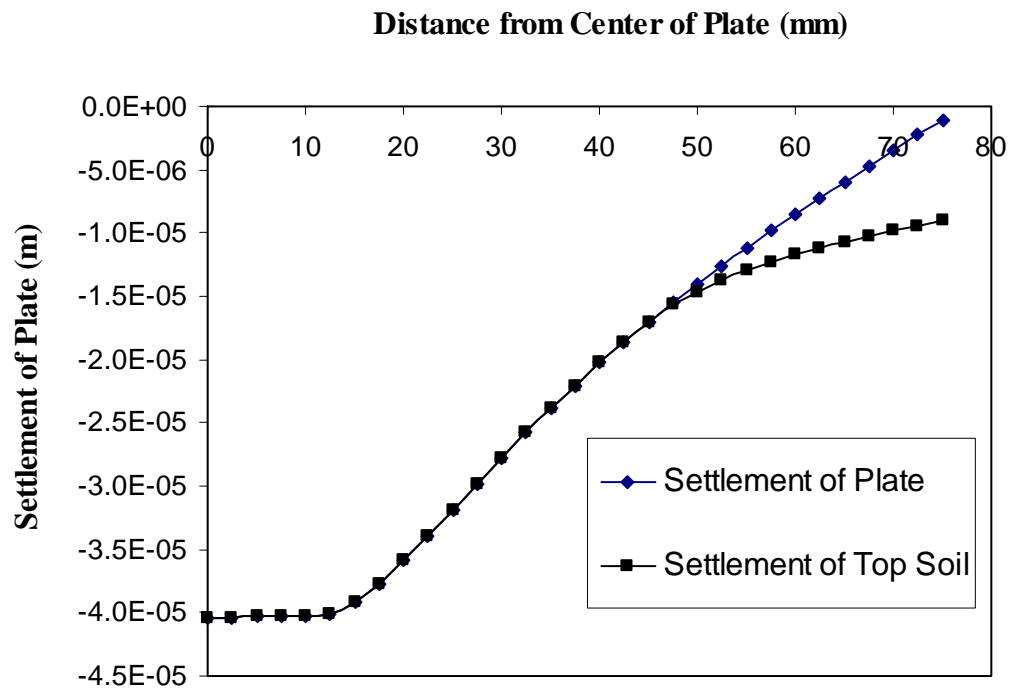


Fig.4.4 Separation between Plate and Soil

Table 4.1 Thickness of Plate and Corresponding Moduli when Plate and Soil Separates

<b>Thickness of Plate (mm)</b>	2.5	3.175	4	4.75	5
<b>Soil Modulus when Soil and Plate Start Separating (MPa)</b>	30	60	100	160	200



As we can see from Table 4.1, for certain plate thickness, there is a soil modulus at which the plate and soil start separating. Fig.4.4 is for 3.175 mm plate on 100MPa soil. The actual contact radius is about 45mm, not 75 mm.

#### **4.4 Comparison between Plate Theory and Numerical Simulation**

We have both finite element method and plate theory to study the problem of plate on elastic foundation. From 4.2, the procedure of solving the problem by using plate theory is very complicated and needs a lot of hand calculations. The plate theory is based on the assumption that soil is Winkler foundation which is not the case in the real world and the plate theory can't predict the separation between plate and soil. Furthermore, the results from the plate theory just give the settlement of plate and second derivation of settlement is needed to calculate the bending moment of plate. While the ABAQUS simulation can conveniently give the settlement of plate, bending moments and strains in radial and hoop directions in the output files. Before we use ABAQUS to simulate BCD on soil, we need to validate the simulation results by comparing the plate theory and ABAQUS simulation result. Fig.4.5 is an example plot in which a 2.5mm thick steel plate with 150 mm in diameter is being applied a 500 N load at the center of plate.

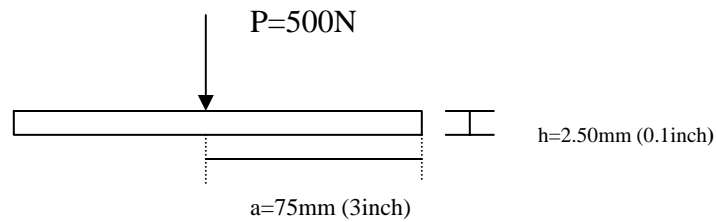


Fig.4.5 Example Plot of Plate on Elastic Foundation

The parameters in the calculation are listed below:

D=Flexural rigidity of plate

$E_p$ =Modulus of plate (2.0E5 MPa)

$E_s$ =Modulus of soil under plate (935.1 kPa)

$\nu$ =Poisson Ratio (0.3)

$h$ =Thickness of plate

$B$ =Diameter of the plate

$A_1, A_2, A_3$ =Parameters in the equation of deflection

$r$ =Radius of the plate

$l$ =Introduced length

$w$ =Deflection of plate

$x$ =Dimensionless length of plate,  $x = r/l$

$z$ =Dimensionless deflection of plate,  $z = w/l$

The flexural rigidity of plate:

$$D = \frac{E_p h^3}{12(1-\nu^2)} = 286.2 \text{ Pa}\cdot\text{m}^3 \quad (4.26)$$

Using the relationship between modulus E and subgrade reaction k:

$$k = \frac{4E_s}{(1-\nu^2)\pi B} = 9045.3 \text{ kPa/m} \quad (4.27)$$

$$l = \sqrt[4]{\frac{D}{k}} = 0.075 \text{ m} = a \quad (4.28)$$

$$A_4 = \frac{P}{8\pi k l^3} = \frac{500 \text{ N}}{8 \times \pi \times 9045.3 \text{ kPa/m} \times 0.075^3 \text{ m}^3} = 5.213 \times 10^{-3} \quad (4.29)$$

At the boundary of the plate,  $x = r/l = 1.0$ . Using Eq.4.19, Eqs.4.20 and 4.21 reduces to:

$$0.5A_1 + 0.25A_2 = 4.062A_4 \quad (4.30)$$

$$0.687A_1 - 8.483A_2 = 11.09A_4$$

These equations give:

$$A_1 = 8.436A_4 = 43.98 \times 10^{-3} \quad (4.31)$$

$$A_2 = -0.624A_4 = -3.253 \times 10^{-3}$$

The deflection of plate:

$$w = lz = 0.075 \times z$$

$$z = 43.98 \times 10^{-3} \left( 1 - \frac{x^4}{2^2 \cdot 4^2} + \frac{x^8}{2^2 \cdot 4^2 \cdot 6^2 \cdot 8^2} - \dots \right) - 3.253 \times 10^{-3} \left( x^2 - \frac{x^6}{4^2 \cdot 6^2} + \frac{x^{10}}{4^2 \cdot 6^2 \cdot 8^2 \cdot 10^2} - \dots \right) + 5.213 \times 10^{-3} \left[ \left( x^2 - \frac{x^6}{4^2 \cdot 6^2} + \frac{x^{10}}{4^2 \cdot 6^2 \cdot 8^2 \cdot 10^2} - \dots \right) \log x + \frac{5}{3,456} x^6 - \frac{1,540 \cdot 10^{-4}}{442,368} x^{10} + \dots \right] \quad (4.32)$$

For estimation, if we just use the first term including x, we can get:

$$w = lz = 0.075 \left\{ 43.98 \times 10^{-3} \left( 1 - \frac{x^4}{2^2 \times 4^2} \right) - 3.253 \times 10^{-3} x^2 + 5.213 \times 10^{-3} [\log(x) \times x^2] \right\} \quad (4.33)$$

At center of the plate,  $x=0$ , the deflection  $w=3.2985 \times 10^{-3}$  m

At edge of plate,  $x = r/l=1$ , the deflection  $w=3.00 \times 10^{-3}$  m

Because the more terms used in the plate theory calculation, the more accurate the result will be. In the comparison between numerical simulation and plate theory, three x terms of the theoretical solution Eq.4.32 was used.

Because the plate is laid on Winkler foundation in the plate theory calculation, the soil under plate is simulated by Spring Element in the ABAQUS numerical simulations. In ABAQUS, Spring Elements are used to model actual physical springs as well as

idealizations of axial or torsional components. Element SPRING2 was used between nodes of plate and soil, acting in a fixed direction. The spring behavior can be linear or nonlinear. The relative displacement across a SPRING2 element is the difference between the  $i$ th component of displacement of the spring's first node and the  $j$ th component of displacement of the spring's second node. In the BCD ABAQUS simulation, SPRING element is linear and the stiffness of SPRING element is determined by multiplying area corresponding to each spring to the subgrade reaction  $k$  of the soil from Eq.4.27.

The comparison of the plate settlement and bending moment are shown in Fig.4.6 and Fig.4.7. The ABAQUS simulation result for plate on elastic half space is also included. From Fig.4.6 and Fig.4.7, we can see that the ABAQUS simulation on Winkler foundation is much closer to plate theory result than simulation on elastic half space. This is because the plate theory is based on the assumption of soil as Winkler foundation. 11, 31 and 61 spring elements were used in the simulations and the more spring element used, the more accurate the result will be. The plots for 11 and 31 Spring Elements are shown in Figs.4.8 and 4.9. Because bending moment is the second derivative of settlement, the errors in the calculation of settlement will become larger in the calculation of bending moment. Fig.4.6 gives a better comparison than Fig.4.7.

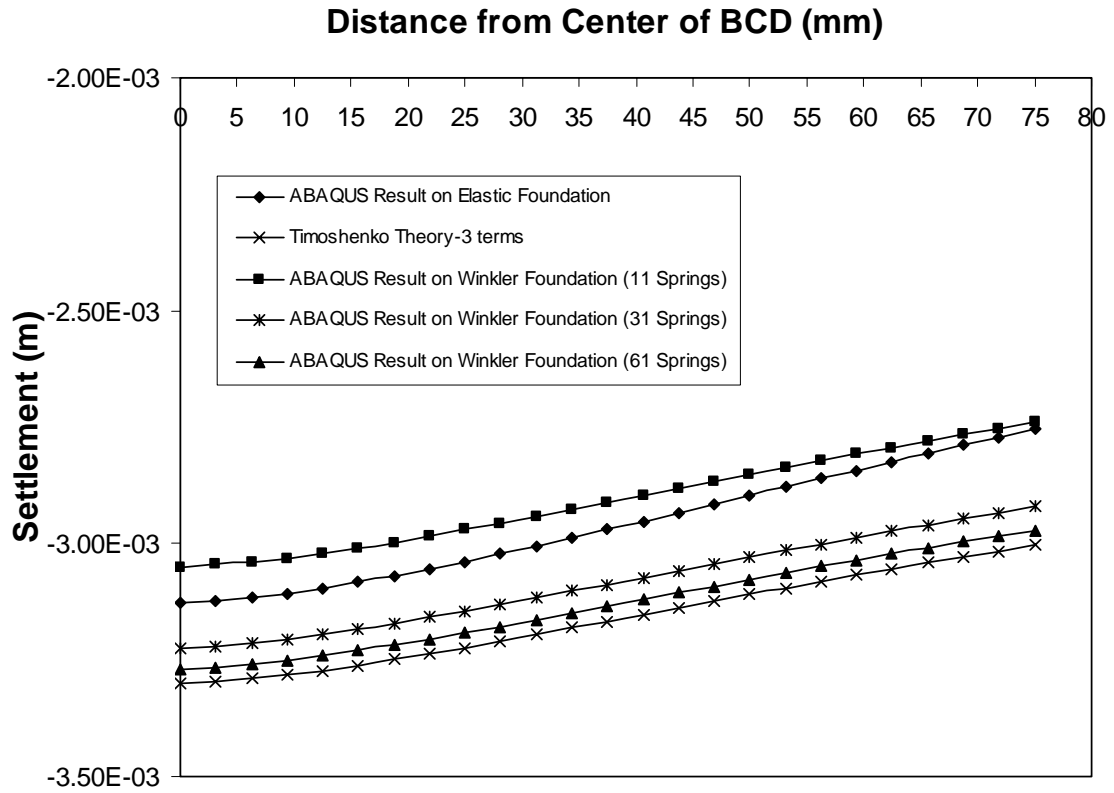


Fig.4.6 Comparison of Settlement of Plate between ABAQUS Simulation and Plate Theory

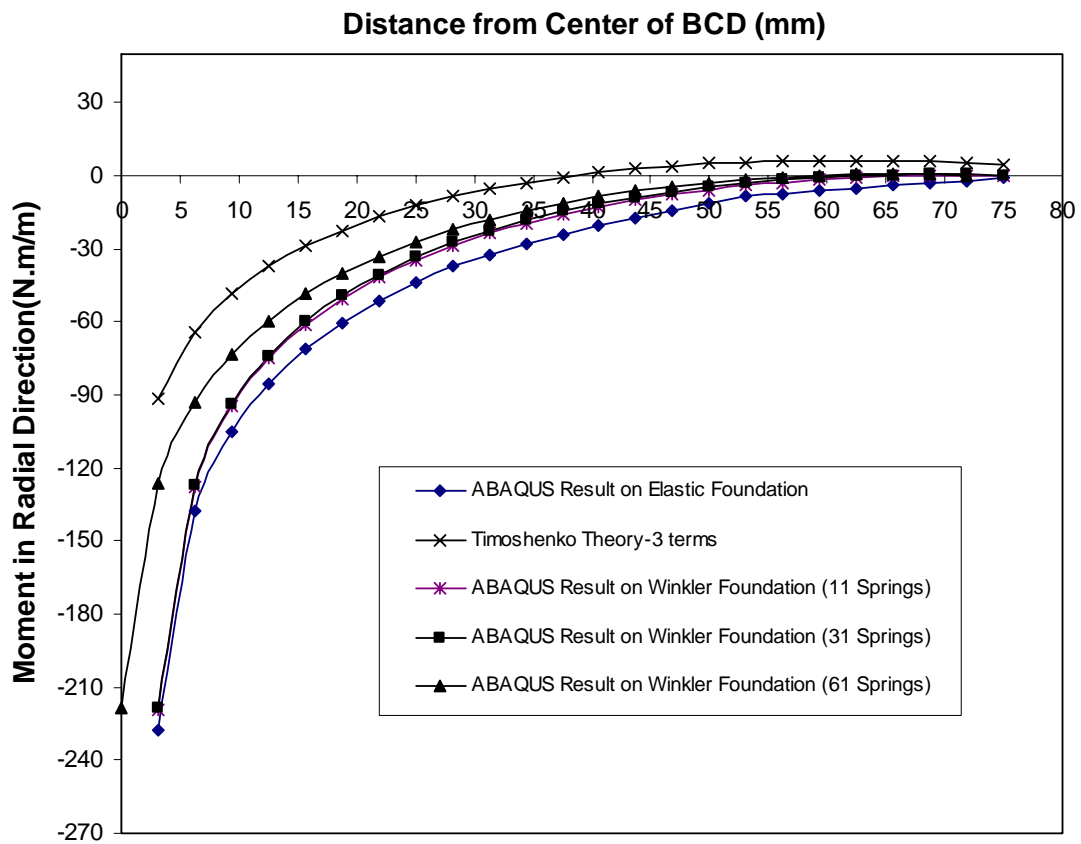


Fig.4.7 Comparison of Bending Moment between ABAQUS Simulation and Plate Theory

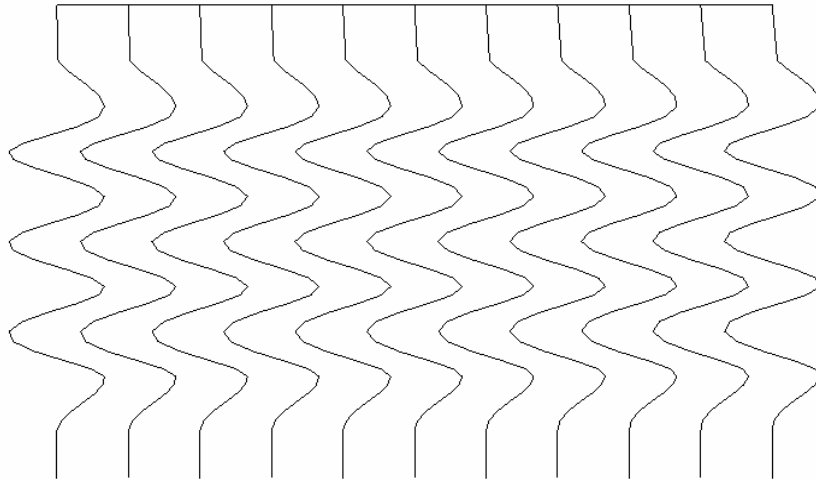


Fig. 4.8 Winkler Foundation with 11 Springs

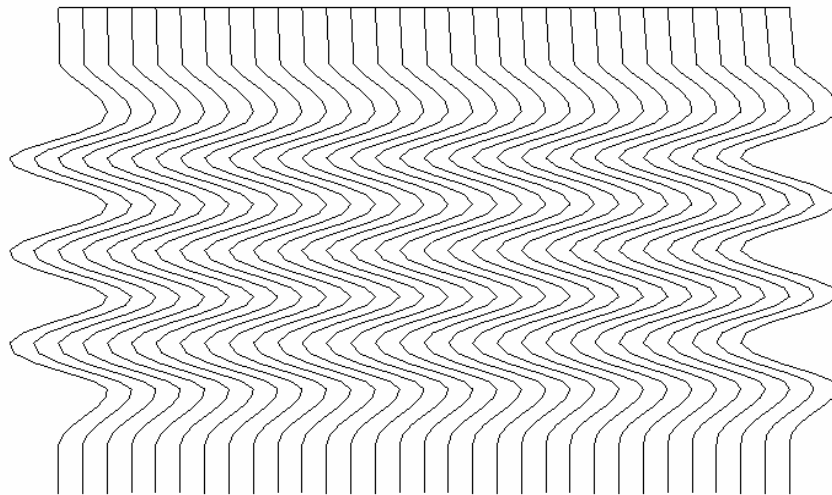


Fig. 4.9 Winkler Foundation with 31 Springs



#### 4.5 Dimensional Analysis of BCD

A dimensional analysis was done to study the BCD on soil. From Fig.4.10, a plate with diameter  $D$  is laid on soil of modulus  $E_s$ . The force applied on the BCD is  $F$ .

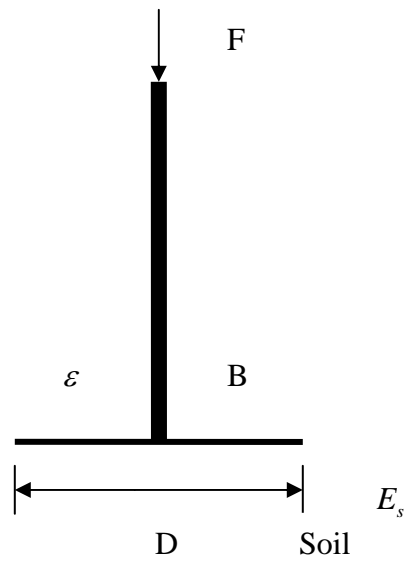


Fig.4.10 Dimensional Analysis of BCD

Where:

$$B = \frac{Eh^3}{12(1-\nu^2)} = \text{flexural rigidity of plate}$$

$E_s$  = modulus of soil under plate

D = diameter of plate

F = force applied on BCD

$\varepsilon$  = strain on top of plate

Symbols:	Dimension:
B	$F.L$
$E_s$	$FL^{-2}$
D	$L$
F	$F$
$\varepsilon$	

Choose B (F group) and D (L group) as repeating variables, so we have three

dimensionless terms:  $\frac{B}{E_s D^3}$ ,  $\frac{B}{FD}$ ,  $\varepsilon$ . According to Buckingham  $\pi$  Theorem,

$$f_1\left(\varepsilon, \frac{B}{E_s D^3}, \frac{B}{FD}\right) = 0 \quad (4.34)$$

$$\varepsilon = f_2\left(\frac{B}{E_s D^3}, \frac{B}{FD}\right) \quad (4.35)$$

Because the Force  $F$ , the diameter of plate  $D$ , flexural rigidity of plate  $B$  are constant, so we can get:

$$\varepsilon = f_3\left(\frac{B}{E_s D^3}\right) \quad (4.36)$$

$$\varepsilon = f_4\left(\frac{1}{E_s}\right) \quad (4.37)$$

$$\frac{1}{\varepsilon} = f_5(E_s) \quad (4.38)$$

$$E_s = f_6\left(\frac{1}{\varepsilon}\right) \quad (4.39)$$

So there is a relationship between Soil Modulus  $E_s$  and the inverse of strain on top of plate. For linear elastic analysis, we can have:

$$E_s = a\frac{1}{\varepsilon} + b \quad (4.40)$$

Where  $a$  and  $b$  are parameters. Eq.4.40 shows that there is a linear relationship between soil modulus  $E_s$  and the inverse of strain on top of plate.

#### **4.6 Depth of Influence of BCD**

We also need to know the depth of influence of BCD to determine the measuring range of BCD. If we define the depth of influence of BCD as the depth from the top of soil to the point where the vertical stress on soil is 10% of the stress at the top, we can find that the depth of influence is changing with the change of soil modulus. The higher the soil modulus, the smaller the depth of influence will be. From Fig.4.11, when the soil modulus changes from 3 MPa to 300 MPa, the depth of influence decreases from 311 mm to 121 mm.

### Distribution of Vertical Stress Under Center of BCD (10%)

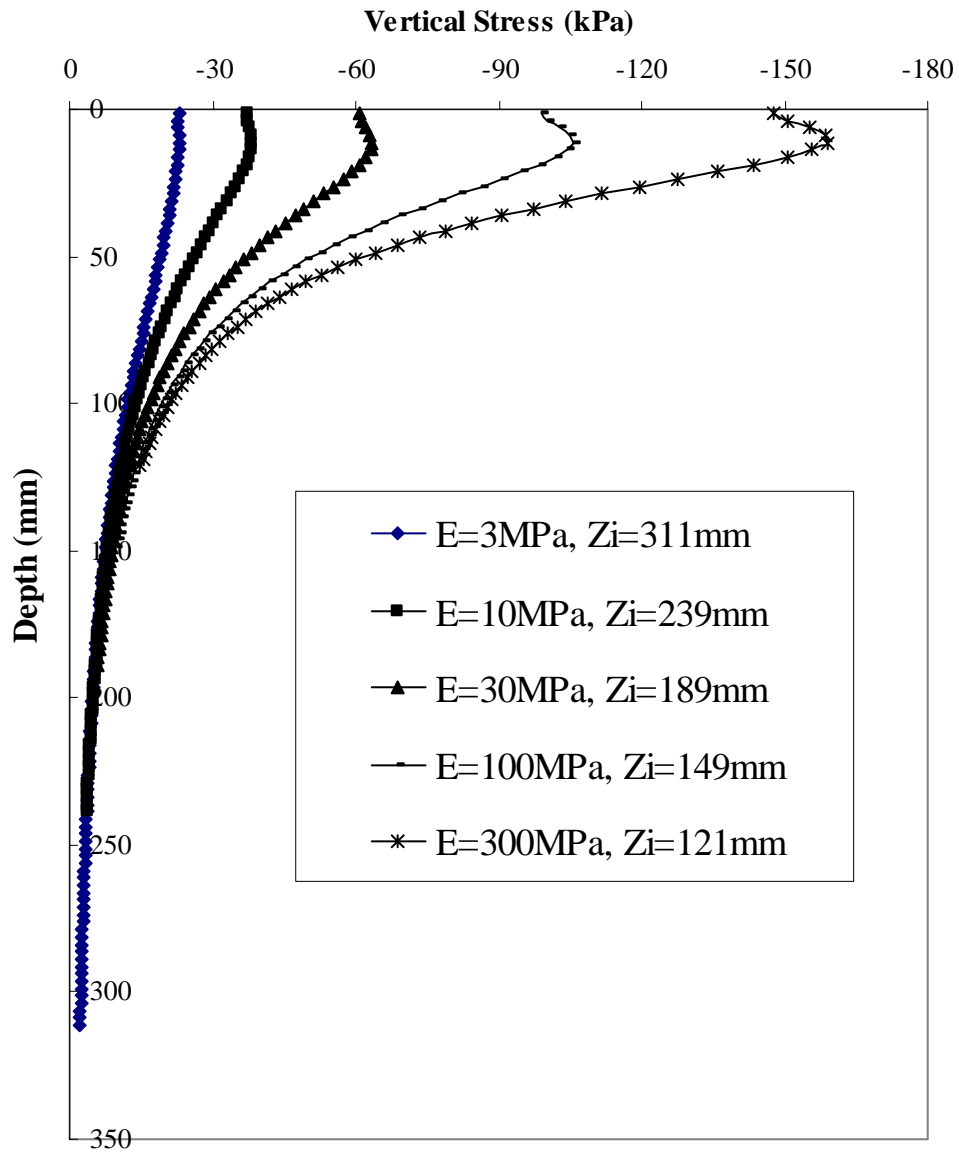


Fig.4.11 Depth of Influence of BCD

#### 4.7 Upper and Lower Limit of BCD

The previous analysis of the BCD is based on an elastic analysis. However, in reality, the soil is not elastic materials. We need to find a more realistic soil model to simulate the soil behavior in the analysis. There are some existing soil models in ABAQUS, for example, EPP (Elastic-Perfect Plastic), Cam-Clay and Mohr-Coulomb. We selected the EPP model because it is easy to use as a first step. The Stress-Strain relationship for the EPP model is shown in Fig. 4.12.

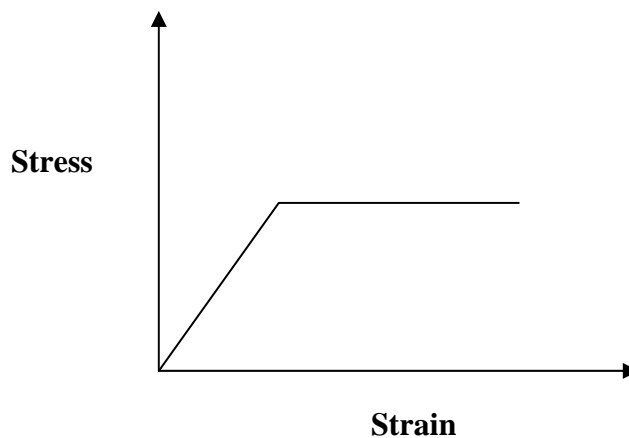


Fig. 4.12 Typical Stress- Strain Curve of EPP Model

To use the EPP model, we must determine the undrained shear strength of the soil first. An empirical relationship between the Young's Modulus of the soil  $E$  and its undrained shear strength  $S_u$  (Fig.4.13) was used to estimate the undrained shear strength of soil knowing the soil modulus.

In our analysis, we used  $E_u/C_u=300$  to calculate the undrained shear strength of the soil under the BCD.

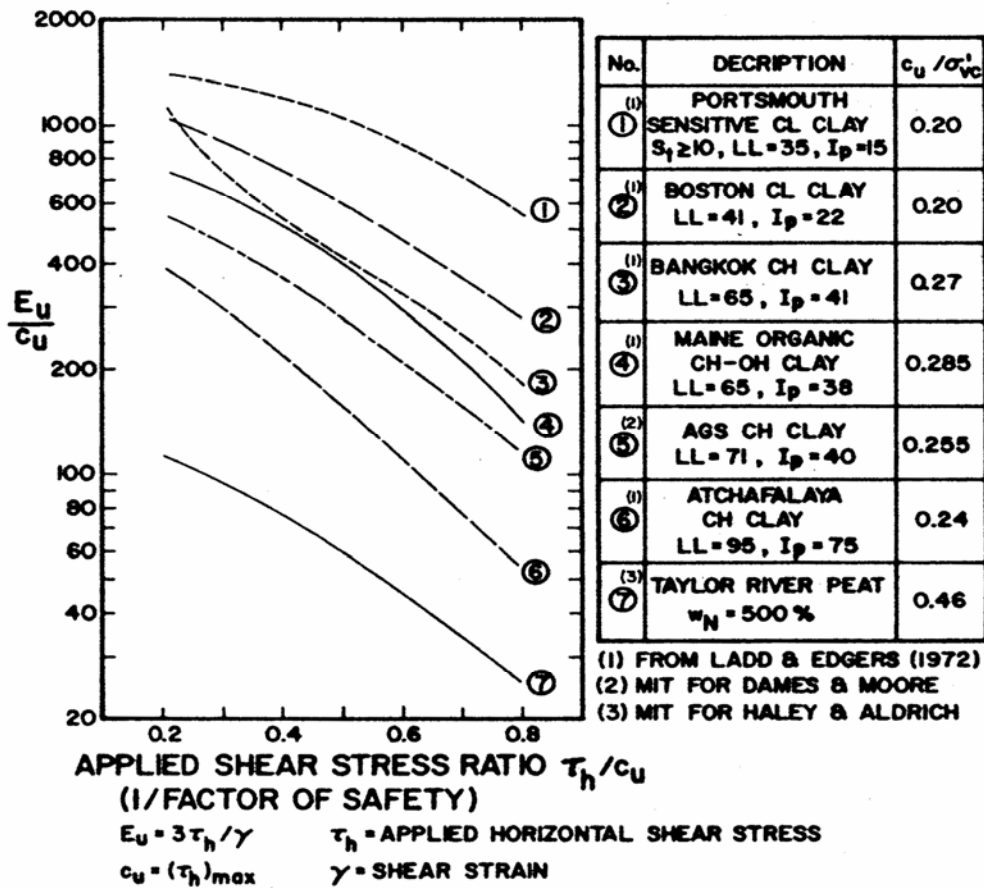


Fig.4.13 Empirical Relationship between Soil Modulus and Undrained Shear Strength (After Roger and Ladd, 1981)

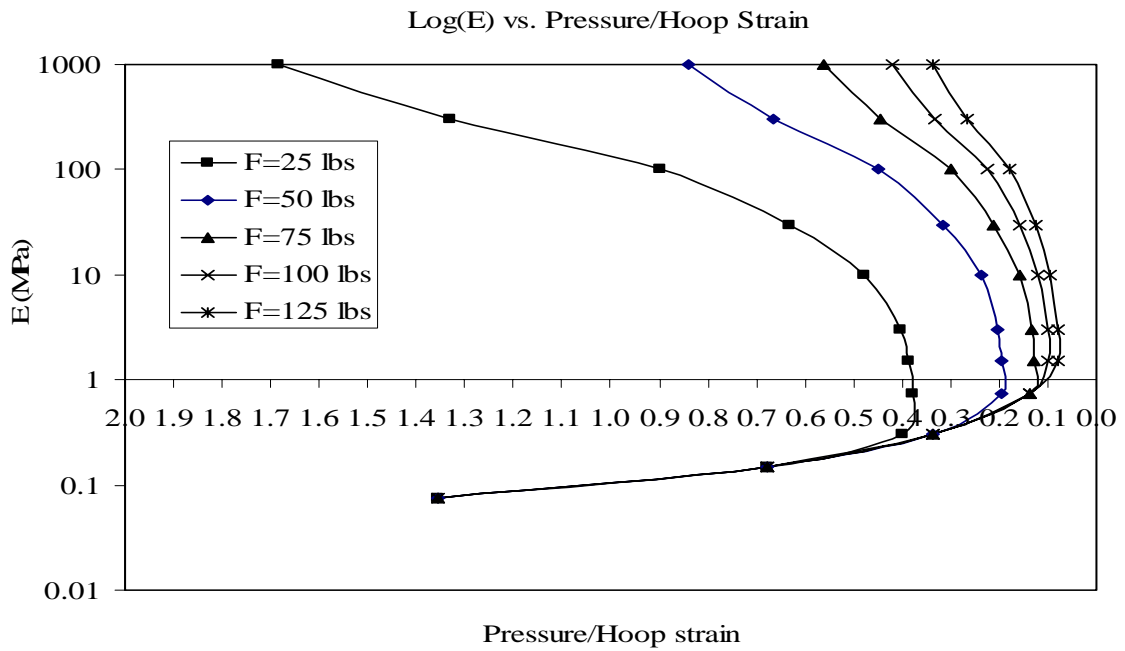
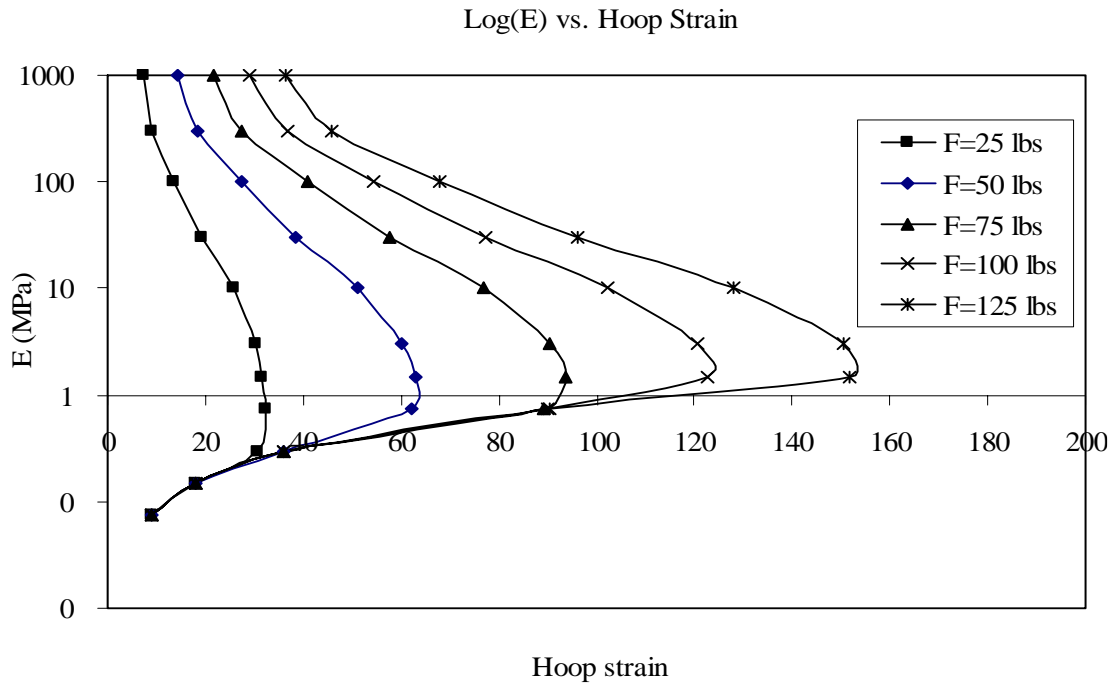


Fig. 4.14 Upper and Lower limit of BCD (2.5mm Plate)



After the Elastic-Plastic analysis of BCD, we found that, within certain range, there is a linear relationship between soil modulus  $E$  and hoop strain measured on top of BCD (Fig.4.14). We can use this range to estimate the upper and lower limit of BCD measurement. BCD upper limit is estimated about 300 MPa and lower limit is about 5 MPa.

#### **4.8 BCD on Two-Layer System**

By using ABAQUS, BCD on two layer system was studied. Four types of two-layer systems were simulated: 10 MPa-20 MPa, 20 MPa-10 MPa, 10 MPa-100 MPa and 100 MPa-10 MPa (Figs.4.15 to 4.18). The depth of each layer is changed in the numerical simulations for each case. For example, in Fig.4.15, the depth of the top layer with modulus of 10 MPa will increase from 0 mm to 300 mm with the increment of 60 mm. The radial strain and hoop strain for each case were output from the simulation results to calculate the BCD modulus. Fig.4.19 gives the correlations to calculate the BCD modulus from radial strain and hoop strain. The predicted BCD modulus versus depth of soil layer for each system is shown in Figs.4.20 to 4.27.

From the Figs.4.20 to 4.27, we can draw the conclusion that the material property of the top 60-120 mm of a soil layer is critical to the BCD measurement. The BCD measurements for two layer system are also affected by the modulus sequence of these two layers. For example, the system with hard layer on top such as 100MPa-10MPa has larger depth of influence than system with soft layer on top (10MPa-100MPa).

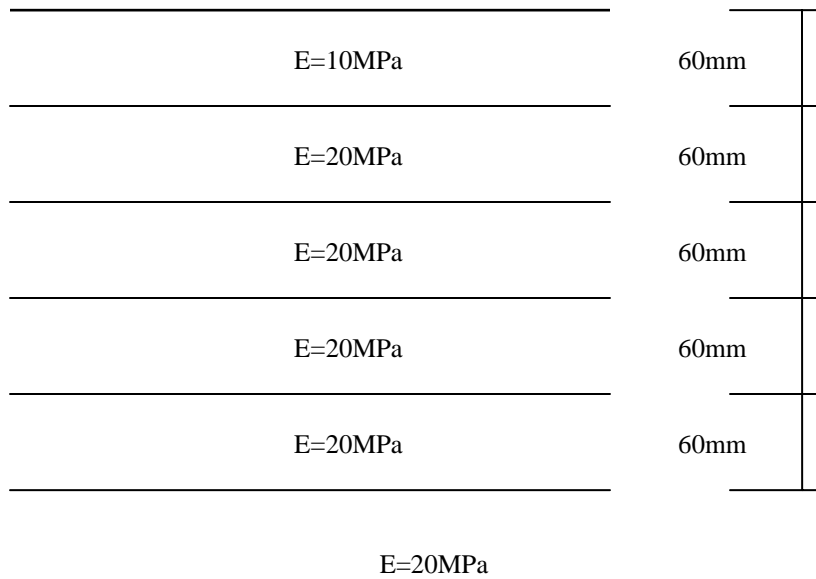


Fig. 4.15 BCD on Two Layer System (10 MPa-20 MPa)

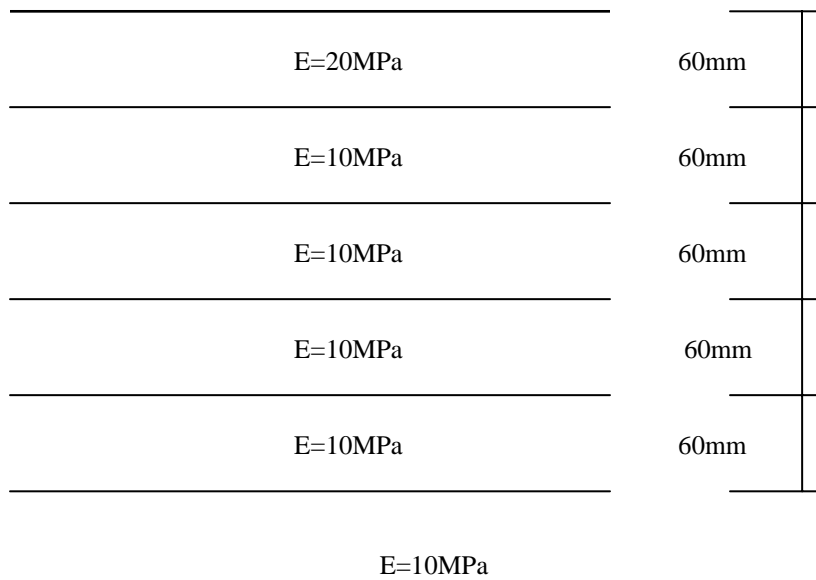


Fig.4.16 BCD on Two Layer System (20 MPa-10 MPa)

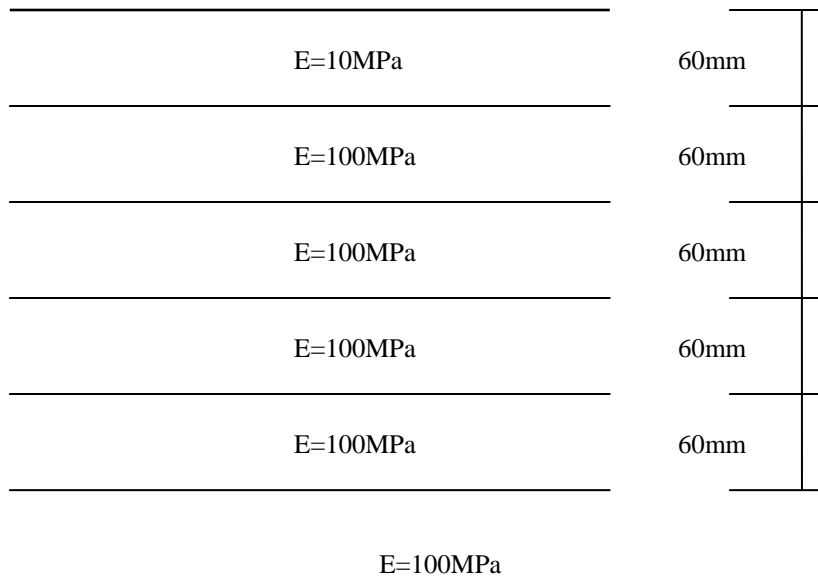


Fig.4.17 BCD on Two Layer System (10 MPa-100 MPa)

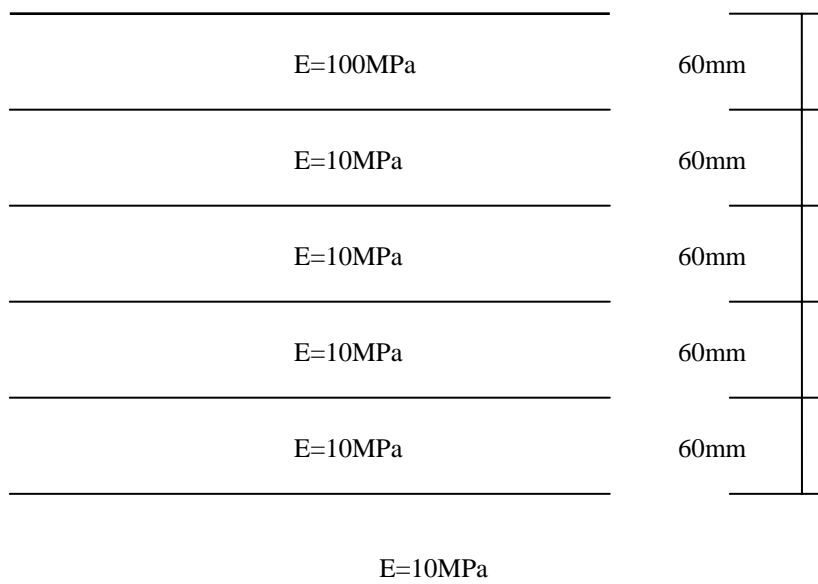


Fig.4.18 BCD on Two Layer System (100 MPa-10 MPa)

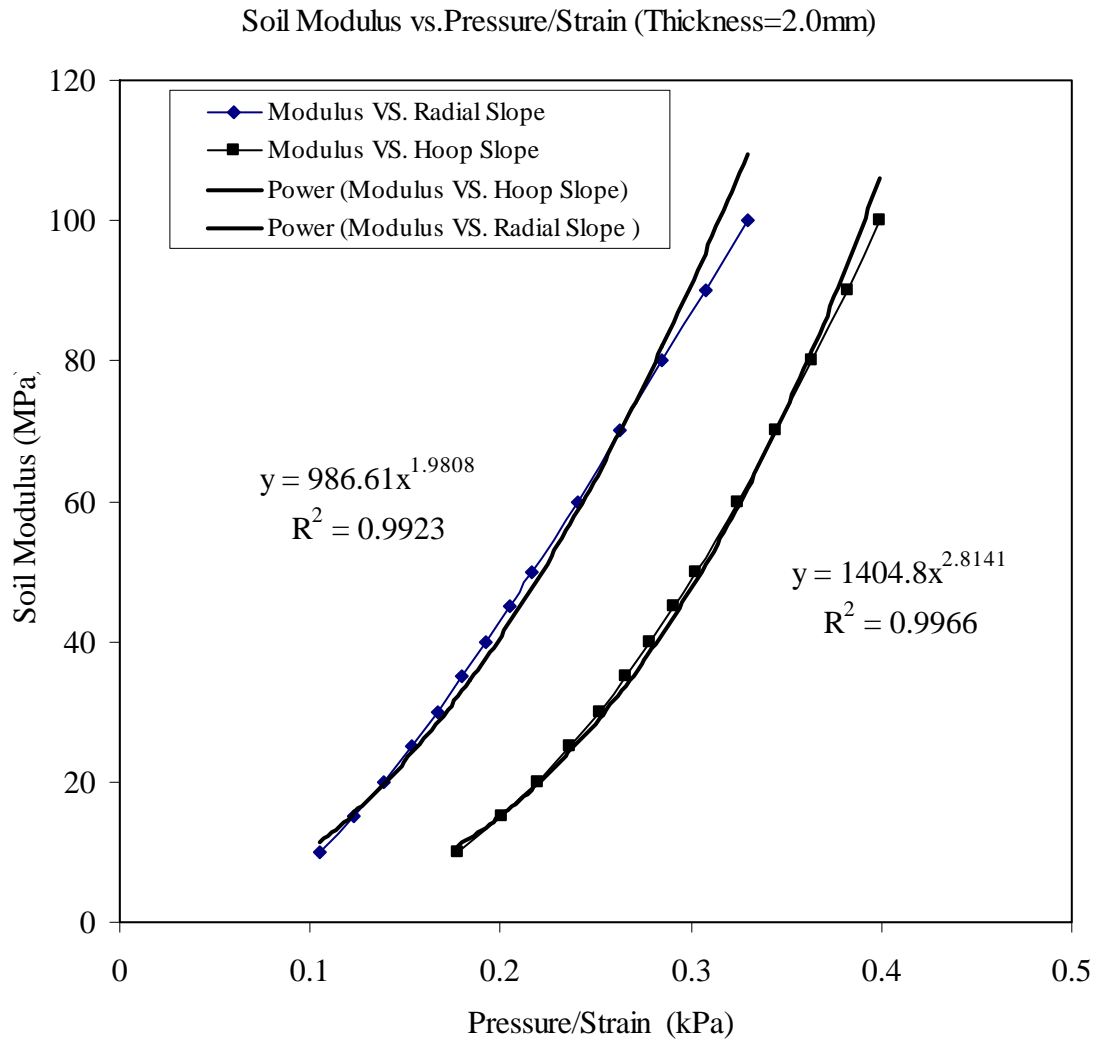


Fig.4.19 Correlations to Calculate Soil Modulus from BCD Result

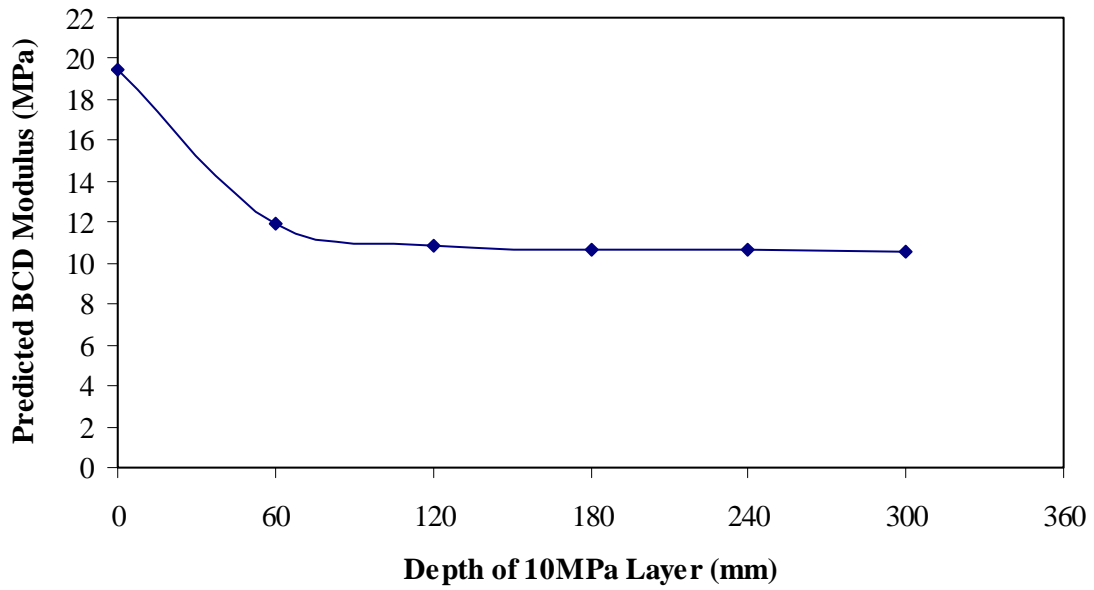


Fig.4.20 Predicted BCD Modulus from Radial Strain for 10 MPa-20 MPa System

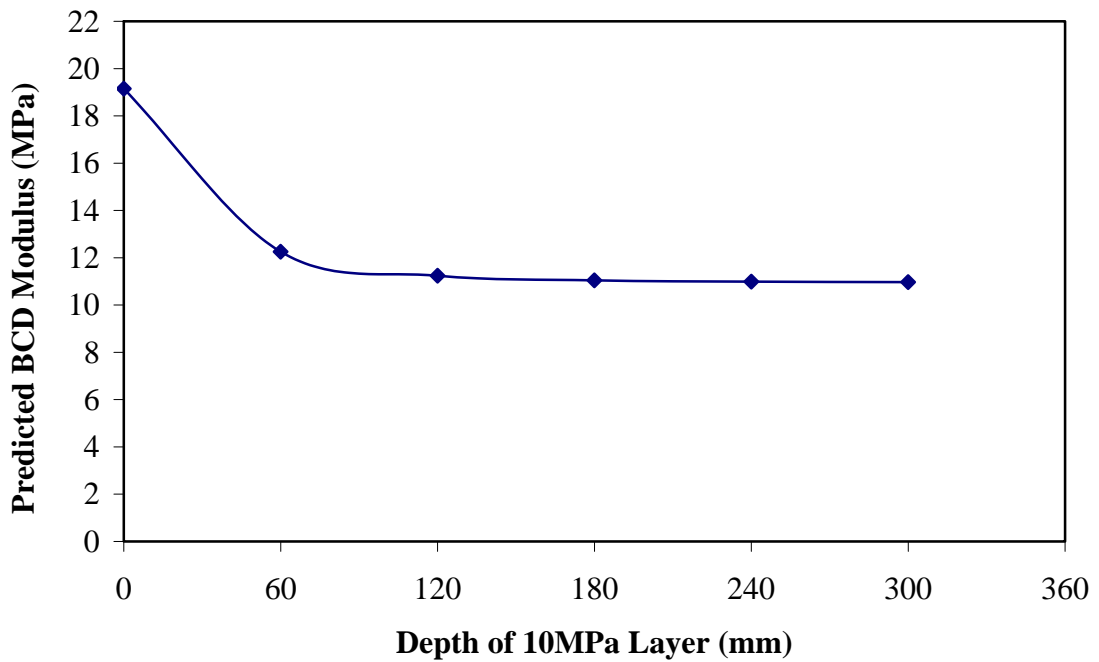


Fig.4.21 Predicted BCD Modulus from Hoop Strain for 10 MPa-20 MPa System

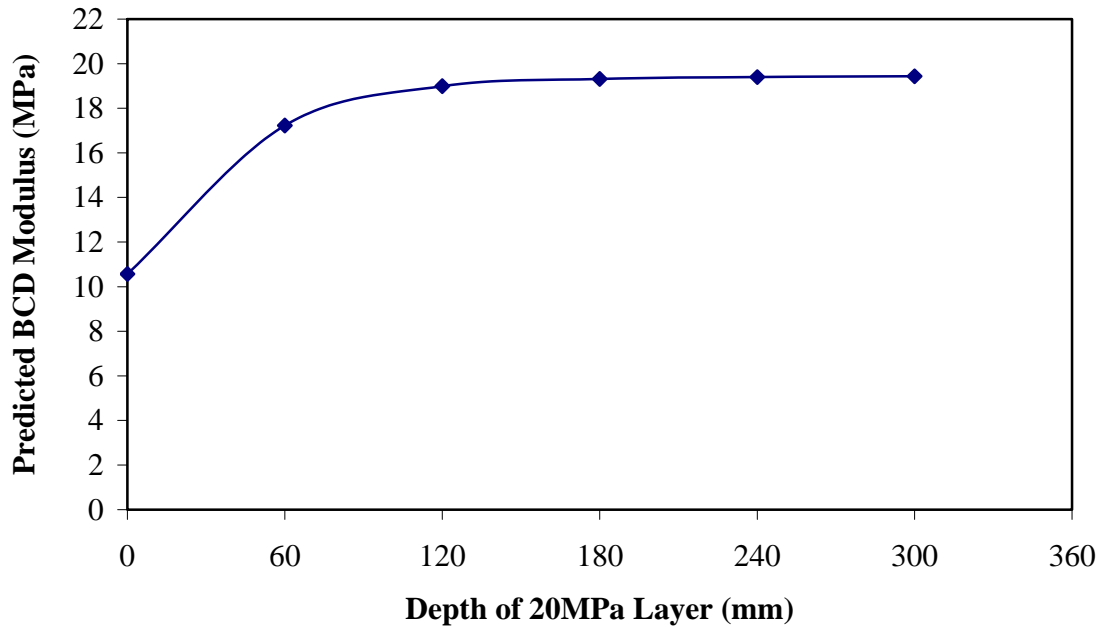


Fig.4.22 Predicted BCD Modulus from Radial Strain for 20 MPa-10 MPa System

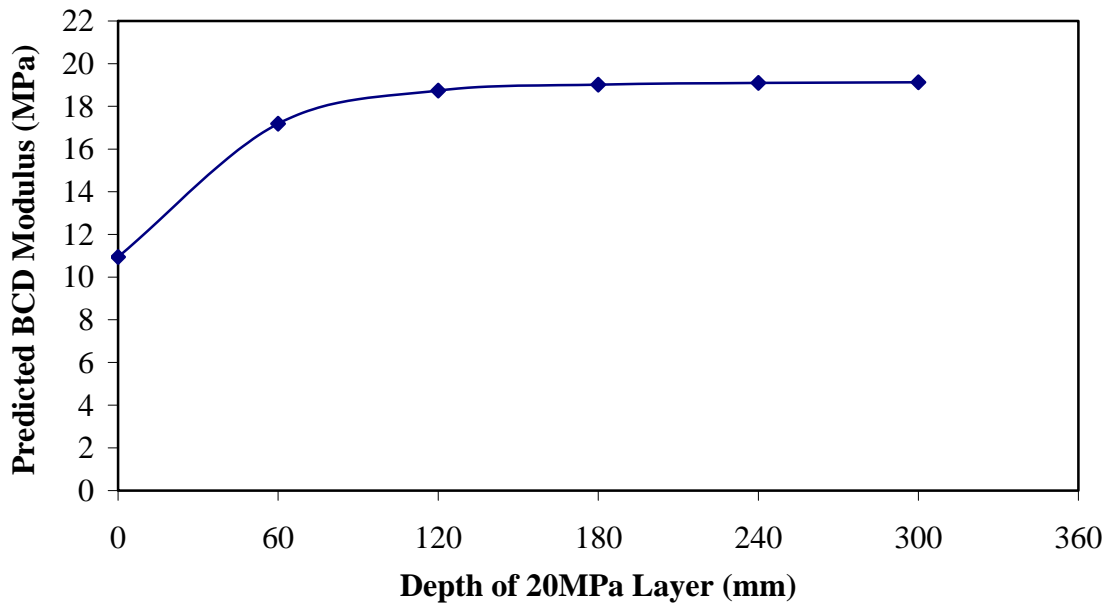


Fig.4.23 Predicted BCD Modulus from Hoop Strain for 20 MPa-10 MPa System

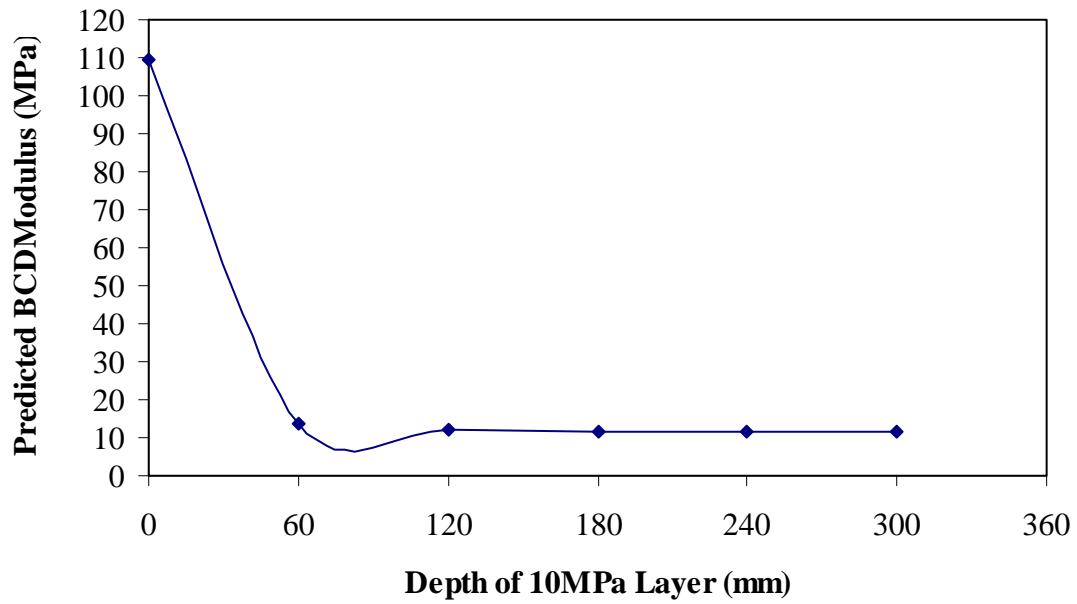


Fig.4.24 Predicted BCD Modulus from Radial Strain for 10 MPa-100 MPa System

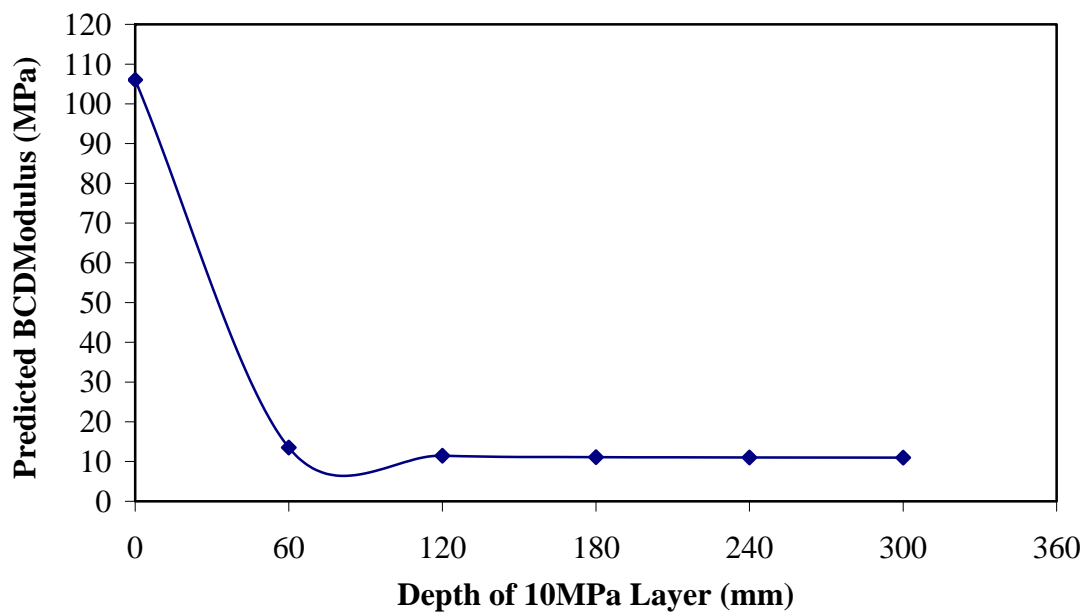


Fig.4.25 Predicted BCD Modulus from Hoop Strain for 10 MPa-100 MPa System

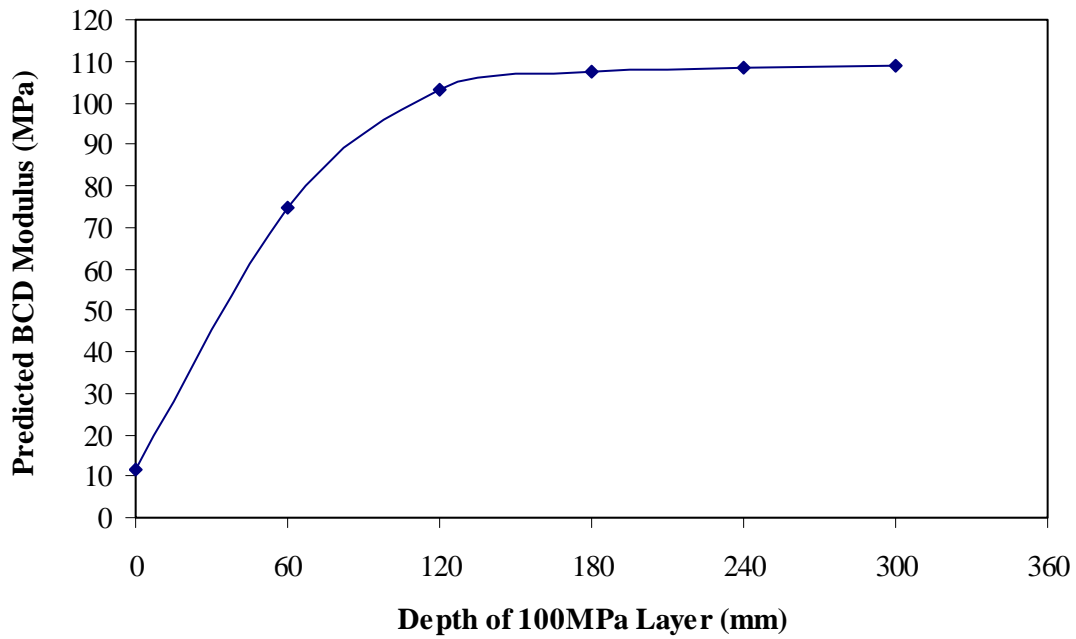


Fig.4.26 Predicted BCD Modulus from Radial Strain for 100 MPa-10 MPa System

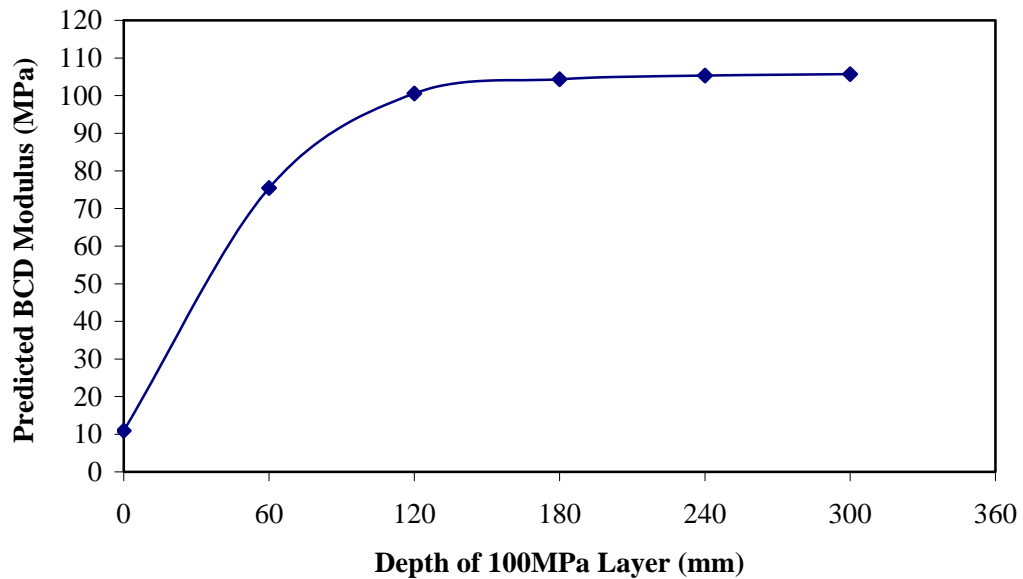


Fig.4.27 Predicted BCD Modulus from Hoop Strain for 100 MPa-10 MPa System



## CHAPTER V

### FIELD TEST AND CALIBRATION OF BCD

#### 5.1 Plate Test-Theory, Apparatus and Procedure

In order to prove that the BCD can measure a soil modulus, rigid plate test in parallel with BCD test were done in the field. The idea of using a plate load test correlation with the BCD modulus was presented by Dr. Jean-Louis Briaud. The idea was to create a small plate load tester with dimensions identical to that of the BCD that could be used in the field with relative ease yet still be large enough to provide an appropriate reaction to obtain useable and reproducible results. The plate load tester is a 0.15 m (6 inch) in diameter, 0.05 m (2 inch) thick full plate with three arms spaced along the circumference of the plate at 120 degrees from each other. The arms are approximately 0.47 m (18.5 inches) long. The weight of the plate load tester is about 20 pounds, which provides the seating load (Fig.5.1).

The idea of plate load test is to have a static load applicator (rigid plate) and manual measuring instruments (dial gauges) to measure deflection at a lateral distance that is far enough so they will not influence the deflection. From elastic analysis, the lateral influence zone of a loaded foundation can be estimated to be around  $3B$ , where  $B$  is the length of the base of the foundation. The distance from the edge of the plate (the source of the load) to the end of the arm is about 18.5 inches. A dial gauge will be placed at the end of each arm that will be attached to a magnetic base. The magnetic

base will be attached to a metal base plate, which is then placed in good contact with the ground. The distance from the end of the arm and the metal base plate is approximately 0.10 m (4 inches). Therefore, the distance from the plate to the measuring point is around 0.56 m (22 inches), which is thought to be out of the lateral zone of influence of the plate.

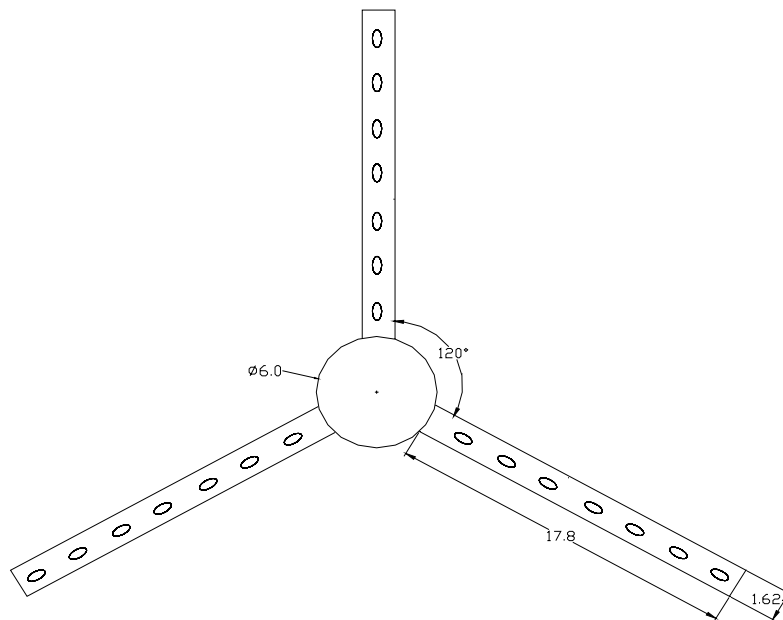


Fig.5.1 Top View of Plate Tester with Dimensions (Unit in Inch)

ABAQUS was used to simulate plate test in the field. The mesh of soil (Figs.5.2 and 5.3) is large enough to simulate elastic half space. Distribution of settlement of plate in Fig.5.4 shows that the dial gauge measurement is 95.5% of the actual settlement

happened underneath the plate. So the measurement is out of the zone of influence and accurate enough.

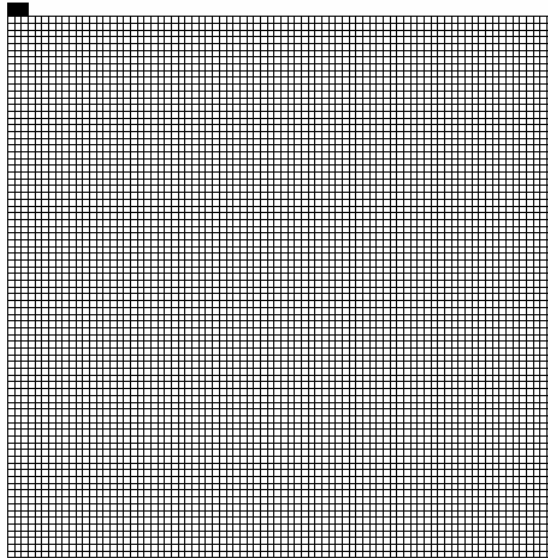


Fig.5.2 Mesh of ABAQUS Simulation of Plate Test

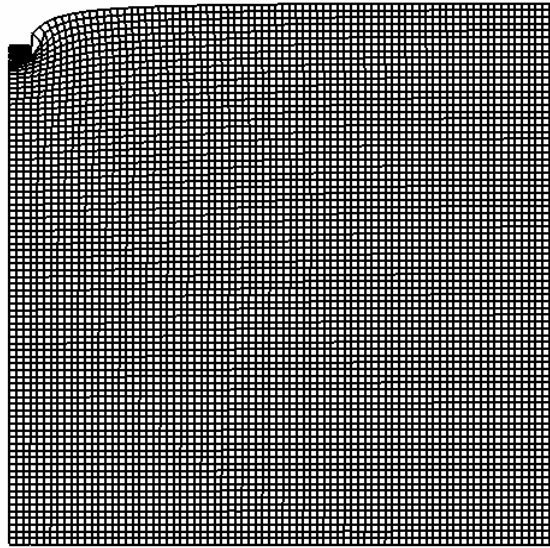


Fig.5.3 Mesh of ABAQUS Simulation of Plate Test (after loading)

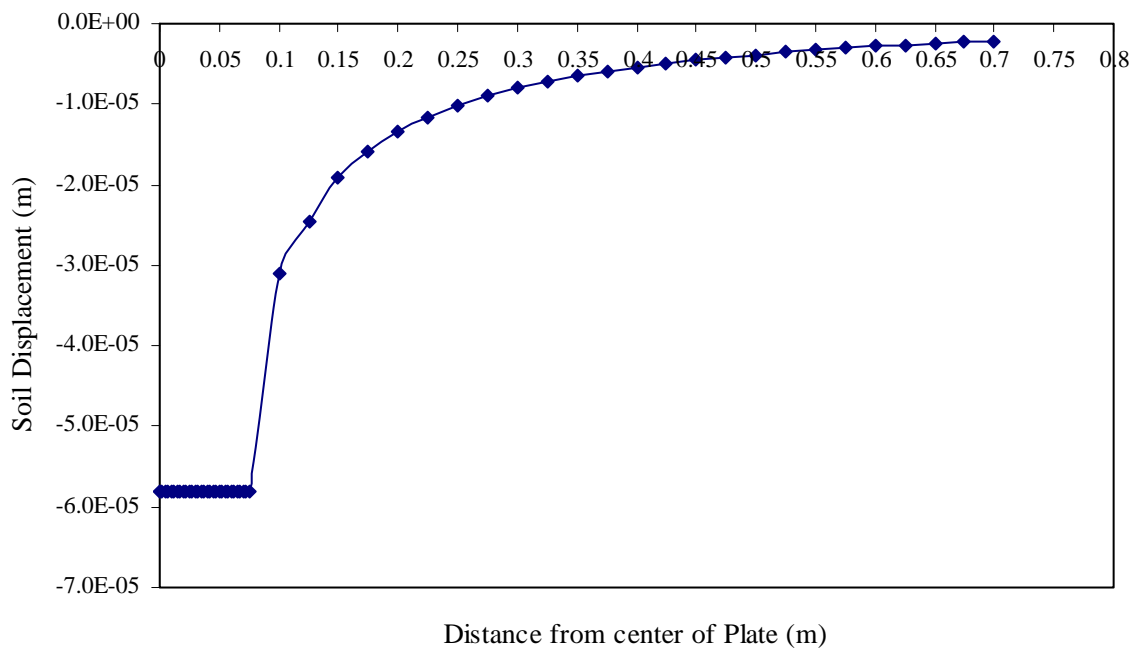


Fig.5.4 Plate Settlement from ABAQUS Simulation

In the field, according to ASTM standard D 1194, the relationship between soil modulus and the load and settlement is found by the equation:

$$E_s = I_w (1 - \nu^2) B \left( \frac{\Delta q}{\Delta s} \right) \quad (5.1)$$

Because  $q = \frac{Q}{I_w B^2}$ , Eq.5.1 reduces to:

$$E_s = \frac{(1 - \nu^2)}{B} x \left( \frac{\Delta Q}{\Delta s} \right) \quad (5.2)$$

where

$E_s$  =soil modulus (psi)

$I_w$  =influence factor,  $\pi/4$  for circular plates

$\nu$  =Poisson's ratio (assume  $\nu = 0.35$ )

$B$  =diameter of the plate (6 inch)

$\frac{\Delta Q}{\Delta s}$  =slope of the load versus settlement curve.

By using Eq.5.2, we can obtain the elastic modulus of the material from the plate test as long as we are using the portion of the load versus settlement curve that is in the elastic region.

The apparatus that are required to run a plate test include the following:

- 1 The plate which is 6 inches in diameter and 2 inches thick. It has three arms extending 18.5 inches at 120 degrees from the edge of the plate;
- 2 Three dial gauges reading in units of 0.0001 inch with a range of 0.4 inch;

- 3 Three magnetic stands to hold the dial gauges and three base plates to place the stands on;
- 4 Dead weights to load the plate (2 weights of 25 pounds each);
- 5 A stop watch to keep track of time.

The procedure that has been adopted for obtaining a good plate modulus is as follows:

- 1 Place the plate at the chosen location and use a sand cushion if necessary. The weight of the plate is around 20 pounds, which is the seating load;
- 2 Set the three dial gauges at the end of the plate arms (the arms holding the dial gauge should be set in the prolongation of the arms of the plate);
- 3 Take a zero reading (Fig.5.5.a);
- 4 Place two dead weights of about 50 pounds on the center of the plate. Wait until the readings stabilize or until one minute has passed, whichever comes first and record the dial gauge readings (Fig.5.5.b);
- 5 Take off the weights and take a reading of the dial gauges;
- 6 Repeat step 4 and get the stable dial gauge readings.



Fig.5.5.a Plate Test in the Field



Fig.5.5.b Plate Test in the Field (loading)

The data reduction steps include the following:

- 1 Draw a “load in pounds versus deflection in inches” curve, including the reloading part.
- 2 Obtain the slope of the loading curve  $(\Delta Q / \Delta S)_{initial}$  and slope of the reloading curve  $(\Delta Q / \Delta S)_{reload}$ . The slopes will be in units of lbs/in.
- 3 Calculate the modulus of the soil from the following equations:
  - a.  $E_L$  (psi) =  $0.146 \times (\Delta Q / \Delta S)_{initial}$  (lbs/in)
  - b.  $E_r$  (psi) =  $0.146 \times (\Delta Q / \Delta S)_{reload}$  (lbs/in).

An example of a typical load reload curve is shown in Fig.5.6.

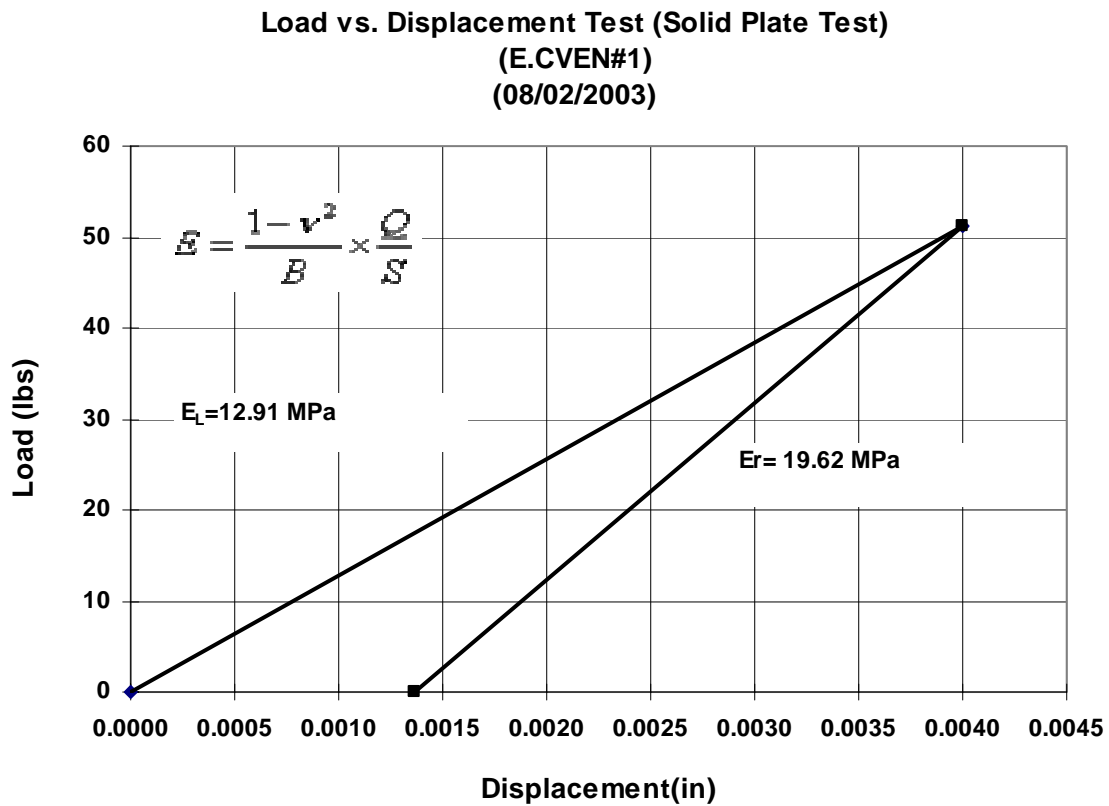


Fig.5.6 A Typical Plate Test Curve



## 5.2 BCD-Procedure

The procedure for doing BCD test in the field is as follows:

- 1 Make the testing surface flat. Sand cushion used if the surface is very uneven and rough;
- 2 Place the plate of BCD on the testing location (Fig.5.7). The self weight of the BCD is around 20 pounds, which is the seating load;
- 3 Adjust the lights in x axis and y axis on the display to the center and zero out the load and strain readings (Fig.5.8);
- 4 Lean on BCD until 50 lbs or close to 50 lbs load is reached. Make sure light is in the center during this loading process;
- 5 Click the trigger under left hand handle and take a strain and modulus reading at 50 lbs or close to 50 lbs;
- 6 Click the display reset button and do step 3, 4 and 5 again.



Fig.5.7 BCD on the Ground



Fig.5.8 Zero Out the Display

### 5.3 Correlations between Plate Test and BCD Test Results

Since October of 2003, the author has conducted 18 plate tests and 18 BCD tests at 7 different locations. A table of the various tests including the locations, date, materials tested and test results can be found in Appendix. A couple of BCD tests were run and immediately followed by the plate test. The plate apparatus was placed directly on the BCD imprint and loaded. With the large amount of data that has been collected over a period of 3 months at a variety of locations, we are able to create a plot relating the pressure/hoop strain of BCD to the plate reload moduli (Fig.5.9).

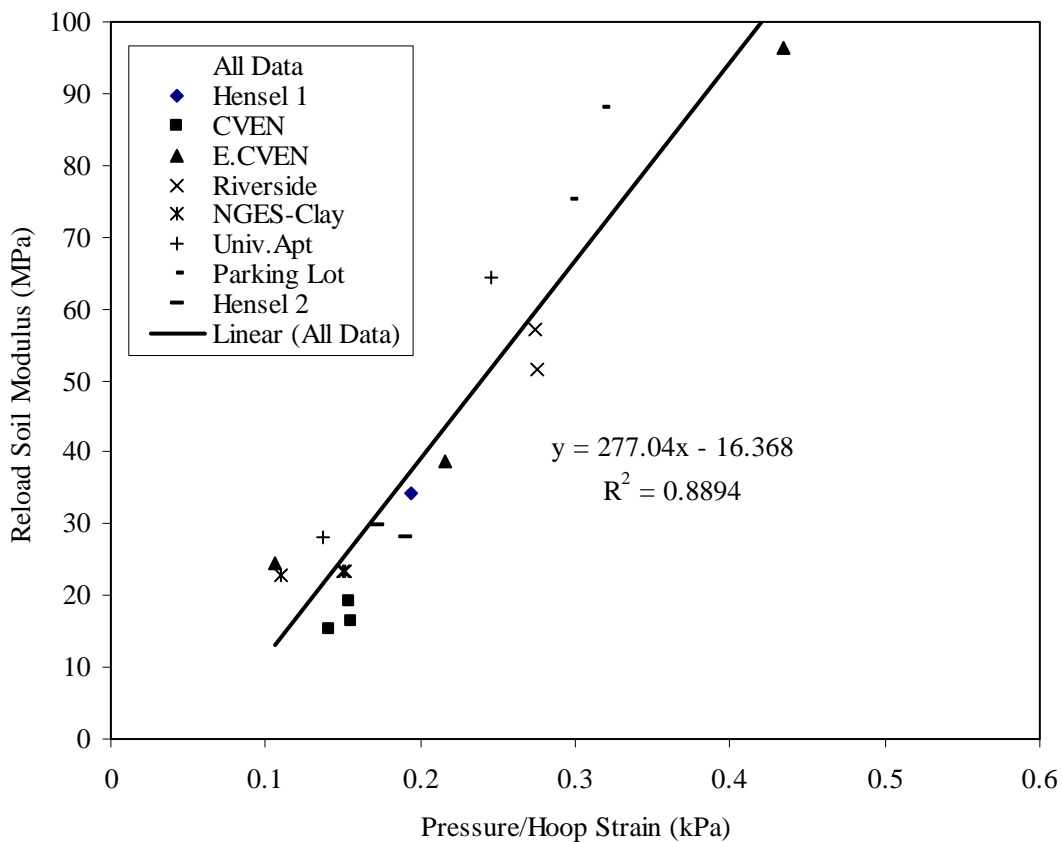


Fig.5.9 Correlation between Plate Test and BCD Test

### 5.3.1 Why There Is an Intercept in Soil Modulus vs. Pressure/Strain Plot?

The intercept of Soil Modulus vs. Pressure/Strain plot depends on the relative rigidity of the plate. The bending and curvature of plate depends on the interaction between plate and the soil underneath. When the soil modulus is very small, the bending and curvature of plate is mainly controlled by the stiffness of the plate. The influence of soil modulus will be small. (BCD will NOT work in this range because the idea of BCD is based on the linear relationship between soil modulus and bending of plate) For example, in Fig.5.10, the soil modulus  $E=0.1\text{MPa}$ , a 2mm plate doesn't have apparent bending while the infinite flexible plate bends a lot.

This can also explain why there is intercept in Soil Modulus vs. Pressure/Strain plot. The reason is when the soil modulus is very small the bending of the plate is controlled by the stiffness of the plate itself as stated before. Stiffer plate has smaller bending and larger intercept. When the thickness of plate changes, say from 0.1 mm to 5 mm, the intercept changes from near 0 to 0.65 (Fig.5.11). So the plate will not bend infinitely, on the contrary, it will bend just a little and the strain is also very small. As a result of this, the pressure/strain will not be zero, so the Soil Modulus vs. Pressure/Strain will not come through origin and there is always an intercept if the plate is not infinite flexible.

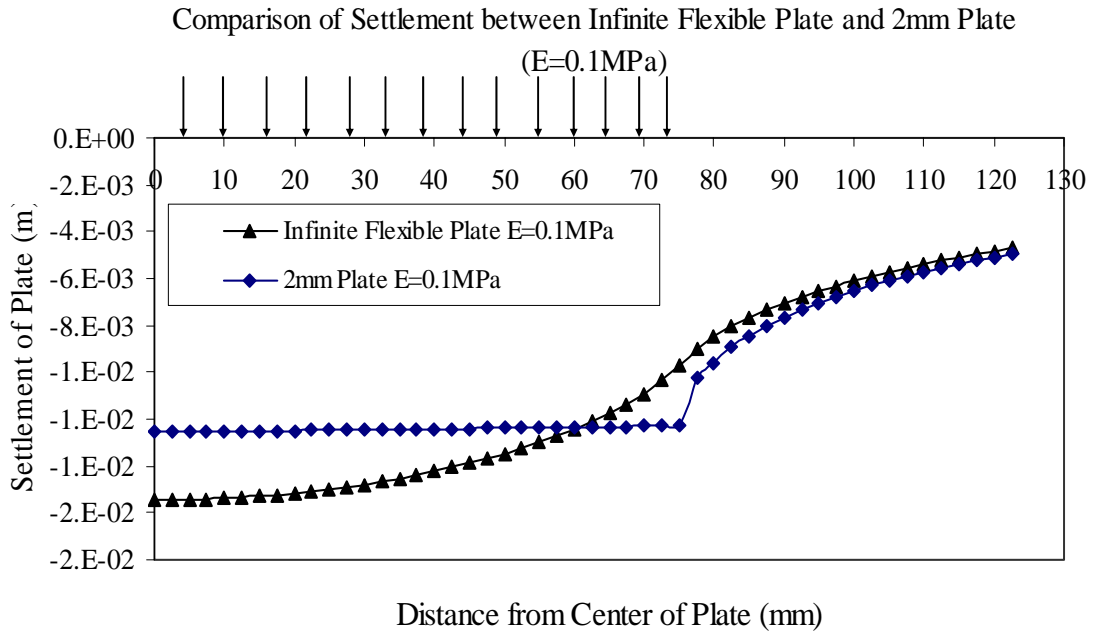


Fig.5.10 Bending of Plate When Soil Modulus is Very Small

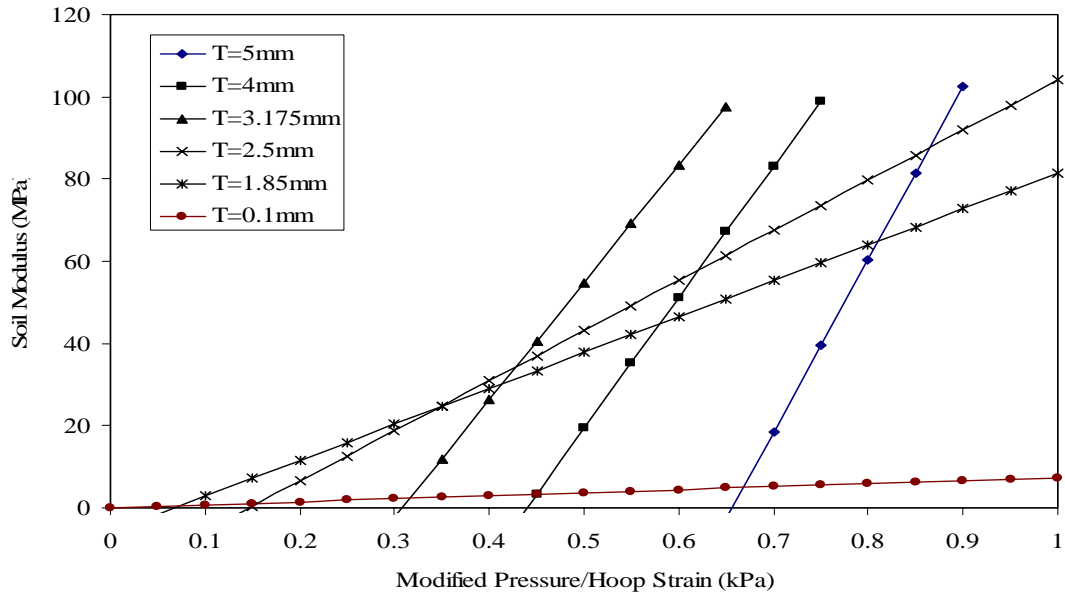


Fig.5.11 The Intercept changing with the Thickness of the Plate

On the other hand, when the soil modulus is not very small, the bending and curvature of plate is mainly controlled by the soil modulus. For example, when soil modulus is 1MPa and 10MPa, the 2mm plate bends more on the 1MPa soil than on the 10MPa soil (Figs.5.12 and 5.13). This is the range where BCD will work.

Basically, when the soil modulus is very small, because the influence of plate stiffness on the bending of plate is increasing, the BCD won't work very well and the result is not accurate. The field tests data can tell this.

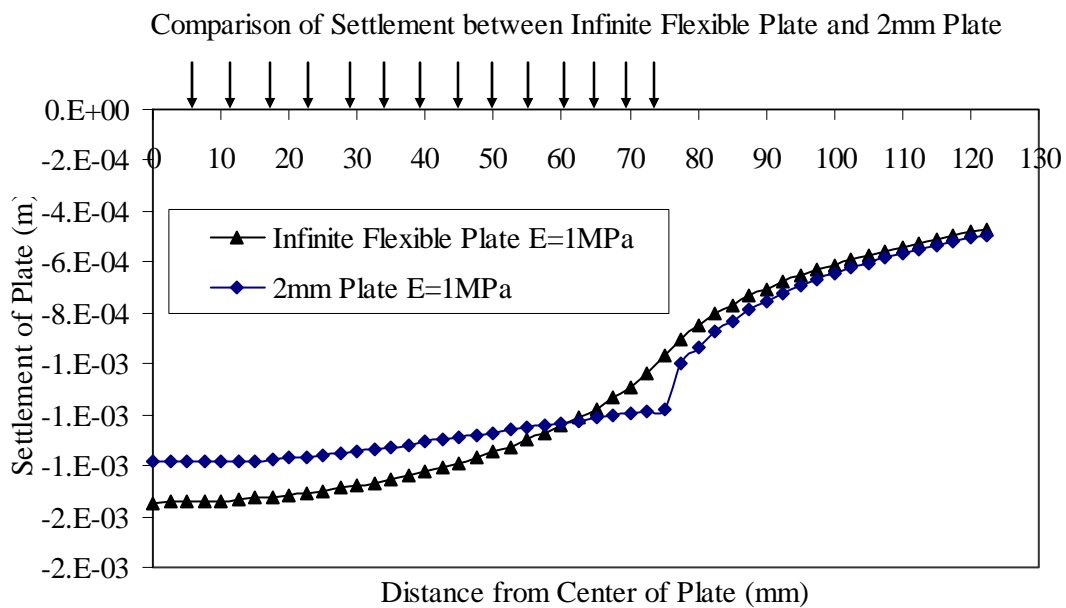


Fig.5.12 Bending of Plate When Soil Modulus E=1MPa

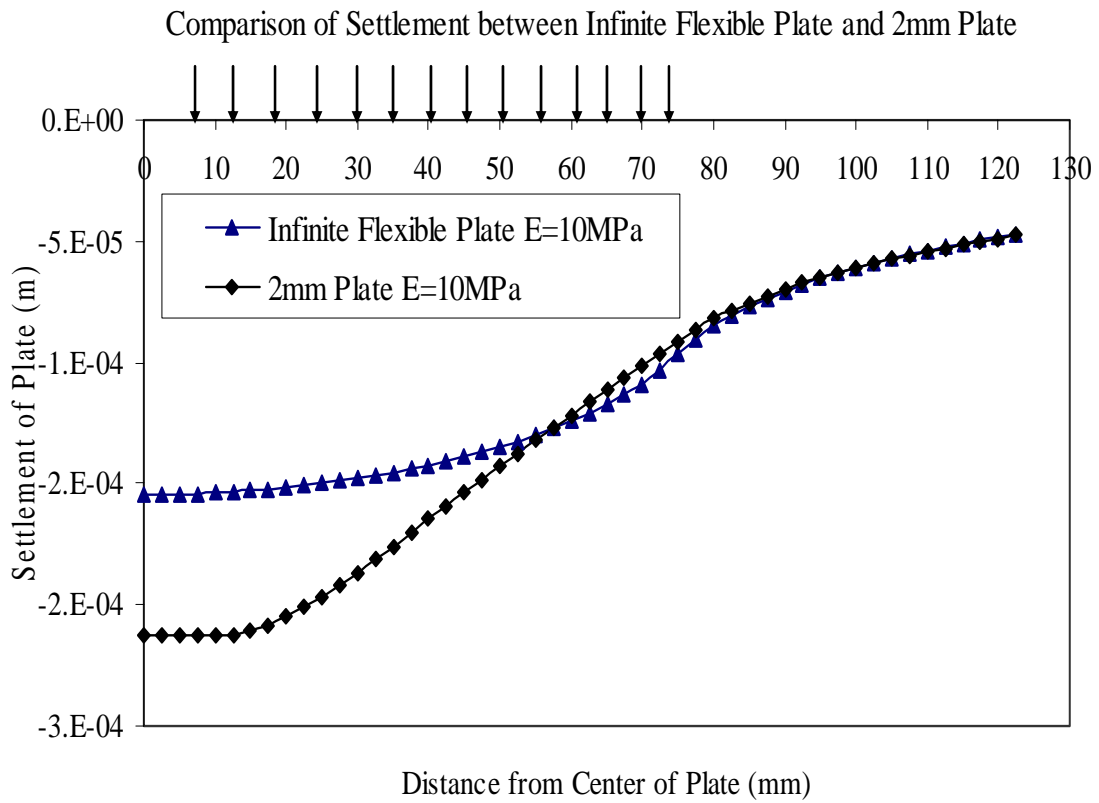


Fig.5.13 Bending of Plate When Soil Modulus  $E=10\text{MPa}$

### 5.3.2 Why the Radial Strain in BCD Doesn't Work?

Although field test shows a good correlation between Plate Reload Soil Modulus and Pressure/Hoop Strain from BCD test (Fig.5.9), the correlation between Reload Soil Modulus and Pressure/Radial Strain is not as good as expected (Fig.5.14). We need to find the reasons why the radial strain on BCD doesn't work well.

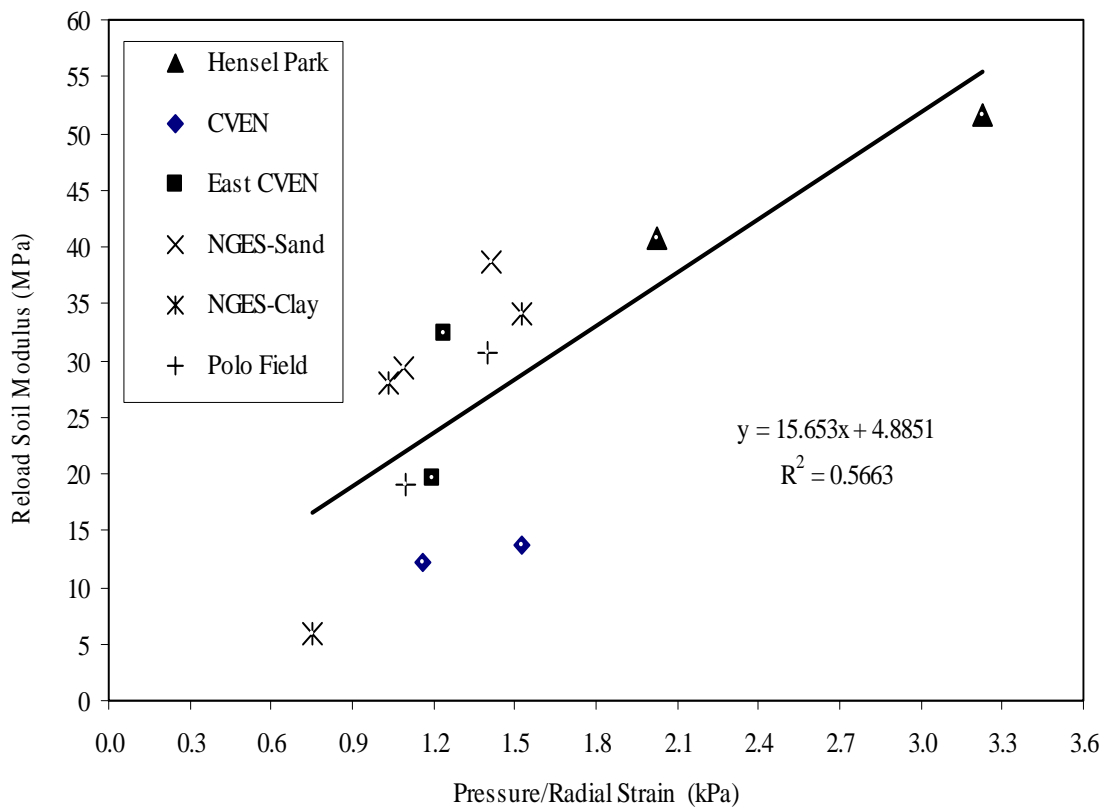


Fig.5.14 Correlation between Plate Test and BCD in Radial Strain (4mm Plate)



Fig.5.15 shows the distribution of radial strain and hoop strain on top of plate when the soil modulus is 20 MPa. From Fig.3.2, we know these strain gauges are glued on a circle with radius 0.75 inch (19.05 mm). The strain gauges in radial direction are perpendicular to the circumference of the circle and strain gauges in hoop direction are along the circumference of the circle. We noticed that in Fig.5.15, at the point where the distance from the center of plate is 19.05 mm, the gradient of radial strain is much larger than the gradient of hoop strain. From Chapter III, we know the length of strain gauges is 1/8 inch (3.2 mm), so the strain gauges are actually measuring average strain happened on a certain range rather than a certain point on the plate.

There are two possible reasons resulting in the problems happened on strain gauges in radial direction:

1. The strain gauges were not glued exactly where they are supposed to be. Because the radial strain has a large gradient around the measuring point, the strain gauges in radial direction have large scatter in measurement than strain gauges in hoop direction.
2. Because the soil is not homogeneous, some part of soil under the BCD plate may be harder than other parts of soil under the BCD. When we apply load on the BCD, the plate will not bend uniformly and the strain gauges in radial direction will actually measure the radial strains happened at different locations and this results in the scatter of measurement in radial strain.

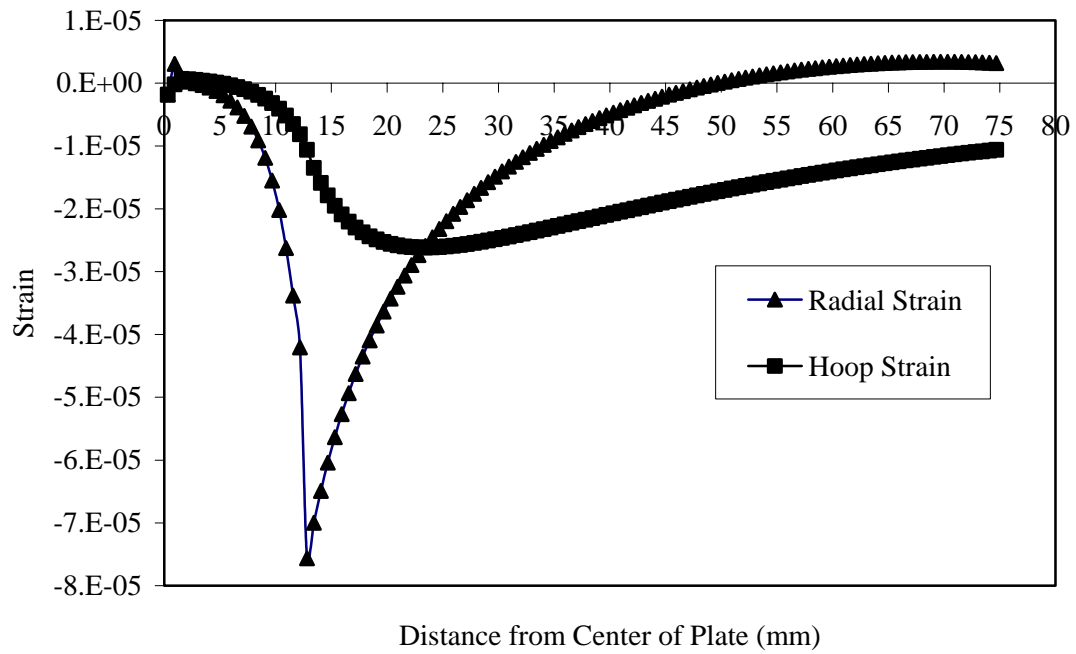


Fig.5.15 Distribution of Strain on Top of Plate (Soil Modulus=20 MPa)

## 5.4 Field Test Results vs. Numerical Simulation Results

The BCD field test results are compared with ABAQUS numerical simulation results in Fig.5.16. The correlations are pretty close to each other. The differences may be coming from the assumption of soil as elastic and homogeneous material in numerical simulation which is not true in the field. The other possible reason for the difference is because the strain output from numerical simulation is just at one certain location (19.05 mm from the center) while the strain gauges in BCD are actually measuring average strains happened in a certain range.

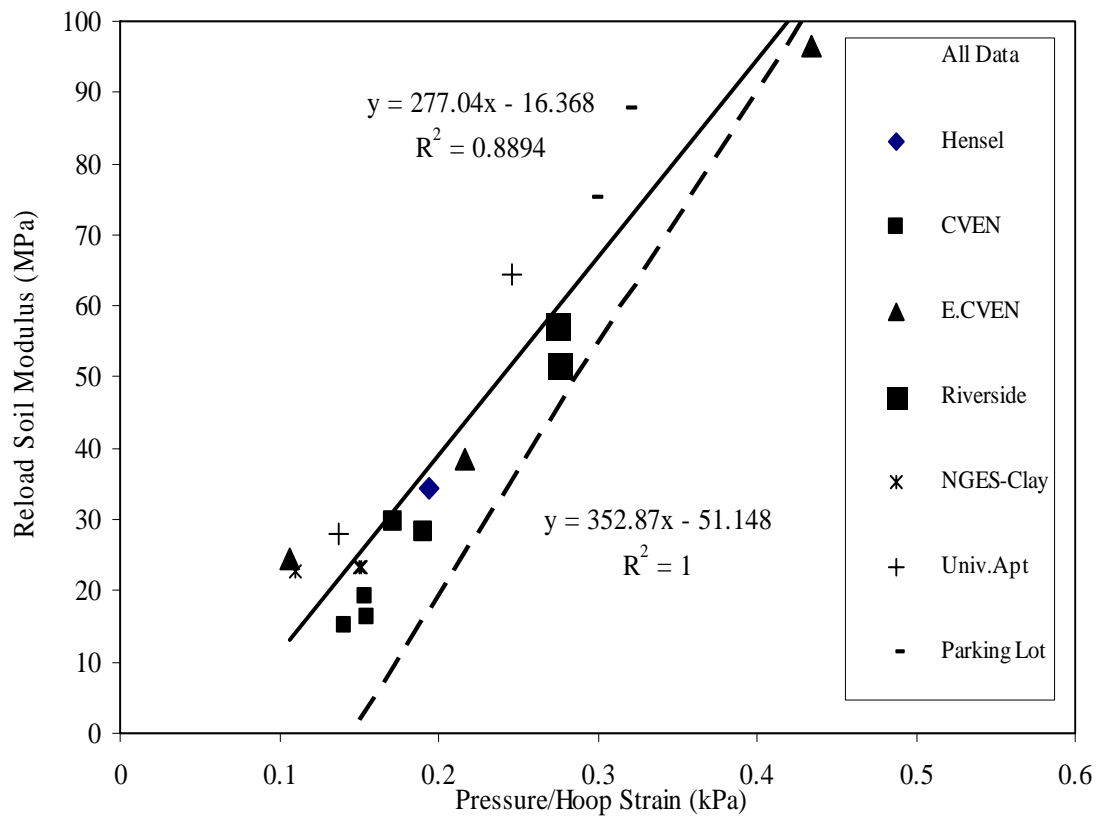


Fig.5.16 Comparison between Numerical Simulation and Field Tests

## 5.5 Influence of Rough Surface on BCD Results

BCD test needs to be done on flat surface to ensure the accuracy of test results. We also studied the influence of rough surface on the BCD result. Two types of rough surface were studied: surface with bump and surface with dent.

### 5.5.1 Surface with Bump

Put a small gravel on the concrete floor to test the influence of rough surface on BCD measurement. If we put gravel on soil, it may be squeezed into soil and surface will be flat after one or two tests. This may explain why we need to do BCD test at least twice at one location (especially on soft material) to get a better result. Two sizes of gravel, one is 2 mm×6 mm, the other is 12 mm ×7 mm, were used in this test. In Fig.5.17, the point in the center of the circle is the center of BCD. All the other points indicate the three locations of gravel. The test result is shown in Table 5.1 and Table 5.2. The conclusions from the tests are listed below:

- The location of gravel matters. The farther the gravel away from the center of BCD, the more influence it will have.
- The size of the gravel matters. Larger gravel tends to have more influence.
- We need a sand cushion on hard uneven surface to eliminate or alleviate the influence of rough surface.

Table 5.1 BCD Test for Bump at Different Locations (Gravel Size 2 mm×6 mm)

Location of Gravel	Load (lbs)	Hoop Strain
NO Gravel	50.4	-96
	50.5	-96
	50.2	-94
Center of Plate	49.2	-214
	51.8	-205
	50.4	-201
Between Center and Edge	50.3	-519
	50.8	-386
	51.9	-496
Edge of Plate	50.2	-627
	52.6	-554
	50.8	-594

Table 5.2 BCD Test for Bump at Different Locations (Gravel Size 12 mm×7 mm)

Location of Gravel	Load (lbs)	Hoop Strain
NO Gravel	50.4	-96
	50.5	-96
	50.2	-94
Center of Plate	50.1	-199
	51.9	-197
	49.5	-231
Between Center and Edge	50.4	-557
	50.6	-554
	51.1	-574
Edge of Plate	50.6	-675
	50.9	-645
	51.5	-661

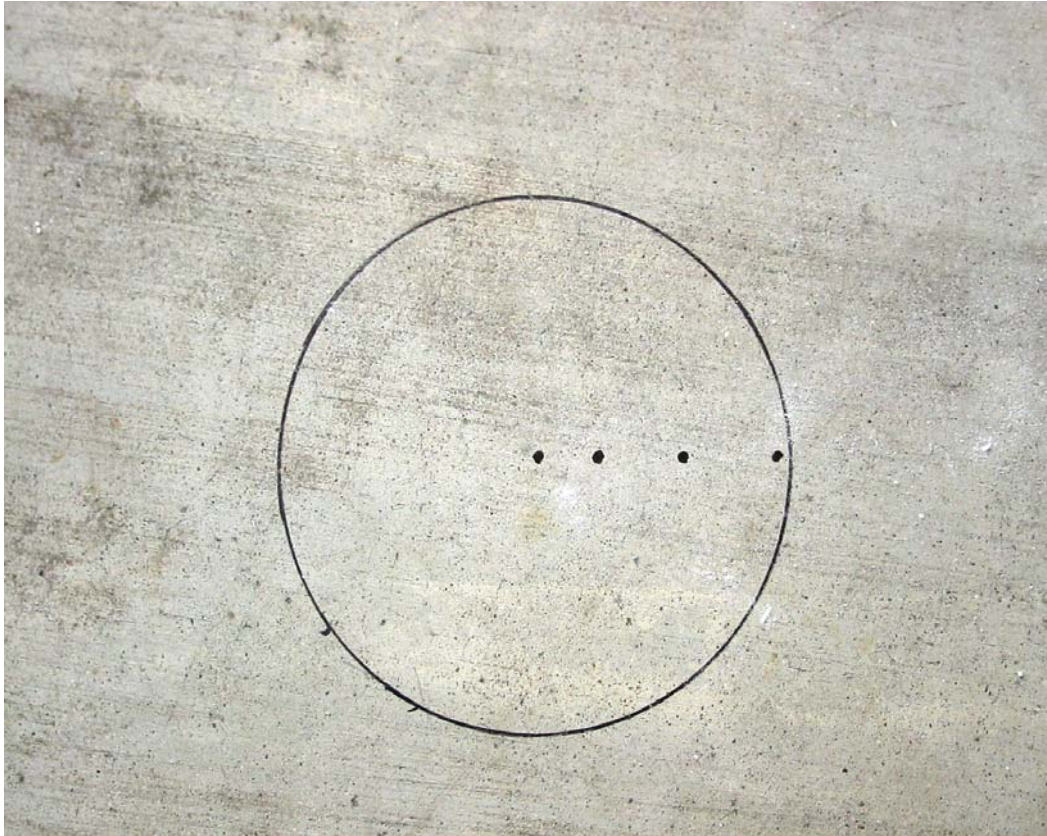


Fig.5.17 Three Locations of Gravel

### 5.5.2 Surface with Dent

ABAQUS was used to simulate the case when there is a dent (2.5 mm×2.5 mm) on the soil surface. The dent was created at three locations under BCD: center of BCD, edge of BCD and between center and edge. Simulation results show that there is no big influence on BCD measurements. The mesh of ABAQUS simulation for dent at center of BCD is shown in Fig.5.18. The test result is shown in Table 5.3.

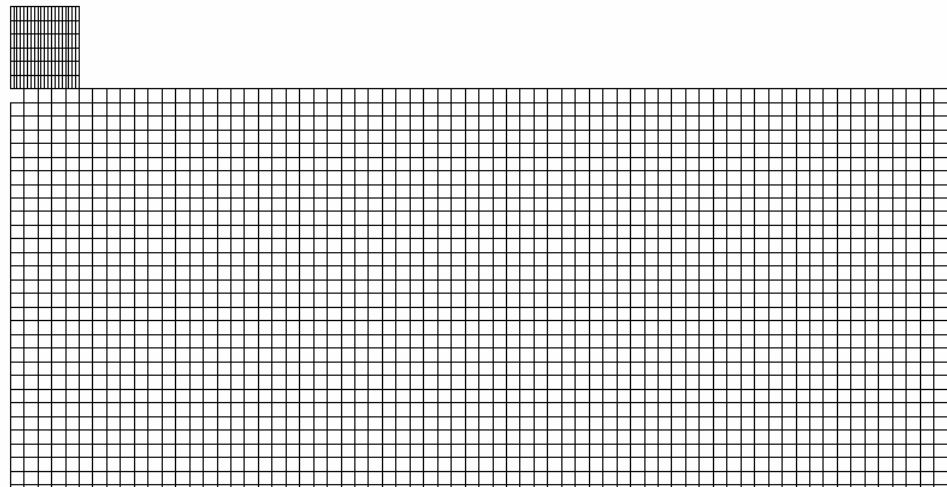


Fig.5.18 Dent at Center of BCD



Table 5.3 ABAQUS Simulation Results with Dent at Three Locations

<b>Location of Dent</b>	<b>Radial Strain</b>	<b>Hoop Strain</b>
No Dent	38.56	24.88
Dent at Center	38.57	24.88
Dent between Center and Edge	38.61	24.89
Dent at Edge	38.56	24.88

### 5.6 Influence of Sand Cushion on BCD Results

To study the influence of sand cushion, a small gravel (2 mm×6 mm) was put on the concrete floor, then a thin layer of moist sand was put in the area of BCD to make the surface flat (Fig.5.19). The gravel was put on the same three locations as in Chapter 5.5.1 and the result is shown in Table 5.4. From Table 5.4, we found that the sand cushion can give similar result as on flat surface (when there is no gravel). So it is not necessary to use sand cushion on flat surface.

When there is gravel in the sand cushion, sand cushion can alleviate the influence of gravel but can't totally eliminate the influence of gravel. So we should always do BCD test on a flat surface. If there is no flat surface in the testing location, we should make the surface relatively flat and then use a sand cushion to ensure the quality of test result.



Fig.5.19 Sand Cushion with Gravel on the Ground

Table 5.4 BCD Test for Bump at Different Locations with Sand Cushion  
(Gravel Size 2 mm×6 mm)

Location of Gravel	Load (lbs)	Hoop Strain
NO Gravel, No Sand Cushion	50.4	-96
	50.5	-96
	50.2	-94
No Gravel with Sand Cushion	50.6	-113
	50.5	-106
	50.8	-80
Gravel at Center with Sand Cushion	50.0	-239
	50.5	-246
	52.2	-256
Gravel between Center and Edge with Sand Cushion	50.6	-274
	49.8	-216
	50.8	-225
Gravel at Edge with sand Cushion	50.5	-123
	53.0	-133
	50.4	-112

### 5.7 Repeatability of BCD

Repeatability of BCD test result is a very important issue when using BCD in the field. Two field tests have been done to check the repeatability of BCD. In this test, BCD tests were done back and forth between two locations in front of CVEN building. At each location, twelve BCD tests were done and the results are shown in Figs. 5.20 and 5.21. The test result shows that the BCD has a very good repeatability and the Coefficient of Variance (COV) is below 4% at both locations.

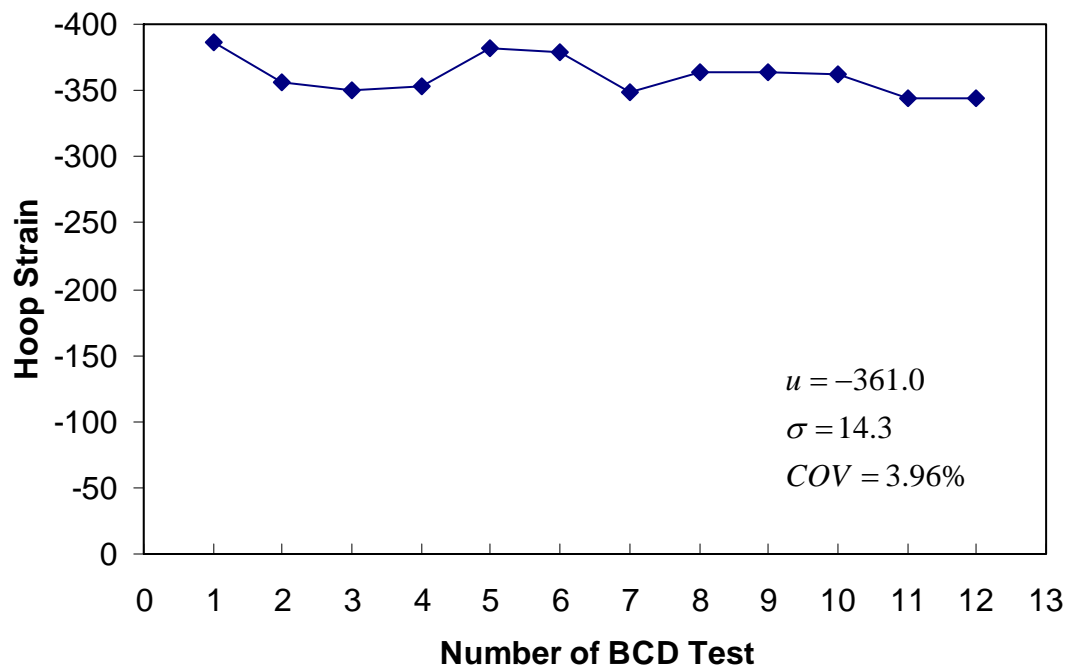


Fig.5.20 Repeatability Test of BCD at Location #1

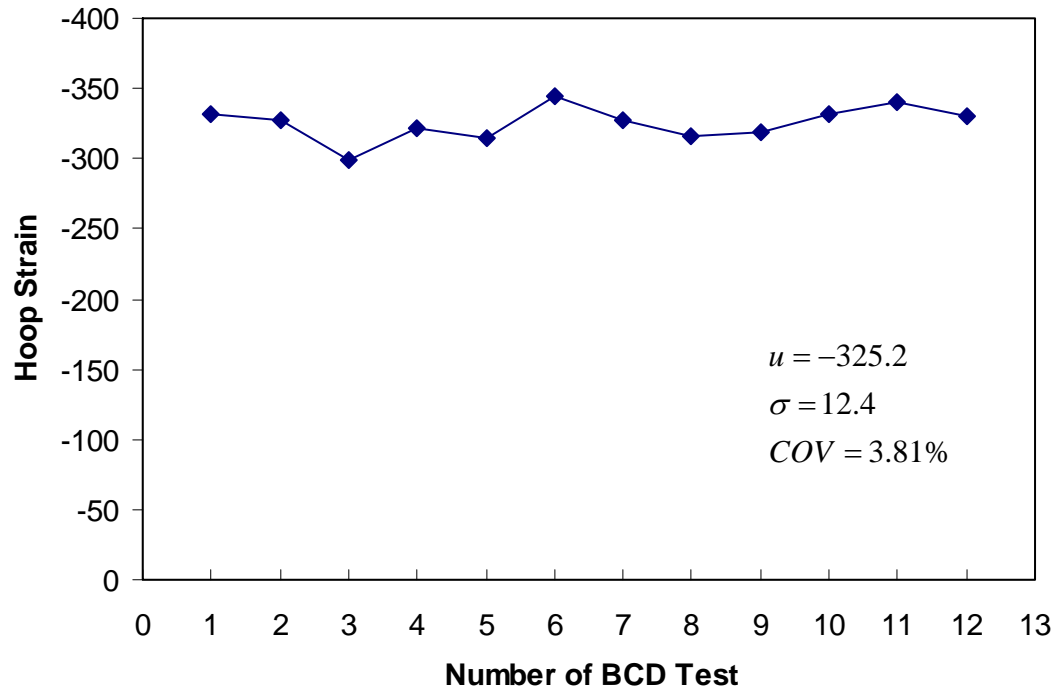


Fig.5.21 Repeatability Test of BCD at Location #2

## 5.8 Calibration of BCD

After long time use of BCD, we must calibrate it to make sure it is working properly. For calibration purpose, two piece of neoprene spring rubber pad were used. The neoprene spring rubber pads were ordered from McMaster-Carr Company ([www.mcmaster.com](http://www.mcmaster.com)). The rubber pad is 1 ft square and 3 inches thick. The tensile strength is 1700 psi and durometer hardness is shore A: 70.

Plate test and BCD test were done on two pads to check if they have same properties. Two rubber pads were laid on concrete floor and the center of each rubber pad was determined before test. The plate of BCD and rigid plate of plate tester were put on the center of rubber pad before the tests. The results of plate test show that rubber pad 1 is 14.65 MPa and rubber pad 2 is 13.88 MPa. Ten independent BCD tests have also been done on each rubber pad (Fig.5.22). The results of BCD tests are in Table 5.5 and Table 5.6. Statistic analysis shows that with 95% confidence, the hoop strain of BCD tests done on rubber pad 1 is in the range of  $-337.7 \pm 10.8$ , while hoop strain of BCD tests done on rubber pad 2 is in the range of  $-331.8 \pm 13.1$ . Both plate test and BCD test show that the two rubber pads have similar material properties and we can use one of them for calibration.

BCD tests were also done when two rubber pads stacked together. The results of BCD tests are in Table 5.7 to 5.8. When pad 1 was put above pad 2, the hoop strain is in the range of  $-319.7 \pm 15.6$ . When pad 2 was put above pad1, the hoop strain is in the range of  $-315.2 \pm 10.4$ .



Fig.5.22 Calibration of BCD

Table 5.5 BCD Test Result on Rubber Pad 1

<b>Load</b>	<b>Hoop Strain</b>	<b>Modified Hoop Strain</b>
50.1	-313	-312.38
50.4	-318	-317.37
50.7	-348	-347.31
51	-332	-331.34
50.1	-350	-349.30
49.8	-346	-345.31
51	-358	-357.29
51	-335	-334.33
50.9	-353	-352.30
50.1	-331	-330.34

Table 5.6 BCD Test Result on Rubber Pad 2

<b>Load</b>	<b>Hoop Strain</b>	<b>Modified Hoop Strain</b>
51.2	-333	-325.20
50.6	-310	-306.32
49.9	-316	-316.63
50.5	-347	-343.56
51.9	-353	-340.08
50.5	-342	-338.61
50.2	-312	-310.76
50.8	-361	-355.31
50.6	-364	-359.68
49.8	-321	-322.29



Table 5.7 BCD Test Result on Rubber Pad 1 above Pad 2

<b>Load</b>	<b>Hoop Strain</b>	<b>Modified Hoop Strain</b>
52.1	-321	-308.06
50.3	-333	-331.01
50.1	-322	-321.36
52.7	-351	-333.02
50.5	-343	-339.60
50.6	-346	-341.90
50.7	-273	-269.23
50.4	-307	-304.56
50	-332	-332.00
51.8	-328	-316.60

Table 5.8 BCD Test Result on Rubber Pad 2 above Pad 1

<b>Load</b>	<b>Hoop Strain</b>	<b>Modified Hoop Strain</b>
50.7	-336	-331.36
51.1	-317	-310.18
50.3	-306	-304.17
50.9	-313	-307.47
50.8	-312	-307.09
51.1	-337	-329.75
50.6	-345	-340.91
50.4	-299	-296.63
50.2	-305	-303.78
50.7	-325	-320.51

To test the possible influence of material under rubber pad to the calibration result, BCD calibration tests were done on rubber pad at three different locations: 1” thick wooden plate, concrete floor and soil. Ten BCD tests were done at each location and the results are listed at Table 5.9-5.11. The hoop strains were modified as to 50 lbs load because the load for each test was not exactly 50 lbs. Statistic analysis shows that with 95% confidence, the hoop strain of BCD tests done on 1” thick wooden plate is in the range of  $-340.5 \pm 12.9$ , on concrete floor, the range is  $-337.2 \pm 13.4$  and on soil, the range is  $-314.5 \pm 12.3$ . The first two tests results are similar and the last test gave different results with the other two. The results show that calibration must be done on some hard layer such like concrete floor.

Table 5.9 Test Result of Rubber Pad on 1” Thick Wooden Plate

<b>Load</b>	<b>Hoop Strain</b>	<b>Modified Hoop Strain</b>
50.2	-362	-360.56
50.2	-320	-318.73
50.1	-324	-323.35
50.4	-321	-318.45
50.2	-343	-341.63
50.1	-357	-356.28
50.2	-323	-321.71
50.1	-355	-354.29
50.7	-356	-351.08
50.1	-360	-359.28

Table 5.10 Test Result of Rubber Pad on Concrete Floor

<b>Load</b>	<b>Hoop Strain</b>	<b>Modified Hoop Strain</b>
50.6	-332	-328.06
51.5	-339	-329.13
52.5	-358	-340.95
51.1	-336	-328.78
50	-337	-337.00
50	-298	-298.00
50.1	-339	-338.32
50.2	-323	-321.71
50.9	-369	-362.48
49.6	-365	-367.94
52.5	-375	-357.14

Table 5.11 Test Result of Rubber Pad on Soil

<b>Load</b>	<b>Hoop Strain</b>	<b>Modified Hoop Strain</b>
52.7	-310	-294.11
51.7	-330	-319.14
53.2	-369	-346.80
50.8	-303	-298.22
51	-332	-325.49
53	-344	-324.52
51.6	-317	-307.17
50	-321	-321.00
52	-331	-318.27
50.4	-293	-290.67

## CHAPTER VI

### LAB TEST OF BCD

#### 6.1. Introduction

Compaction control using dry density as a parameter consists of

1. Performing a laboratory test (ASTM Standard Proctor Test) to obtain the dry density versus water content curve,
2. Establishing the target density and water content values and
3. Verifying that these target values have been obtained in the field by independent measurements.

One of the problems associated with using the modulus as a compaction control parameter instead of the dry density is that there is no established way to obtain a target modulus value. The BCD provides a means of measuring a modulus in the field (step 3) but there are no recommendations on how to obtain the corresponding target modulus value (steps 1 and 2 above). There are two problems associated with this target modulus value:

1. Modulus, unlike dry density, depends on many factors as described in Chapter II
2. The variation of the modulus as a function of the water content has not been studied extensively.

In an effort to solve the target modulus value problem, the author proceeded to perform BCD tests in the laboratory in order to obtain the BCD modulus versus water

content curve. At this time, BCD can just give the strain value and the boundary condition in the laboratory is different from that of the field test case. We can't just use the correlation between soil modulus and pressure/strain developed in Chapter V to calculate the soil modulus in the mold. Plate test was also performed on the compacted soil to get the soil modulus. The relationship between soil modulus from plate test and pressure/strain from BCD is also studied in the laboratory test.

BCD tests were performed in the laboratory on top of a sample compacted inside the proctor mold followed by plate tests. The intent was to develop a soil modulus versus water content curve which would parallel the approach for the dry density versus water content. If successful this modulus versus water content curve would give the target value needed to use in the specifications and needed to be verified in the field.

Until we understand better how the soil modulus is influenced by the water content for many different soils, it will be very difficult to confidently move to a modulus based compaction control. The best way to transition from dry density based compaction control to modulus based compaction control is to find a way to obtain a modulus versus water content curve similar to the dry density curve. The BCD laboratory test or some similar test needs to be developed into a standard test before one can confidently move to a modulus based compaction control.

## **6.2 Lab Test of BCD**

In the lab test of BCD, two compaction molds with label #5 and label #6 were used. Two operators compact the same soil at certain water content in these two molds individually. Both plate test and BCD test were done on two soil samples and the results were compared. After the test, some soil was taken out from the samples to measure the actual water content.

### **6.2.1 Compaction Test in the Lab**

ASTM (D 698-91) covers laboratory compaction procedures used to determine the relationship between water content and dry unit weight of soils compacted in a 4 or 6 inch diameter mold with a 5.5 lbf rammer dropped from a height of 12 inch producing a standard compactive effort of 12,400 ft.lbf/ft<sup>3</sup>. In our lab tests, two 6 inch molds were used because the diameters of BCD and plate tester are both 6 inch.

During the compaction, soil at a selected water content was placed in three layers into a 6 inch mold, with each layer compacted by 56 blows of a 5.5 lbf rammer dropped from a distance of 12 inch, subjecting the soil to a total compactive effort of about 12,400 ft.lbf/ft<sup>3</sup>. A compacted soil sample is shown in Fig.6.1. The resulting dry unit weight is determined. The procedure is repeated for sufficient number of water contents to establish a relationship between the dry unit weight and the water content for the soil. This data, when plotted, represents a curvilinear relationship known as the

compaction curve. The values of optimum water content and standard maximum dry unit weight are determined from the compaction curve.



Fig.6.1 Compacted Soil in Mold

### 6.2.2 BCD and Plate Test on Compacted Soil

After the compaction, BCD tests were done on two soil samples and followed by plate tests. Both tests were done according to the procedures mentioned in Chapter V. The BCD tests were done three times to check the repeatability of test results. Because the diameters of BCD and plate tester are 150 mm which is near to the diameter of proctor mold, contact between the BCD or plate with the edge of mold must be avoided to ensure the quality of test data. The tests are shown in Fig.6.2 and Fig.6.3 respectively.



Fig.6.2 Plate Test on Compaction Mold





### 6.2.3 ABAQUS Simulation of BCD and Plate on Compaction Mold

ABAQUS was used to simulate the BCD and plate test on proctor mold. Two boundary conditions between soil and mold were simulated. One is sliding boundary condition and the other is fixed boundary condition. In fixed boundary condition case, the top nodes were released to sliding and the corresponding coefficients were also given. The meshes of BCD on compaction mold before and after loading are shown in Figs.6.4 and 6.5. The meshes of plate on compaction mold before and after loading are shown in Figs.6.6 and 6.7.

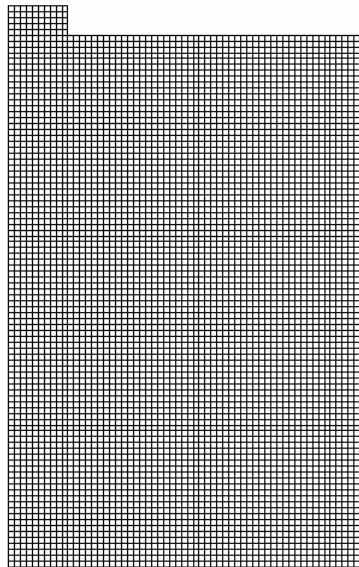


Fig.6.4 Mesh of BCD on Proctor Mold

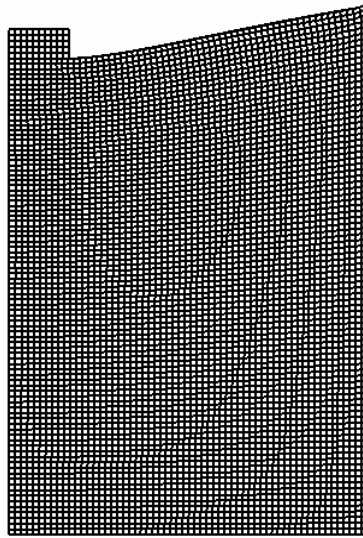


Fig.6.5 BCD on Proctor Mold after Loading (Fixed Boundary)

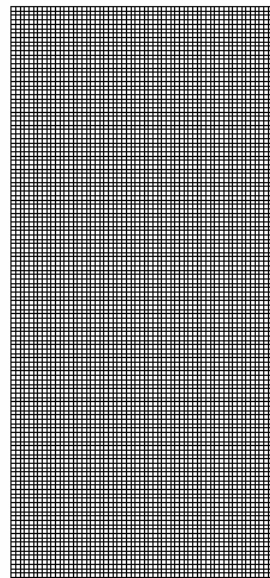


Fig.6.6 Mesh of Plate on Proctor Mold

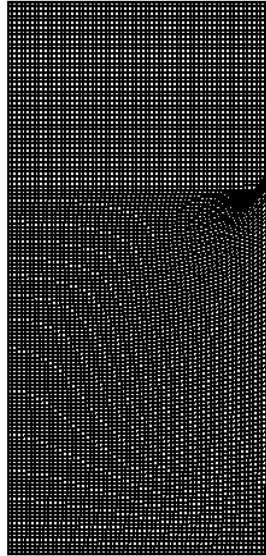


Fig.6.7 Plate on Proctor Mold after Loading (Fixed Boundary)

For plate test on proctor mold, from Eq.5.1, we can get:

$$E_R = I(1-\nu^2) \frac{Q}{BS} \quad (6.1)$$

$E_R$  -Reload soil modulus (20 MPa in simulation);

$I$  -Coefficient depending on the boundary conditions;

$\nu$  -Poisson's ratio (0.35);

$Q$  -Load applied on plate (50lbs=222.73N);

$B$  -Diameter of plate (0.14986m);

$S$  -Settlement of plate

In the numerical simulation, the values of  $E_R$ ,  $\nu$ ,  $Q$  and  $B$  have been given. Based on the output of settlement  $S$  under different boundary conditions, we can calculate the corresponding coefficient  $I$ .

For fixed boundary condition: settlement of plate  $S = 1.144 \times 10^{-5}$  m,  $I = 0.1754$

For sliding boundary condition: settlement of plate  $S = 4.3504 \times 10^{-5}$  m,  $I = 0.667$

For free boundary condition: settlement of plate  $S = 6.319 \times 10^{-5}$  m,  $I = 0.969$

From the comparison tests conducted in the laboratory for compacted soil samples in the Proctor mold and out of the mold, we found that the boundary condition for soil in the mold is close to sliding case and the coefficient we should use is  $I = 0.667$ .

#### **6.2.4 ABAQUS Simulation of the Material under Compaction Mold**

To study the influence of material under the compaction mold to the BCD measurement, three moduli of the material under mold were tried in ABAQUS simulation. The mesh of the compaction mold and material under mold is shown in Fig.6.8. The after loading case is shown in Fig.6.9. The soil modulus in the mold is 20 MPa. When the material under the mold is 20 MPa, the hoop strain output from ABAQUS is 55.36. When the modulus of material under mold increased to 1000 MPa, the hoop strain output from ABAQUS decreased to 55.27. Finally, the modulus of material under mold increased to 200000 MPa which is the modulus of steel, the hoop strain output from ABAQUS is 55.26. The ABAQUS simulation shows that the hoop strain from BCD doesn't change much with the modulus of material under the

compaction mold. This means that we can do the BCD on the compaction mold anywhere no matter what is under the mold. This needs to be testified in the future studies.

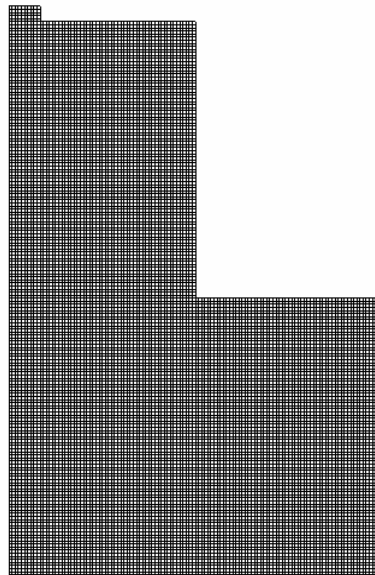


Fig.6.8 Mesh of Mold and Material under Compaction Mold

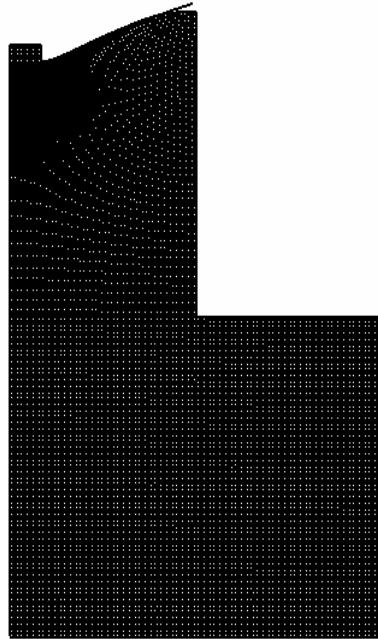


Fig.6.9 Mesh of Mold and Material under Compaction Mold after Loading

### **6.3 BCD Lab Test Result**

Two types of soil have been used in the BCD lab test. One is the soil from National Geotechnical Experimentation Site (NGES) sand site at Texas A&M University riverside campus. The other is a soil mixture of NGES sand and porcelain clay.

### 6.3.1 BCD Lab Test of NGES Sand

For NGES sand, the water content changes from 2% to 12% with the interval of 2%. There are 6 soil samples for each compaction mold. The total number of soil sample is 12.

#### 6.3.1.1 Sieve Analysis of NGES Sand

To study the soil particle distribution of NGES sand, sieve analysis was done according to ASTM D422. In this test, 2000 grams of soil was used. The sieves in order from largest to smallest are listed at Table 6.1.

From the sieve analysis result (Fig.6.10), we know the soil consists of 6.63% gravel, 84.45% sand and 8.92% silt and clay. Effective size  $D_{10}=0.078$  mm,  $D_{30}=0.17$  mm,  $D_{60}=0.27$  mm, Uniformity Coefficient  $C_u=1.59$ , Coefficient of Gradation  $C_c=1.37$ . The NGES sand is poorly graded soil.



Table 6.1 Sieves No. for Sieve Analysis of NGES Sand

Sieve NO.	Opening (mm)
4	4.75
10	2.00
40	0.425
80	0.180
100	0.150
200	0.075

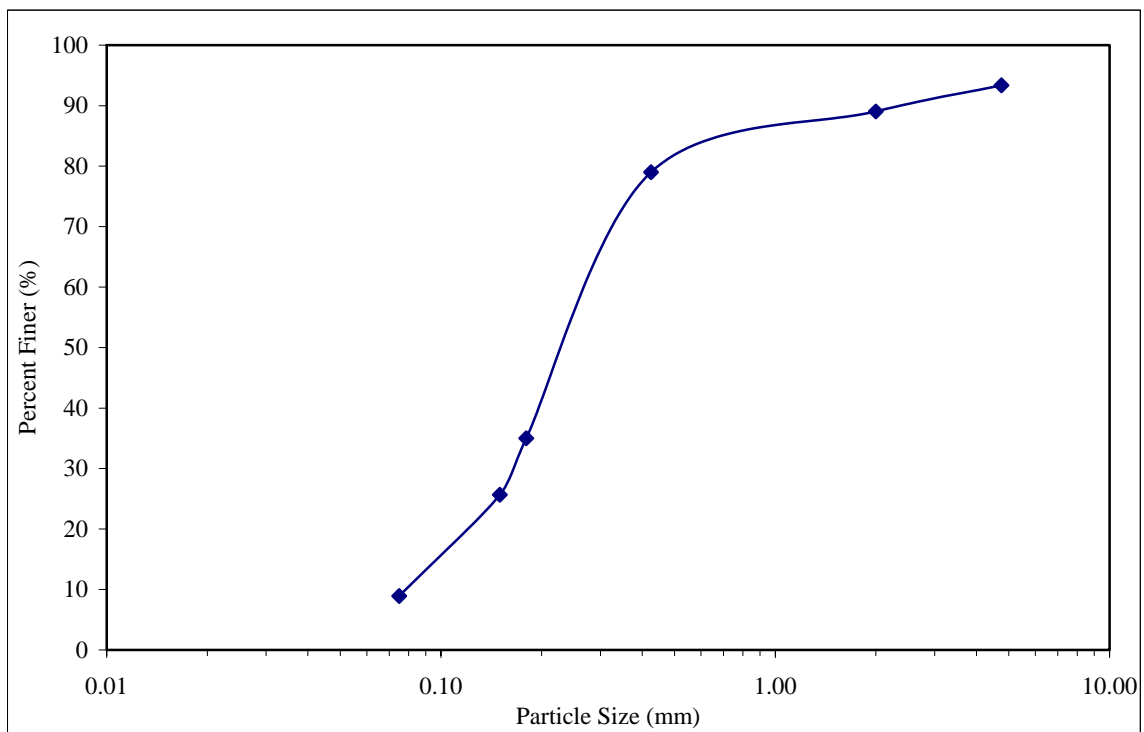


Fig.6.10 Sieve Analysis of NGES Sand

### 6.3.1.2 BCD Lab Test Result of NGES Sand

The compaction curves of NGES sand in two molds are similar to each other (Fig.6.11). From the compaction curves, the optimum water content is about 8% for both molds. The maximum dry unit weight is about  $18.51 \text{ kN}/\text{m}^3$  for mold 5,  $18.75 \text{ kN}/\text{m}^3$  for mold 6.

The plate reload modulus changes with water content. Test results of two molds show the similar trends (Figs.6.12-6.13). Because of suction effect, when water content is smaller than 6%, the plate reload modulus increases with the decrease of water content although the dry unit weight is low for lower water content. When water content is larger than 6%, the suction effect disappears so the plate reload modulus changes in the same trend as the dry unit weight.

Eq.6.1 was used to get the plate reload modulus from plate test. To reasonably reflect the boundary condition between soil and mold, the boundary condition is assumed to be fixed with the top node sliding, so the coefficient  $I$  is 0.4236 in the calculation. The relationship between plate reload modulus and BCD pressure/hoop strain for both molds are shown in Figs.6.14 and 6.15. For mold #6, the correlation is very good with  $R^2 = 0.953$ . But the correlation is not good for mold #5. The reason may be because the diameter of mold #5 is a little smaller than mold #6 which sometimes caused the contact problem between BCD or plate with the edge of mold.

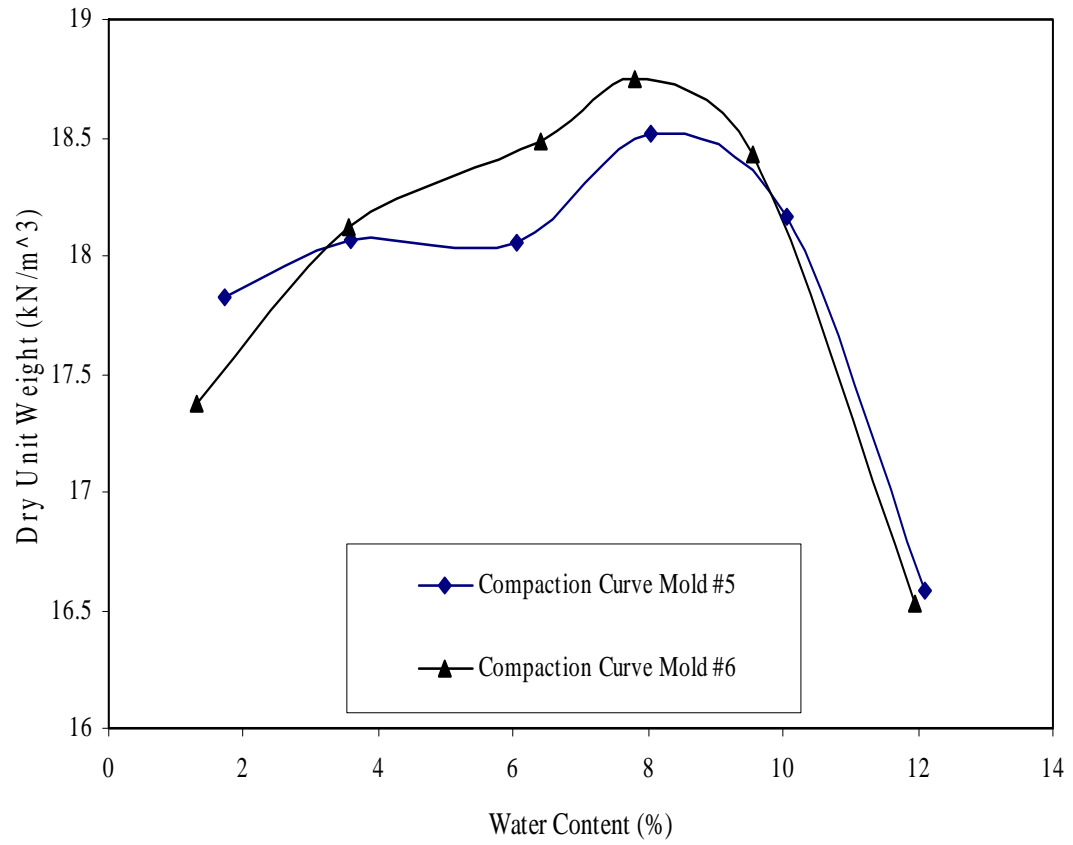


Fig.6.11 Compaction Curve for NGES Sand

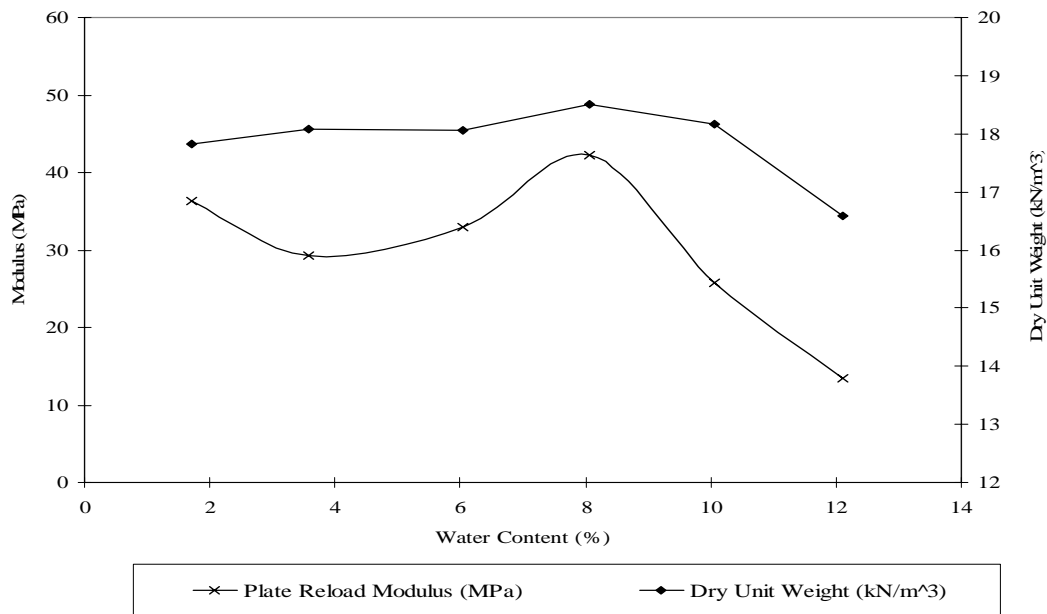


Fig.6.12 Compaction Curve and Plate Modulus vs. Water Content Curve (Mold #5)

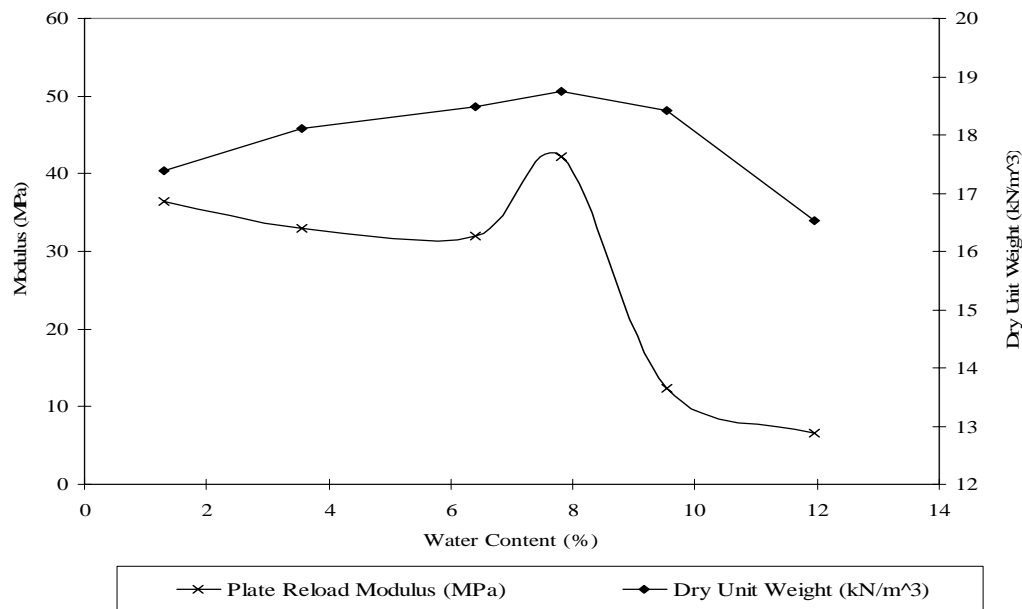


Fig.6.13 Compaction Curve and Plate Modulus vs. Water Content Curve (Mold #6)

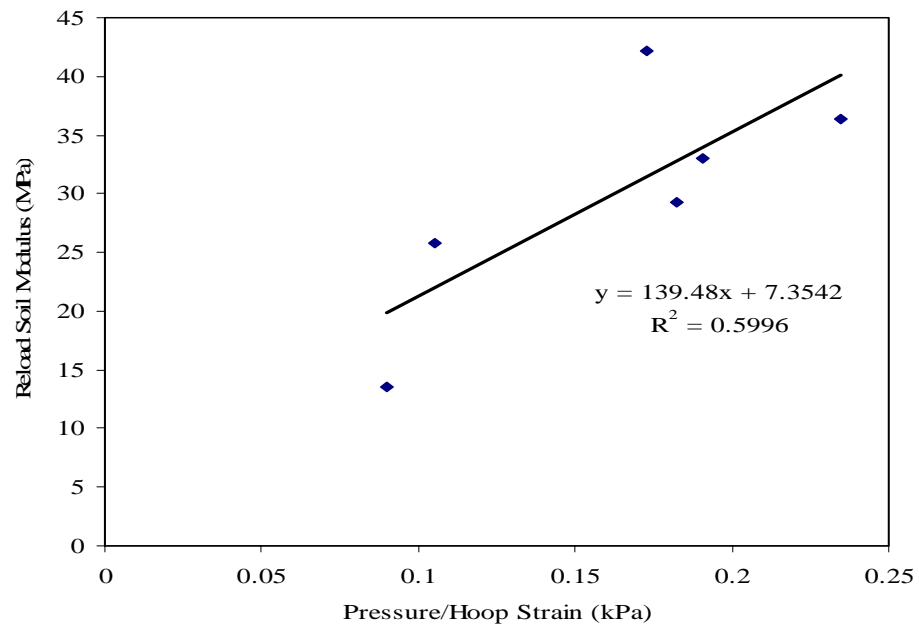


Fig.6.14 Relationship between Plate Modulus and Pressure/Hoop Strain (Mold #5)

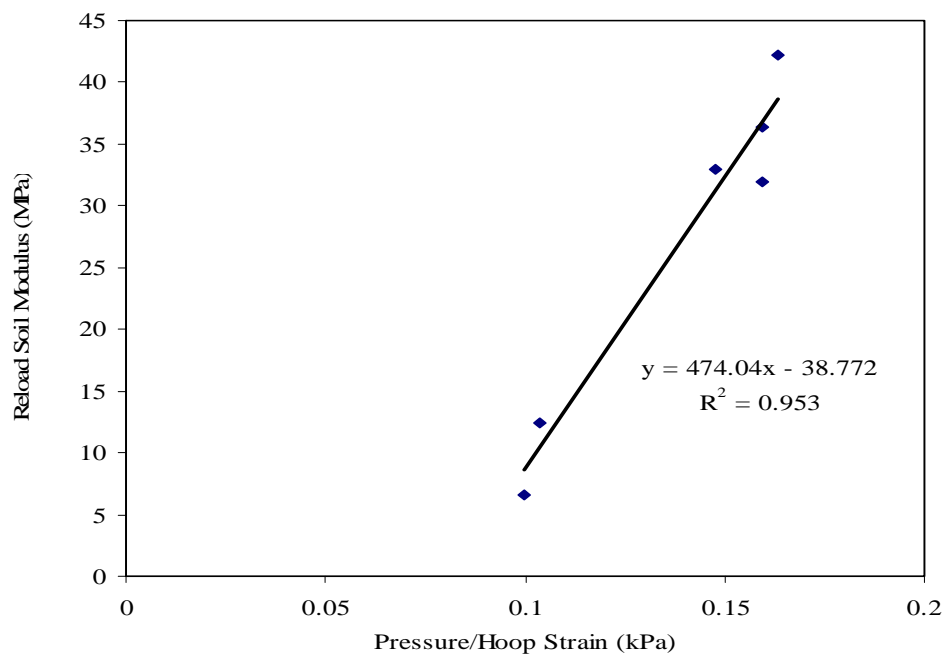


Fig.6.15 Relationship between Plate Modulus and Pressure/Hoop Strain (Mold #6)

### 6.3.2 BCD Lab Test of Mixture of NGES Sand and Porcelain Clay

A new soil was made by mixing the NGES sand with porcelain clay in certain ratio. The water content changes from 4% to 14% with the interval of 2%. There are 6 soil samples for each compaction mold. The total number of soil sample is 12.

#### 6.3.2.1 Sieve Analysis of Mixture of NGES Sand and Porcelain Clay

Based on the sieve analysis of NGES sand, a certain amount of porcelain clay was added to NGES sand and the fine content (passing #200) in the new soil is 40%. The sieve analysis result is shown in Fig.6.16.

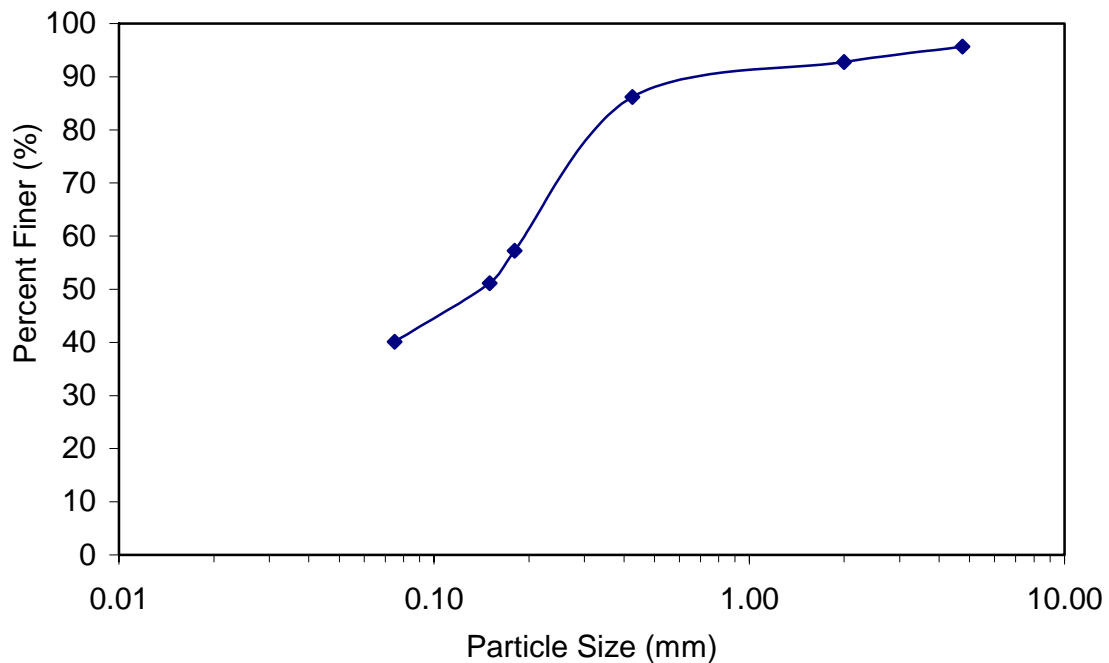


Fig.6.16 Sieve Analysis of Mixture of NGES Sand and Porcelain Clay

### 6.3.2.2 Lab Test Result of Mixture of NGES Sand and Porcelain Clay

The compaction curves of mixture of NGES sand and porcelain clay in two molds are similar to each other (Fig.6.17). Both of them are double peak curves. From the compaction curve, the optimum water content is about 11% for both molds. The maximum dry unit weight is about  $19.01 \text{ kN}/\text{m}^3$  for mold 5,  $19.19 \text{ kN}/\text{m}^3$  for mold 6.

The plate reload modulus changes with water content. Test results of two molds show the similar trends (Figs.6.18-6.19). The highest plate modulus happened around 6%, which is 5% smaller than the optimum water content. When water content smaller than 8%, plate reload modulus change in the same trend as dry unit weight.

The relationship between plate reload modulus and BCD pressure/hoop strain for both mold are shown in Figs.6.20 and 6.21. Because we changed the diameter of plate tester to avoid the contact problem, there are good correlations for both mold #5 and mold #6.

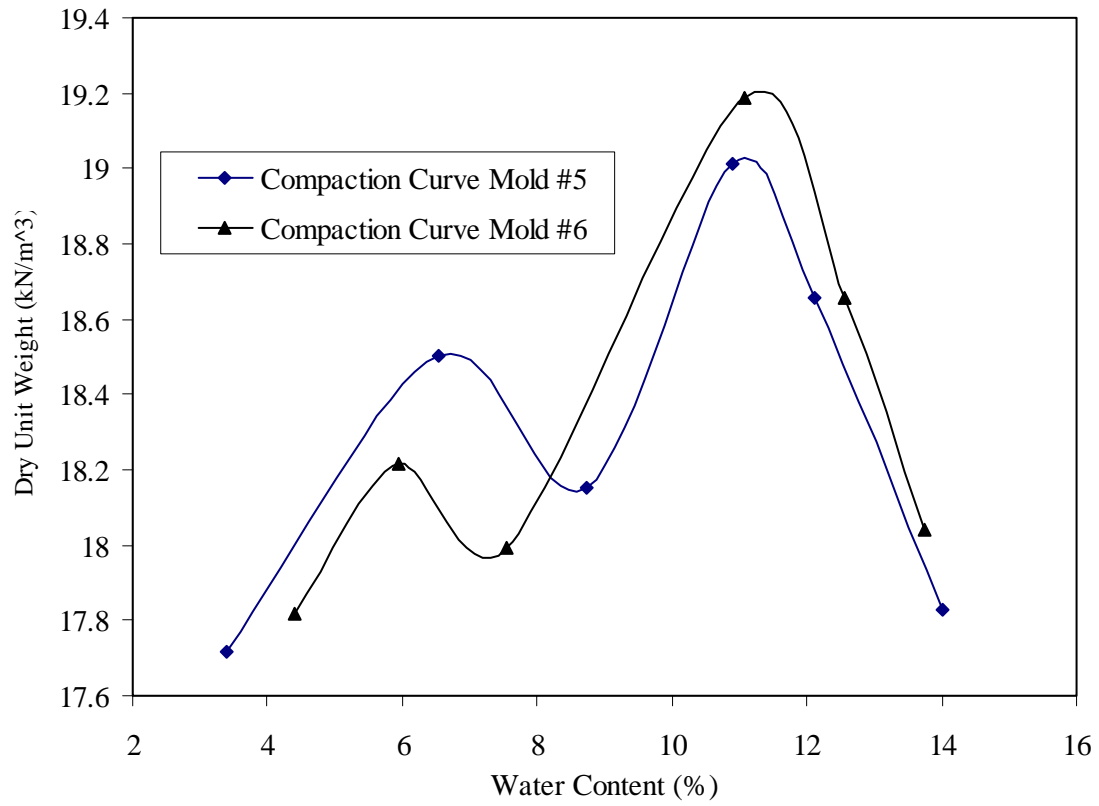


Fig.6.17 Compaction Curve for Mixture of NGES Sand and Porcelain Clay



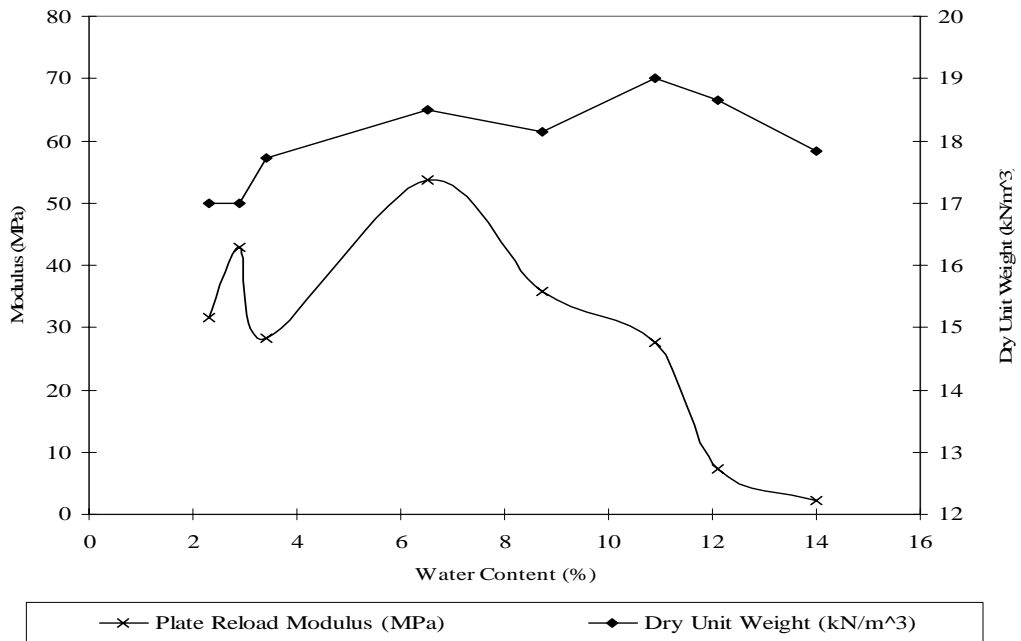


Fig.6.18 Plate Modulus and Dry Unit Weight Change with Water Content (Mold #5)

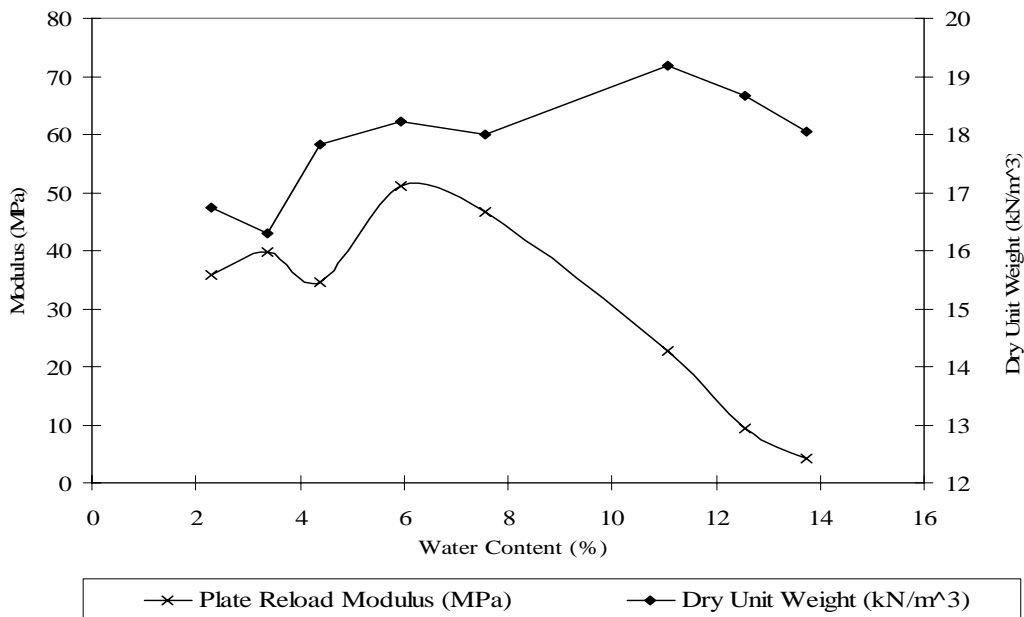


Fig.6.19 Plate Modulus and Dry Unit Weight Change with Water Content (Mold #6)

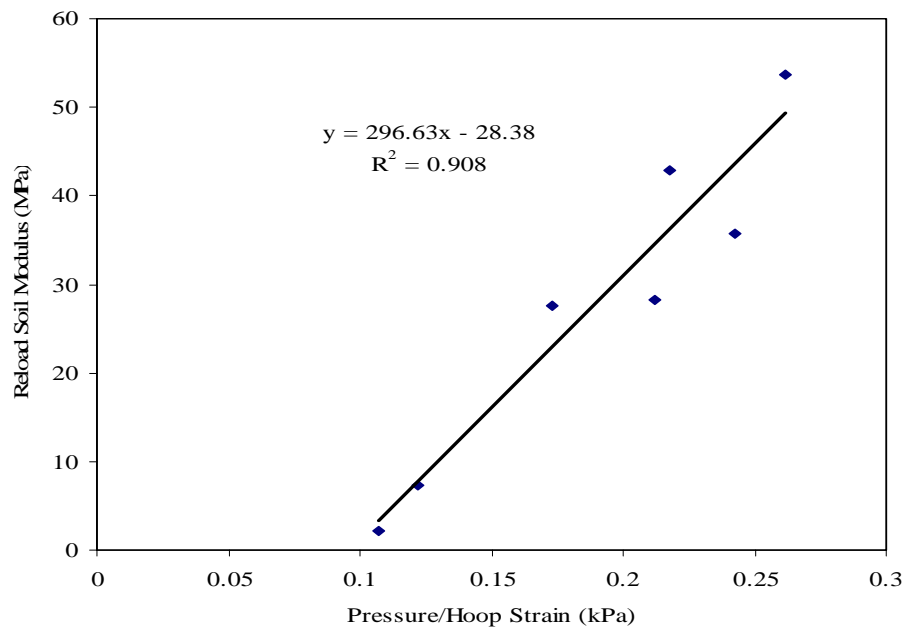


Fig.6.20. Relationship between Plate Modulus and Pressure/Hoop Strain (Mold #5)

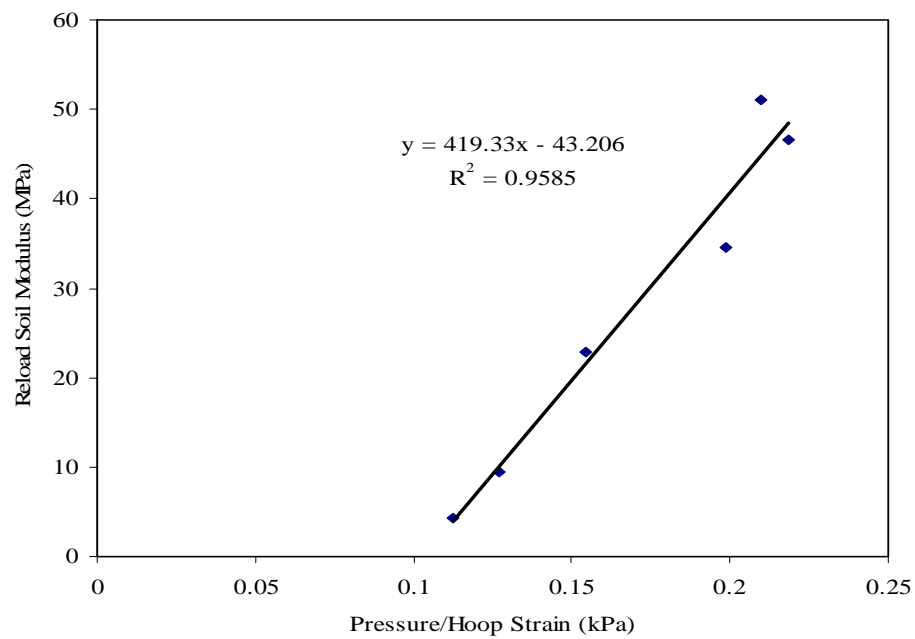


Fig.6.21. Relationship between Plate Modulus and Pressure/Hoop Strain (Mold #6)

### 6.3.3 Combined Results for NGES Sand and Mixture of NGES Sand and Clay

The test results for two types of soil were combined and the relationship between reload plate modulus and pressure/hoop strain for two molds are shown in Figs.6.22 and 6.23. The data for mold #6 shows a better correlation than mold #5 because of the possible contact problem happened on mold #5. The laboratory test needs to be done on more types of soil and the influence of mold on the test result also needs to be studied in the future research.

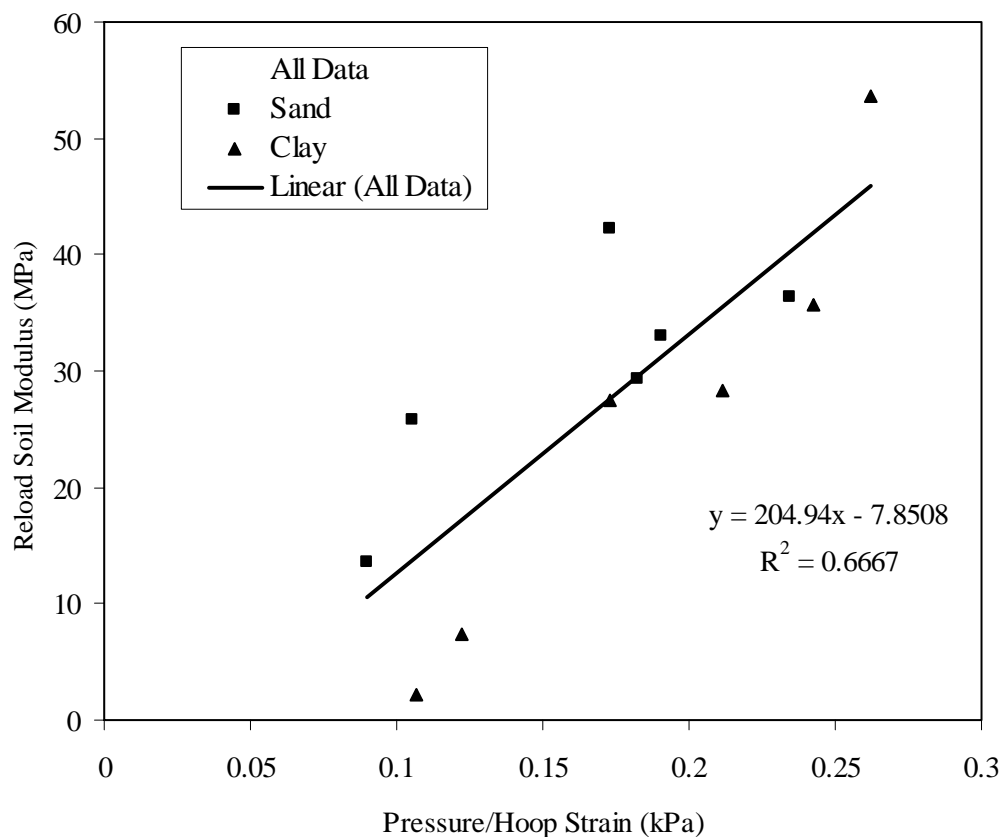


Fig. 6.22 Relationship between Plate Modulus and Pressure/Hoop Strain (Mold #5)

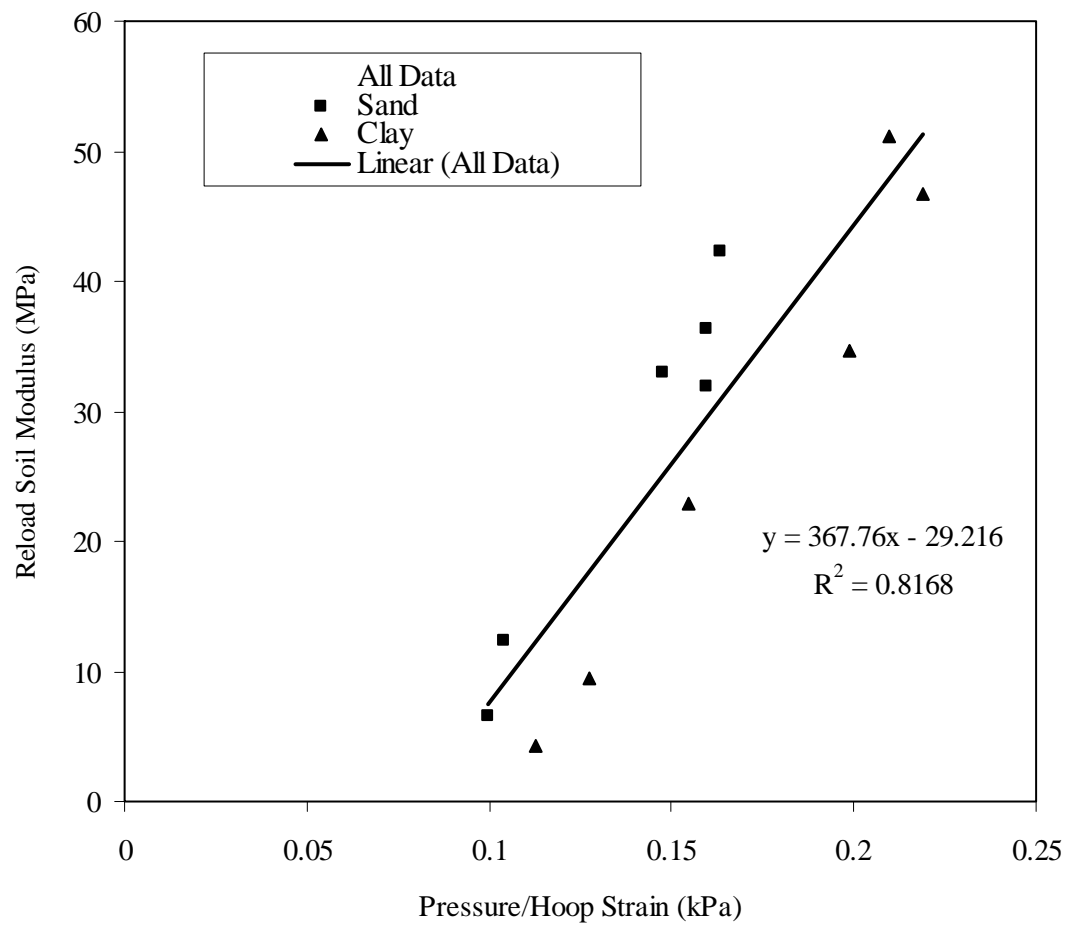


Fig.6.23 Relationship between Plate Modulus and Pressure/Hoop Strain (Mold #6)

## **CHAPTER VII**

### **CONCLUSIONS AND RECOMMENDATIONS**

#### **7.1 Conclusions**

Soil compaction is very important in the construction of highways, airports, buildings and bridges. Currently compaction is controlled by measuring the dry density and the water content of the compacted soil and checking that a target value has been achieved. There is a very strong trend towards measuring the soil modulus instead or in addition to density because the density measurements are made using nuclear density meter, an undesirable tool in today's political environment.

Although there are many apparatus to measure the soil modulus/stiffness in field such as FWD, SPA, DCP and Geogauge, there is a strong need for a lightweight and inexpensive device which can measure the soil modulus fast and accurately.

In response to this need, Briaud Compaction Device (BCD) was invented by Dr. J.L. Briaud in 2002. Since then, two prototypes of BCD have been made. Many numerical simulations have been run to simulate the BCD behavior on soil. BCD test and plate test of the same size have been done in the field to validate the design. BCD tests were done on surface with bump to study the influence of uneven contact surface. A procedure for calibrating BCD was developed by doing BCD on a rubber pad. BCD tests were also done with plate tests on Proctor mold to study the validity of BCD in the laboratory.

The following are the conclusions made from the results obtained in this study.

1. The modulus of a soil is a very complex parameter which depends on many factors. The modulus used in pavement design is very different from the modulus used for embankment settlement or MSE wall backfill compression. Any modulus based compaction control must use a target value and a verification tool consistent with the purpose of the geo-structure.
2. The BCD was invented by Dr. J.L. Briaud and it provides an alternative to control compaction by modulus approach rather than dry density.
3. The depth of influence of BCD is about 120 mm to 310 mm for different soil moduli. The measuring range of BCD is between 5 MPa and 300 MPa.
4. BCD tests and the plate tests have been done at 18 locations. The plate reload modulus and pressure/hoop strain from BCD are correlated on Fig.5.9 with the linear regression  $R^2$  of 0.8894. The correlation is going to be integrated into BCD to show the soil modulus directly on the display of BCD. There is an intercept in the plot of reload modulus vs. pressure/hoop strain due to the interaction between plate and soil.
5. The strain gauges in the radial direction of BCD didn't work very well. One of the reasons is because the locations of these strain gauges are on the place where radial strain changes drastically while hoop strain keeps relatively constant.
6. Doing BCD test on a surface with bump such as a gravel will have big influence on the test result. The bigger the bump, the higher the influence will be. The

location of the bump also has influence on the result. Numerical simulation shows that the surface with a dent has very small influence on the test result.

7. For uneven surface, using a sand cushion can alleviate but can't totally eliminate the influence of bump. If there is no flat surface in the testing location, we should make the surface relatively flat and then use a sand cushion to ensure the quality of test result. Good contact between BCD and soil surface is very important for quality of BCD test results. The surface should be flat enough to get a good test result. This is probably due to the extremely small strain level happened on BCD during testing.
8. For calibration, BCD test can be done at the center of a rubber pad lying on a hard surface such as a concrete floor. The test result should in a certain range to ensure the BCD is working properly.
9. In BCD laboratory test, the modulus versus water content curve was given for two types of soil. When water content is smaller than certain value, the soil modulus gets higher for lower water content due to suction effect. The correlation between reload soil modulus from plate test and pressure/hoop strain from BCD is relatively good for both molds. The small difference in diameters of molds may have influence on the BCD test results.

## 7.2 Recommendations

BCD tests have been conducted at various locations in the field. The correlation between plate reload soil modulus and pressure/hoop strain of BCD is very strong and this demonstrated the validity of BCD. In addition, BCD tests have also been performed on Proctor mold in the laboratory to establish the modulus versus water content curve.

The following are recommended areas for future research:

1. The Briaud Compaction Device-BCD test should be conducted on more soil types at more locations in the field and improved with respect to the accuracy.
2. There is an urgent need to develop a convenient (laboratory) test to obtain a target modulus (and water content) value which would be part of field specifications for modulus based compaction control. This test would be to the modulus what the Proctor test is to the dry density. More laboratory tests with different soil types need to be done to establish the correlations of BCD and plate test on Proctor mold. The influence of different Proctor mold also needs to be studied.
3. The techniques to test soil moisture such like TDR should be integrated into BCD because we can't control the soil compaction by modulus alone. Modulus could be high when the material is loose (dry fine grained soil). It is likely that a combination of modulus and water content will provide a valid compaction control scheme but this needs to be proven.
4. It is highly recommended to measure the soil modulus (in addition to dry density and water content) on compaction jobs because it is the design parameter of choice.



## REFERENCES

- ABAQUS User's and Theory Manuals* (2000). Version 6.1, Hibbit, Karlson & Sorensen, Inc., Pawtucket, RI.
- ASTM D1883-99 "Standard test method for CBR (California Bearing Ratio) of laboratory-compacted soils." *Annual Book of ASTM Standards*, Vol.04.08, American Society for Testing and Materials, West Conshohocken, PA.
- ASTM D4694-96 "Standard test method for deflections with a falling-weight-type impulse load device." *Annual Book of ASTM Standards*, Vol.04.03, American Society for Testing and Materials, West Conshohocken, PA.
- ASTM D5874-02 "Standard test method for determination of the Impact Value (IV) of a soil." *Annual Book of ASTM Standards*, Vol.04.09, American Society for Testing and Materials, West Conshohocken, PA.
- ASTM D6758-02 "Standard test method for measuring stiffness and apparent modulus of soil and soil-aggregate In-place by an Electro-Mechanical method." *Annual Book of ASTM Standards*, Vol.04.09, American Society for Testing and Materials, West Conshohocken, PA.
- Briaud, J. L. (2001). "Introduction to soil moduli." *Geotechnical News*, Vol.19.02 BiTech Publishers, Richmond, B.C., Canada.
- Briaud, J. L., Jaynes, N., Rhee, K. and Li, Y. (2003). *Geogauge and compaction control*. Research report for Federal Highway Administration, Washington, DC.

- Chen, D.-H. and Bilyeu, J. (1999). "Comparison of resilient moduli between field and laboratory testing: a case study." Internal Document, Texas Department of Transportation, Design Pavement Section, Austin, TX.
- Das, B. M. (1998). *Principles of Geotechnical Engineering*, 4<sup>th</sup> Edition. PWS Publishing Company, Boston, MA.
- Duncan, J. M., and Chang, C-Y. (1970). "Nonlinear analysis of stress and strain in soils." *J. Soil Mech. And Found. Div.*, ASCE, 18(5), 495-498.
- Eduard, V. and Theodor, K. (2001). *Thin Plates and Shells*, Marcel Dekker, Inc., New York.
- Fleming, P.R. (2000). "Small-scale dynamic devices for the measurement of elastic stiffness modulus on pavement foundations." *Nondestructive Testing of Pavements and Backcalculation of Moduli*, ASTM STP, Vol.3, 1375.
- Holtz, R. D and Kovacs, W. D. (1981). *An Introduction to Geotechnical Engineering*, Prentice-Hall, Englewood Cliffs, NJ.
- Janbu, N. (1963). "Soil compressibility as determined by oedometer and triaxial tests." *ECSMFE*, Weisbaden, Germany, 1, 19-25.
- Liu, C. and Evett, J. B. (2001). *Soils and Foundations*, 5<sup>th</sup> Edition. Prentice Hall. Englewood Cliffs, NJ.
- McKane, R. (2000). "In situ field testing of mechanical properties." University of Minnesota 48th Annual Geotechnical Engineering Conference-Young Engineer Paper Competition, Obtained by Mel Main-Humboldt Mfg. Company, 7300 West Agatite, Norridge, IL. 60706.

Nebraska Department of Roads. "NDR standard method T205."

([www.nebraskatransportation.org](http://www.nebraskatransportation.org), date of access: 05/28/2004).

Petersen, L. Peterson, R. and Nelson, C. (2002). "Comparison of Quasi-Static Plate Load Test with the Humboldt Geogauge." Internal Document, CNA Consulting Engineers. Obtained from Mel Main, Humboldt Mfg. Company, 7300 West Agatite, Norridge, IL.

Roger, F. and Ladd, C.C. (1981) "Undrained settlement of plastic and organic clays." *Journal of Geotechnical Engineering*, ASCE, Vol. 107, No. 8, 1079-1095.

Sargand, S.M., Edwards, W.F. and Salimath, S. (2001). "Evaluation of soil stiffness via non-destructive testing-final report." Ohio Research Institute for Transportation and the Environment, Athens, OH.

Timoshenko, S. (1987) *Theory of Plates and Shells*, McGraw-Hill, Inc., New York.

### **Supplemental Sources**

Jaynes, N. (2002). "The Humboldt Geogauge research." Master of Engineering Report, Department of Civil Engineering, Texas A&M University, College Station.

Nazarian, S., Baker, M.R., and Crain, K. (1993). "Fabrication and Testing of a Seismic Pavement Analyzer." *SHRP Report H-375*. SHRP, National Research Council, Washington, DC.

- Rhee, K. (2004). "Geogauge test in laboratory and ring plate test." Master of Engineering Report, Department of Civil Engineering, Texas A&M University, College Station.
- Seyman, E. (2003). "Laboratory evaluation of in-situ tests as potential quality control/quality assurance tools." M.S. Thesis, Civil and Environmental Engineering Department, Louisiana State University, Baton Rouge, LA.
- Yuan, D., Nazarian, S., Chen, Dar-Hao, and Hugo, F. (1997). "Use of seismic pavement analyzer to monitor degradation of flexible pavement under Texas mobile load simulator." *Transportation Research Record No.1615*. Transportation Research Board. Washington DC. 3-10.

## APPENDIX A

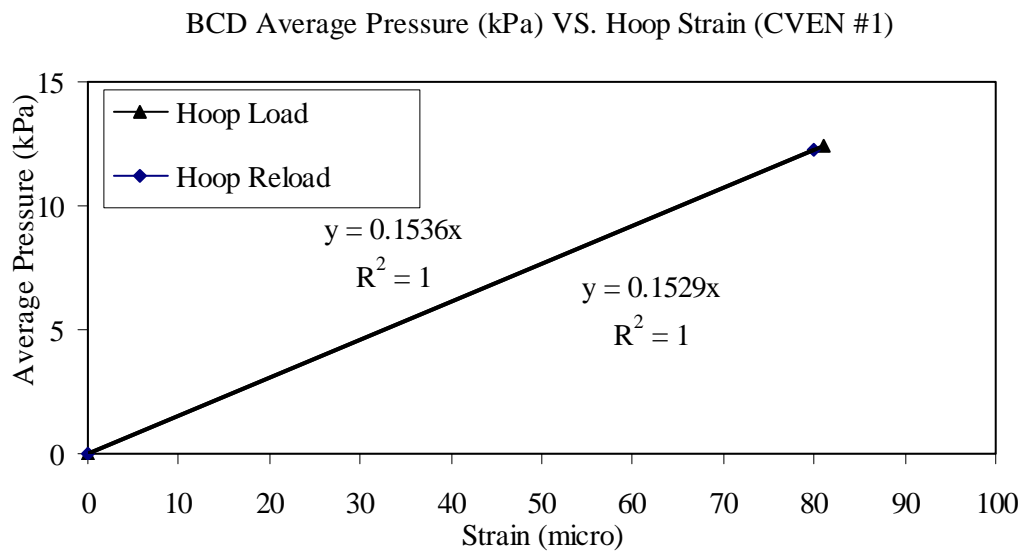
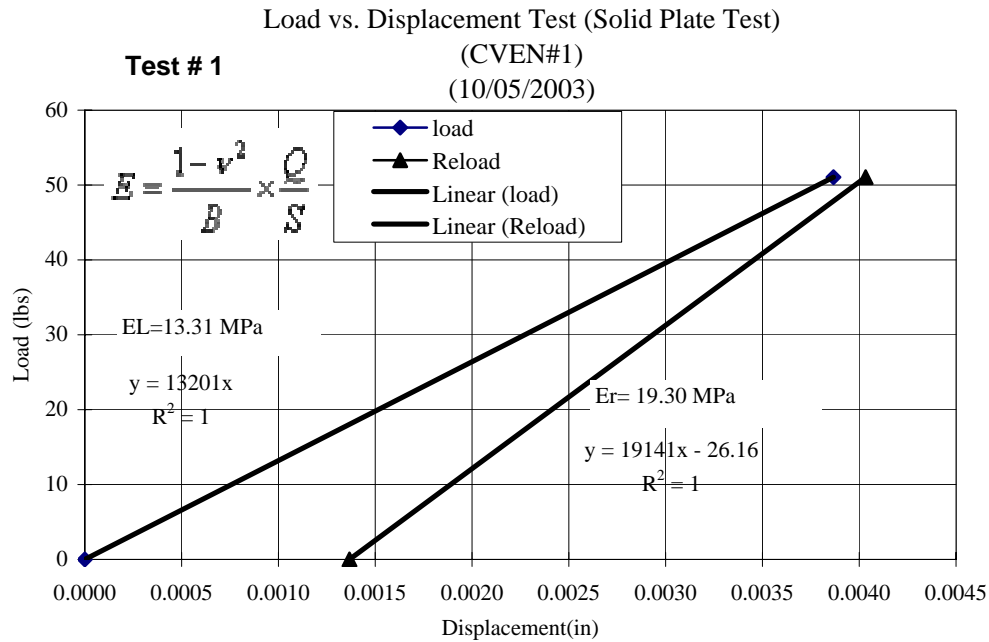
### Rigid plate and BCD Field Test Data Table

Test No.	Site Name	Site Location	Date	Ground Type	Test Description	Load Modulus (Mpa)	Reload Modulus (MPa)	BCD Load Pressure/Hoop Strain (kPa)	BCD Reload Pressure/Hoop Strain (kPa)
1	TAMU CVEN Building Front	College Station TX	10/5/03	Natural ground	Site #1	13.31	19.3	0.1529	0.1536
2	TAMU CVEN Building Front	College Station TX	10/5/03	Natural ground	Site #2	10.8	15.29	0.1457	0.1407
3	TAMU CVEN Building Front	College Station TX	10/5/03	Natural ground	Site #3	12.25	16.43	0.1618	0.1549
4	TAMU CVEN Building East	College Station TX	10/19/03	Natural ground	Site #1	24.13	24.51	0.1011	0.1065
5	TAMU CVEN Building East	College Station TX	10/19/03	Concrete Walkway	Site #2	96.51	96.51	0.4868	0.4345
6	TAMU CVEN Building East	College Station TX	10/19/03	Natural ground	Site #3	27.57	38.6	0.1928	0.2164
7	TAMU Riverside Campus	Bryan TX	10/31/03	4% Cement Treat Base	Site #1	42.89	51.47	0.3288	0.2759
8	TAMU Riverside Campus	Bryan TX	10/31/03	4% Cement Treat Base	Site #2	51.47	57.19	0.2806	0.2746
9	TAMU National Clay Site	College Station TX	11/14/03	Clay	Site #1	9.77	22.71	0.1068	0.1095
10	TAMU National Clay Site	College Station TX	11/14/03	Clay	Site #2	10.31	23.4	0.1563	0.1514
11	TAMU National Clay Site	College Station TX	11/14/03	Clay	Site #3	12.87	23.4	0.1476	0.1500
12	TAMU University Apt.	College Station TX	11/23/03	Road Base	Site #1	32.17	64.34	0.2346	0.2458
13	TAMU University Apt.	College Station TX	11/23/03	Natural ground	Site #2	11.79	28.07	0.1398	0.1376
14	TAMU Parking Lot	College Station TX	11/30/03	Natural ground	Site #1	22.93	87.9	0.2829	0.3184
15	TAMU Parking Lot	College Station TX	11/30/03	Natural ground	Site #2	35.16	75.34	0.2814	0.2973
16	College Station Hensel Park	College Station TX	12/7/03	Road base	Site #1	26.17	34.31	0.1834	0.1943
17	College Station Hensel Park	College Station TX	12/7/03	Road base	Site #2	13.19	28.25	0.2131	0.1902
18	College Station Hensel Park	College Station TX	12/7/03	Road base	Site #3	10.55	29.85	0.1695	0.1717

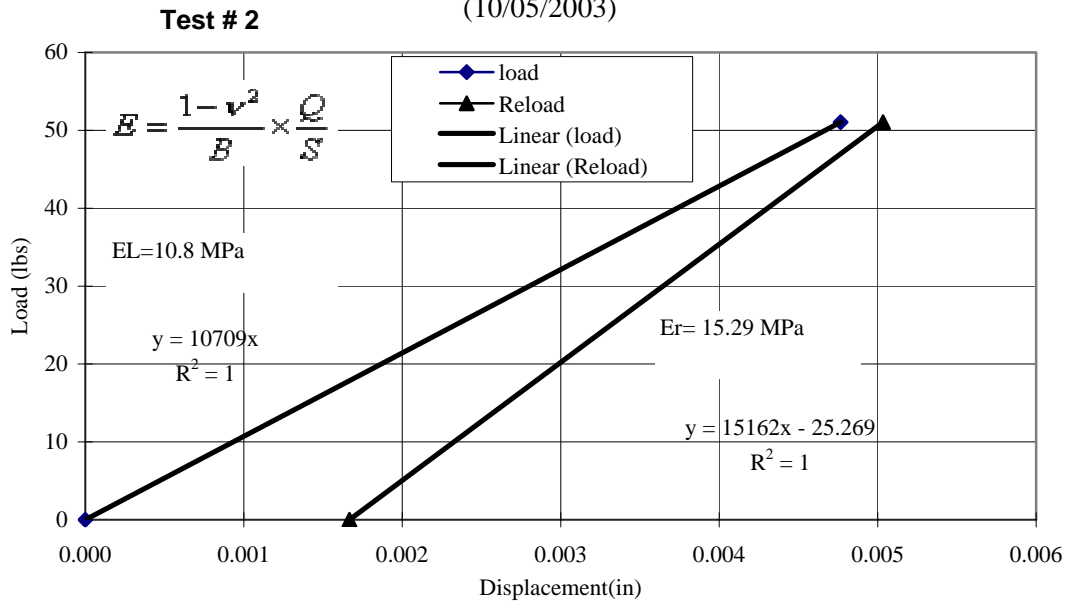
## APPENDIX B

### Plate Test and BCD Hoop Strain Result

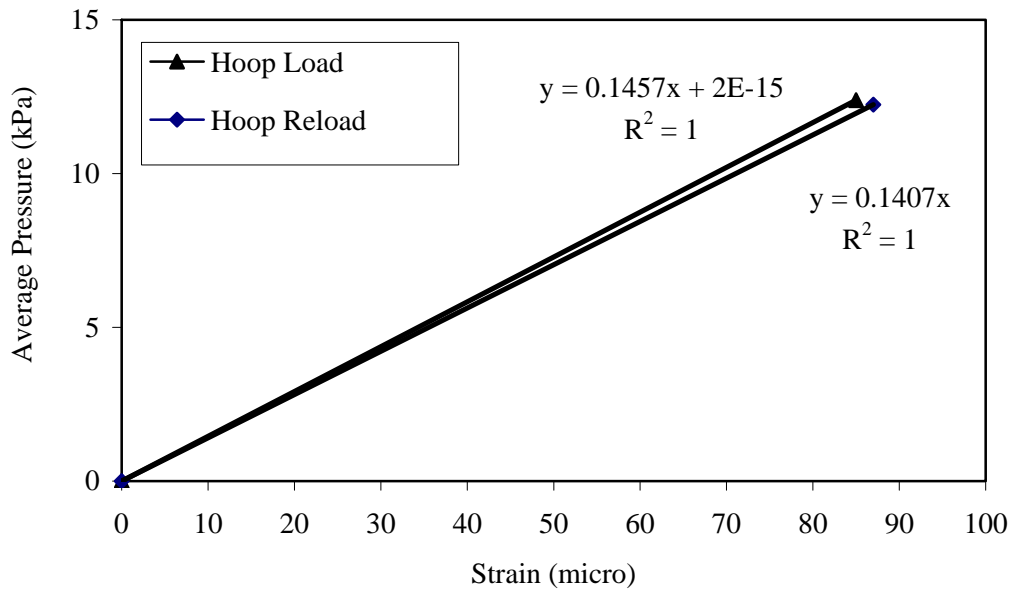
1. TAMU CVEN Building Front



Load vs. Displacement Test (Solid Plate Test)  
(CVEN #2)  
(10/05/2003)



BCD Average Pressure (kPa) VS. Hoop Strain (CVEN #2)

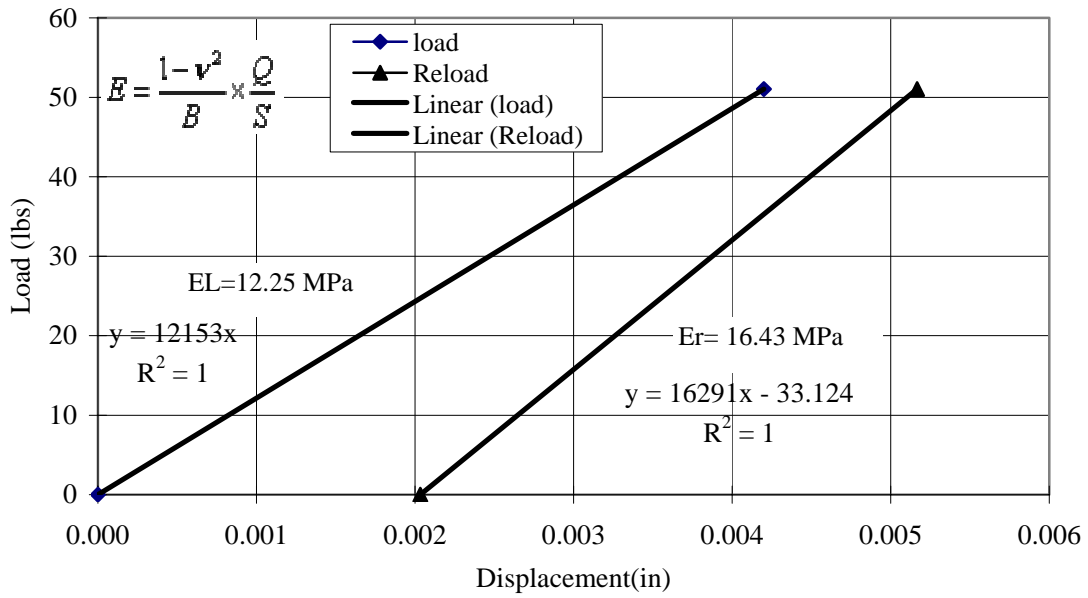


Load vs. Displacement Test (Solid Plate Test)

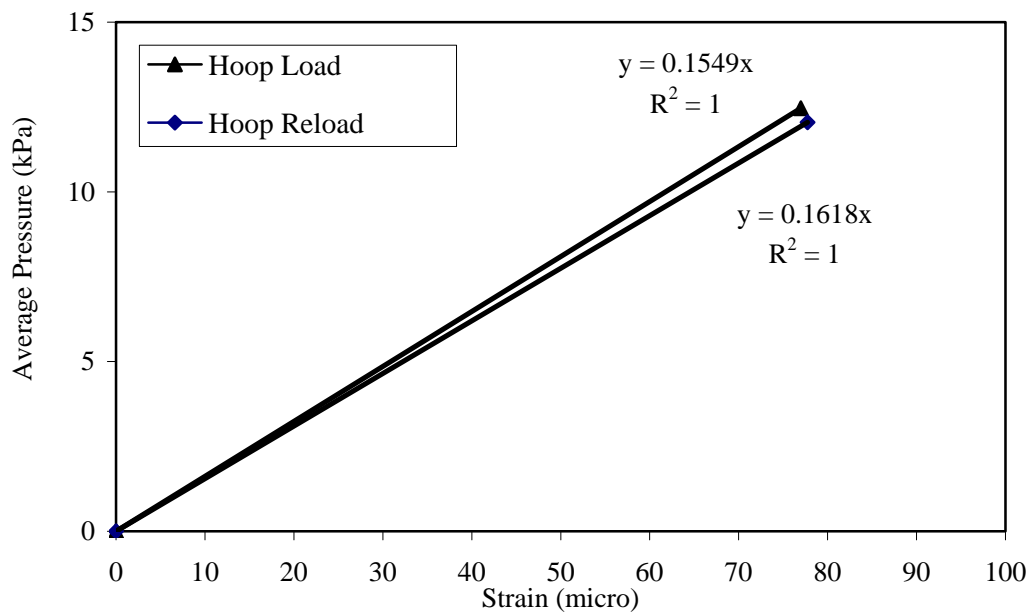
(CVEN #3)

(10/05/2003)

Test # 3

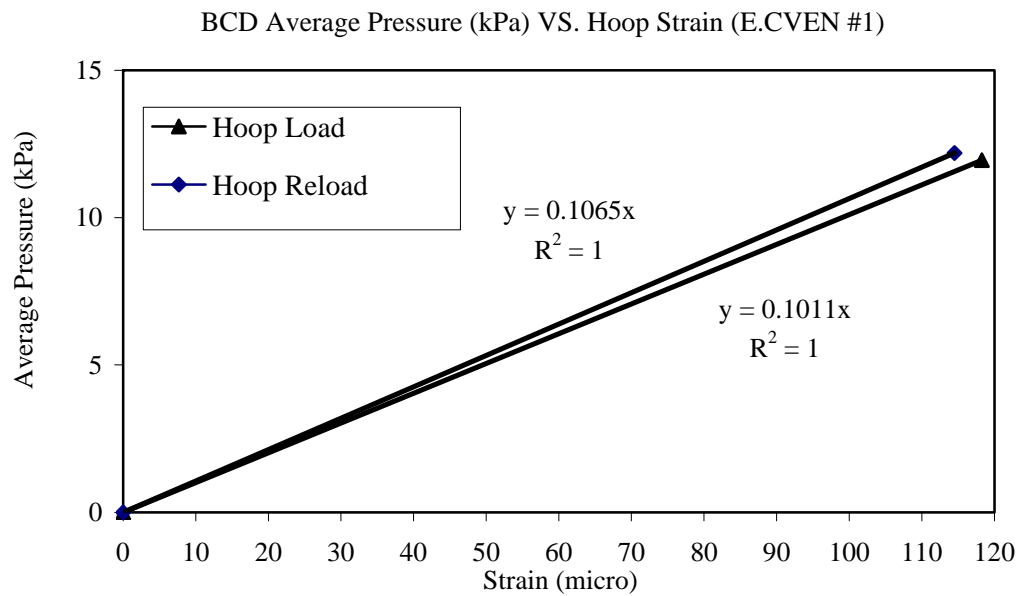
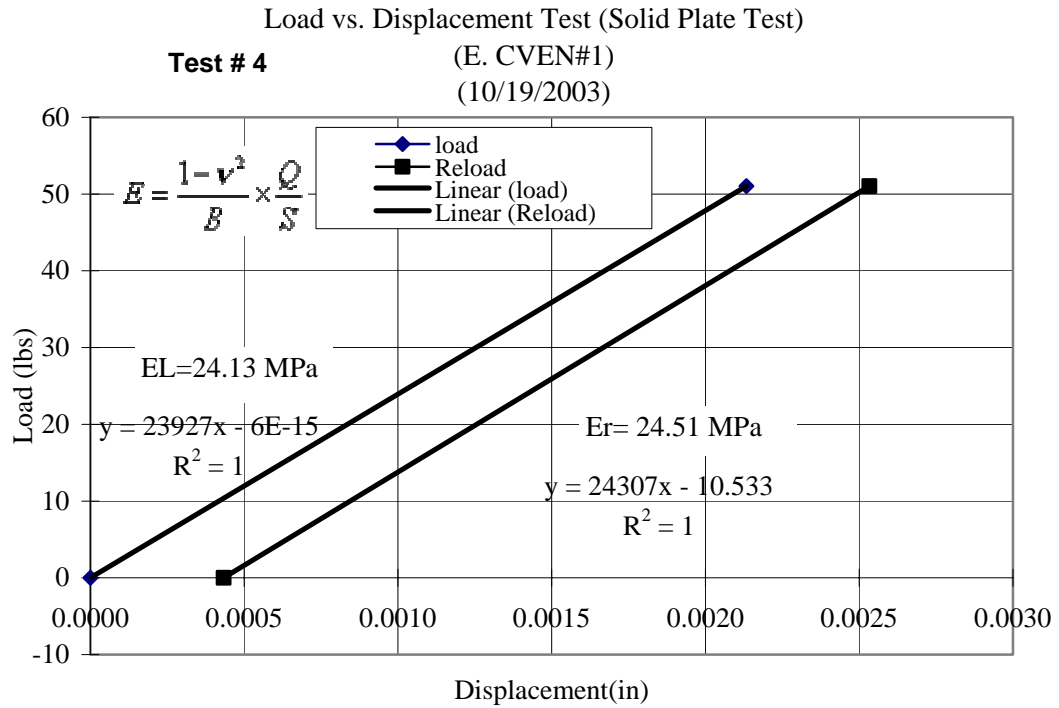


BCD Average Pressure (kPa) VS. Hoop Strain (CVEN #3)

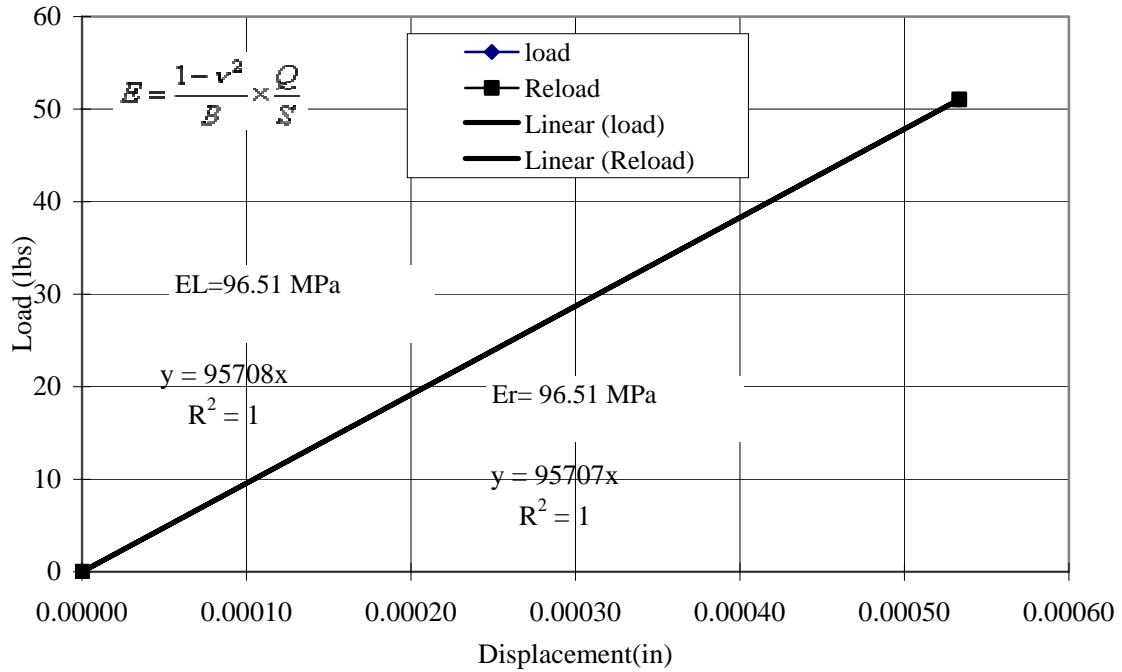




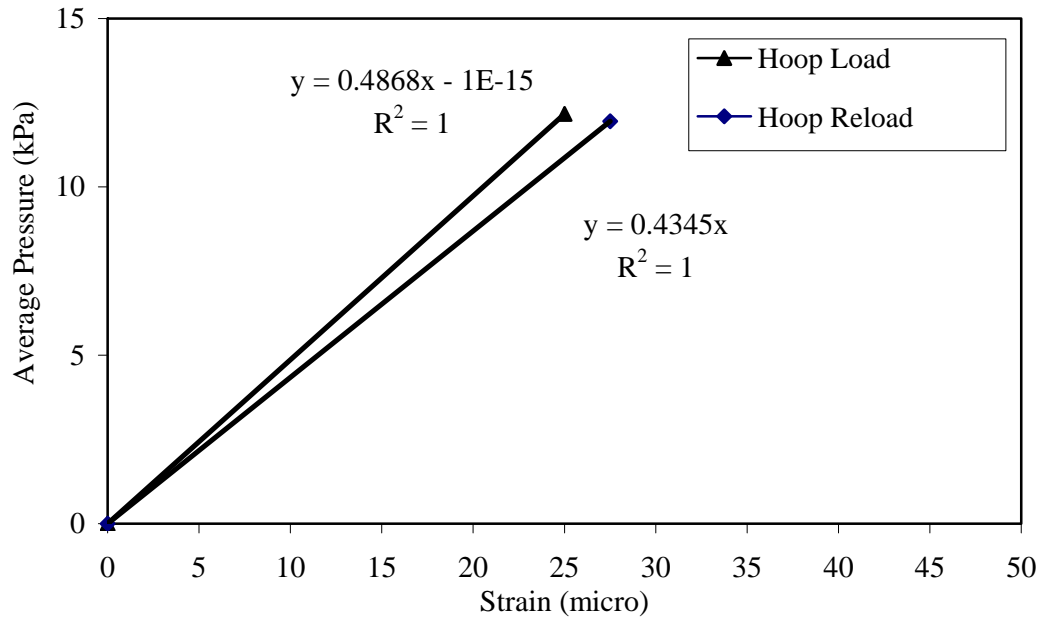
2. TAMU CVEN Building East



Load vs. Displacement Test (Solid Plate Test)  
 (E.CVEN #2)  
 Test # 5  
 (10/19/2003)



BCD Average Pressure (kPa) VS. Hoop Strain (E.CVEN #2)

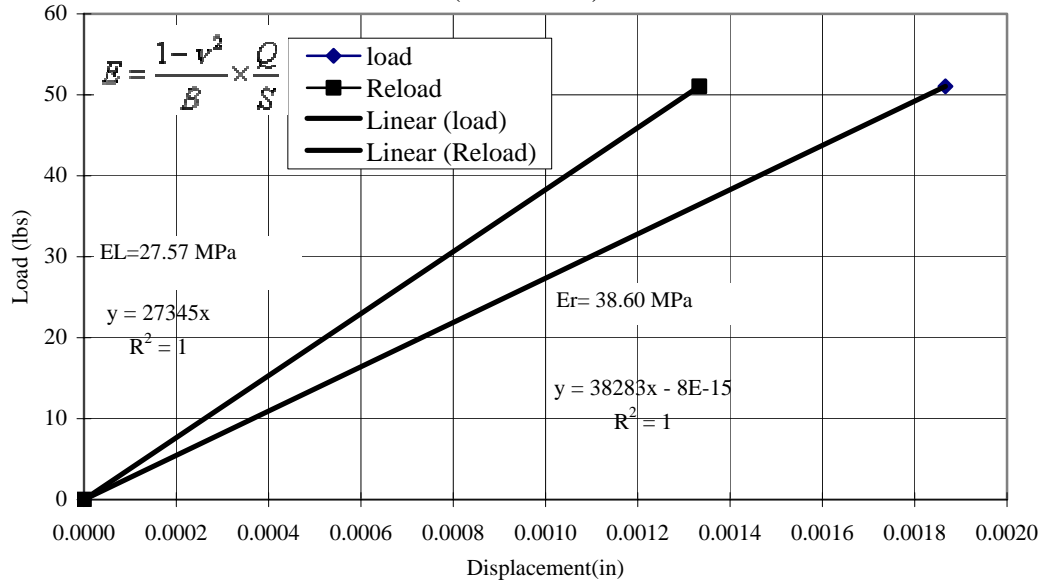


Load vs. Displacement Test (Solid Plate Test)

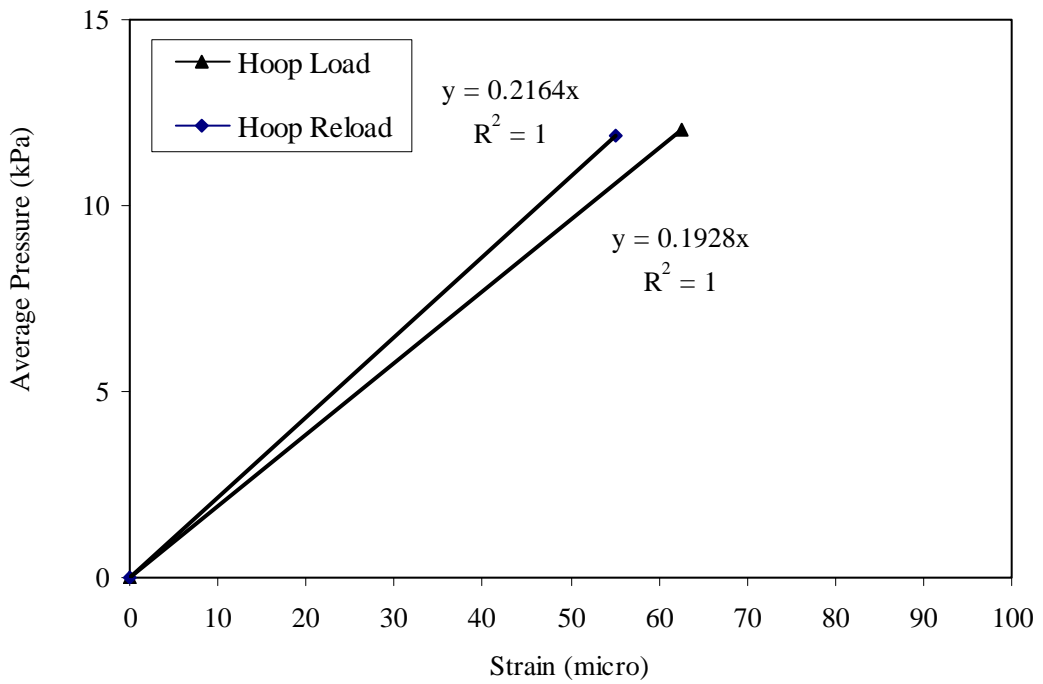
(E.CVEN #3)

(10/19/2003)

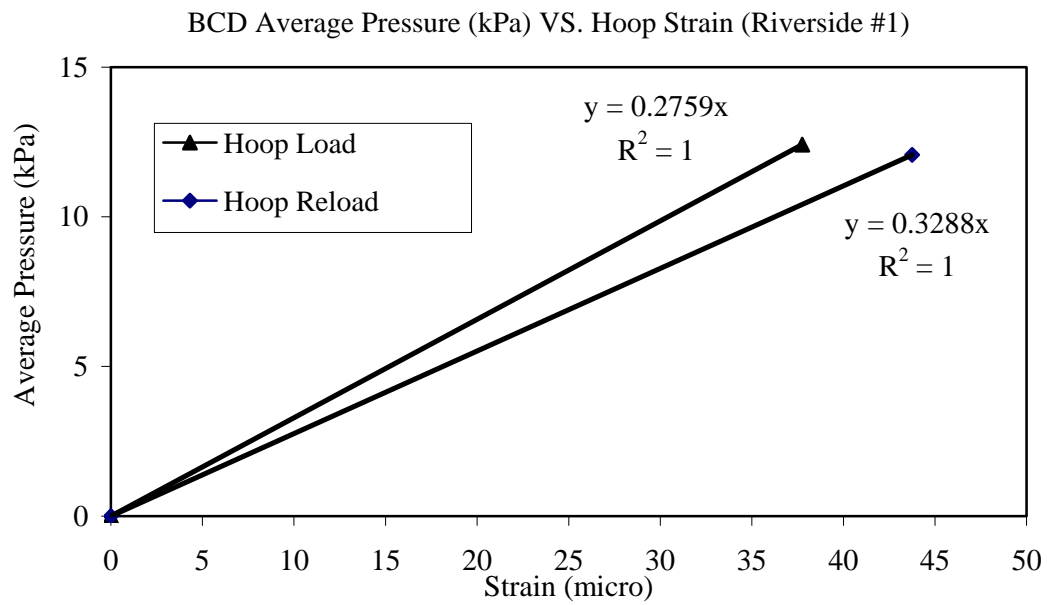
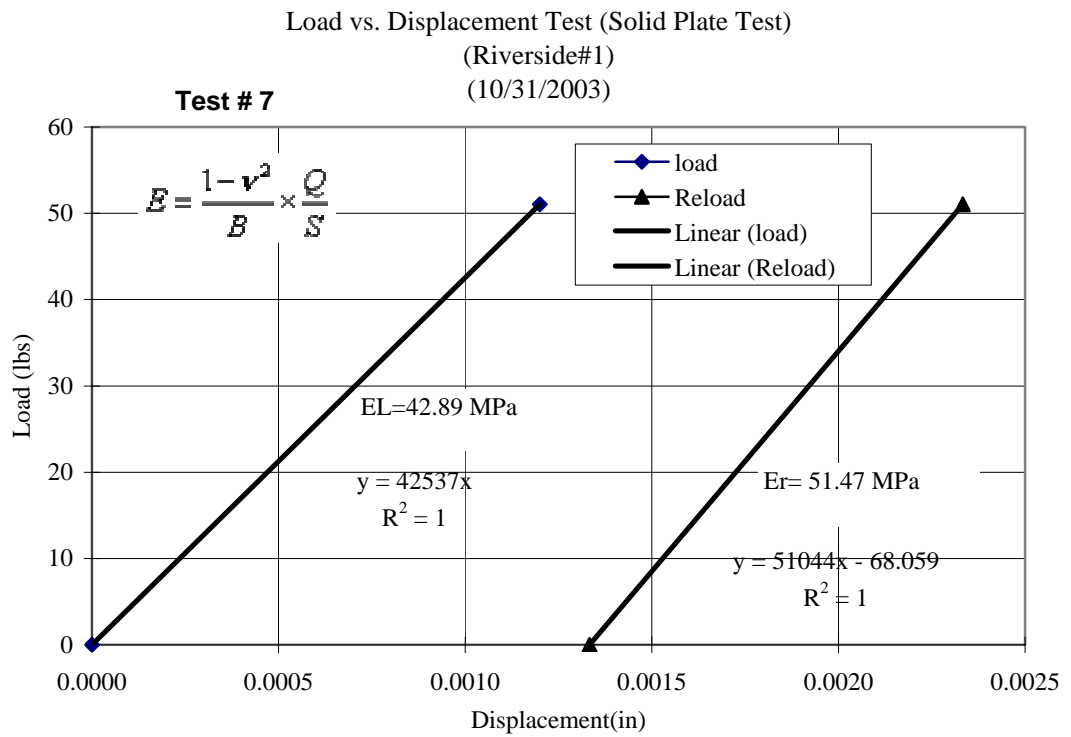
Test # 6



BCD Average Pressure (kPa) VS. Hoop Strain (E.CVEN #3)



3. TAMU Riverside Campus

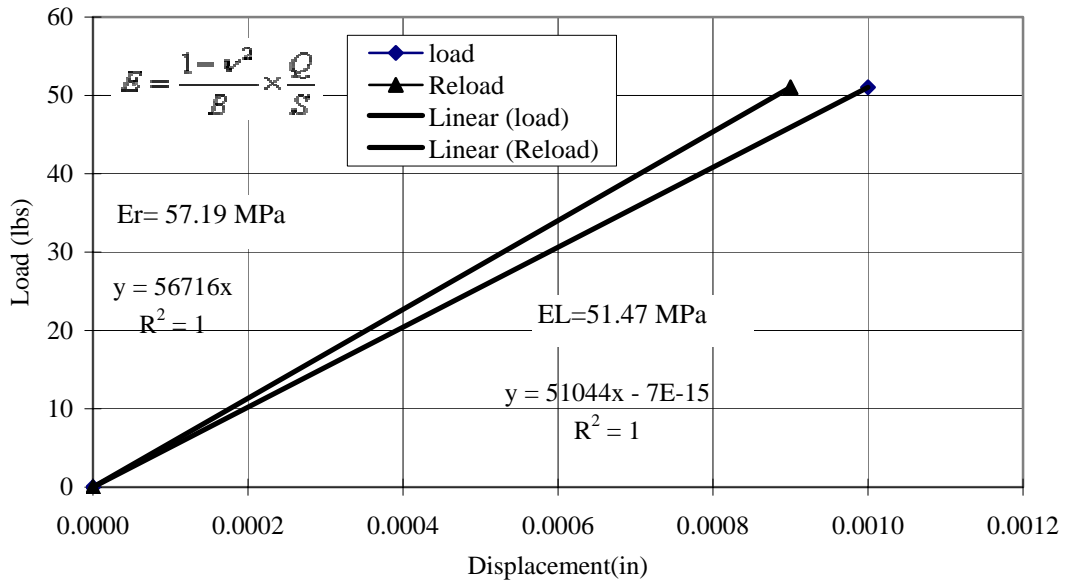


Load vs. Displacement Test (Solid Plate Test)

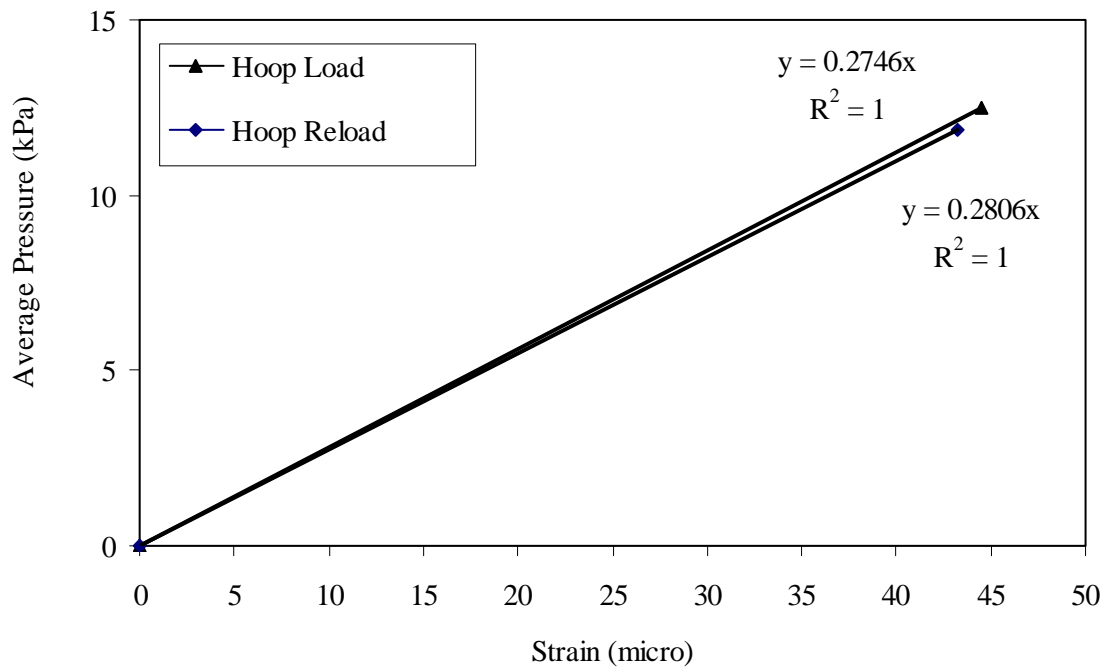
(Riverside #2)

(10/31/2003)

Test # 8

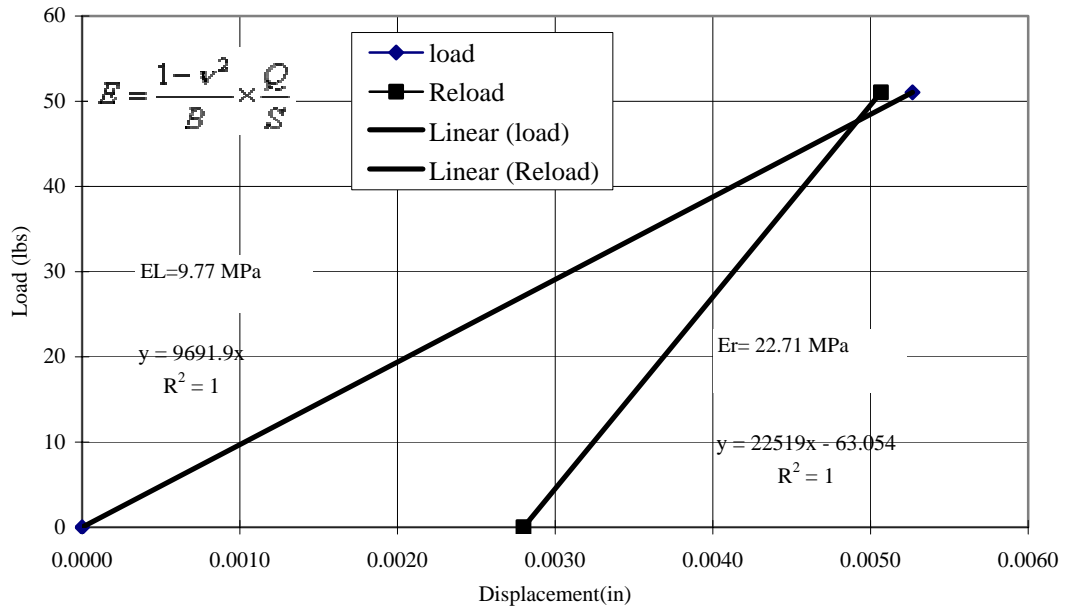


BCD Average Pressure (kPa) VS. Hoop Strain (Riverside #2)

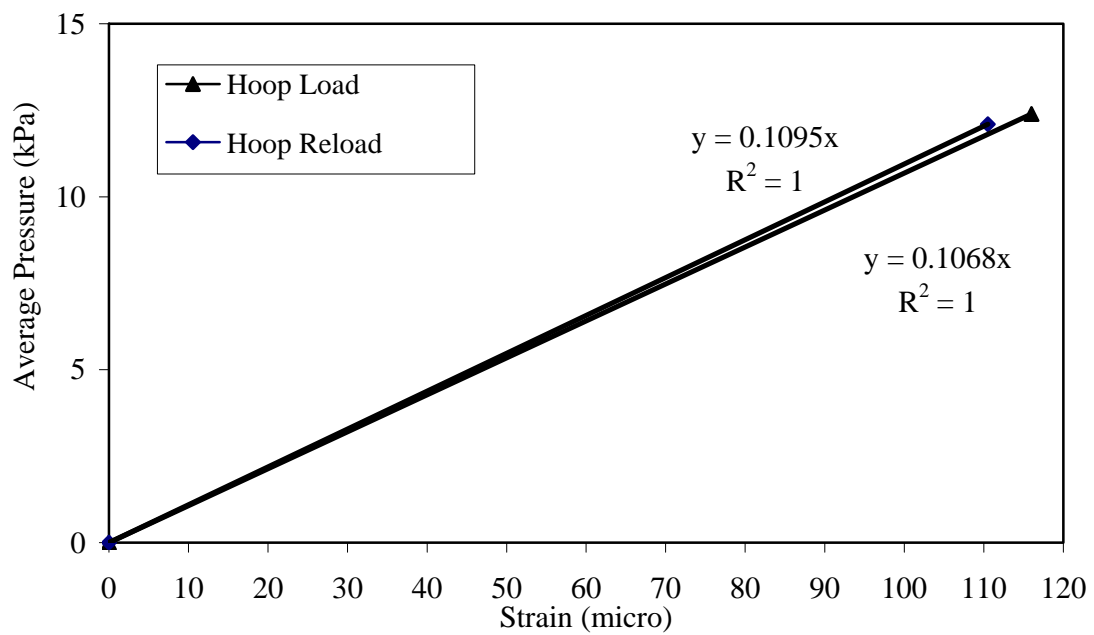


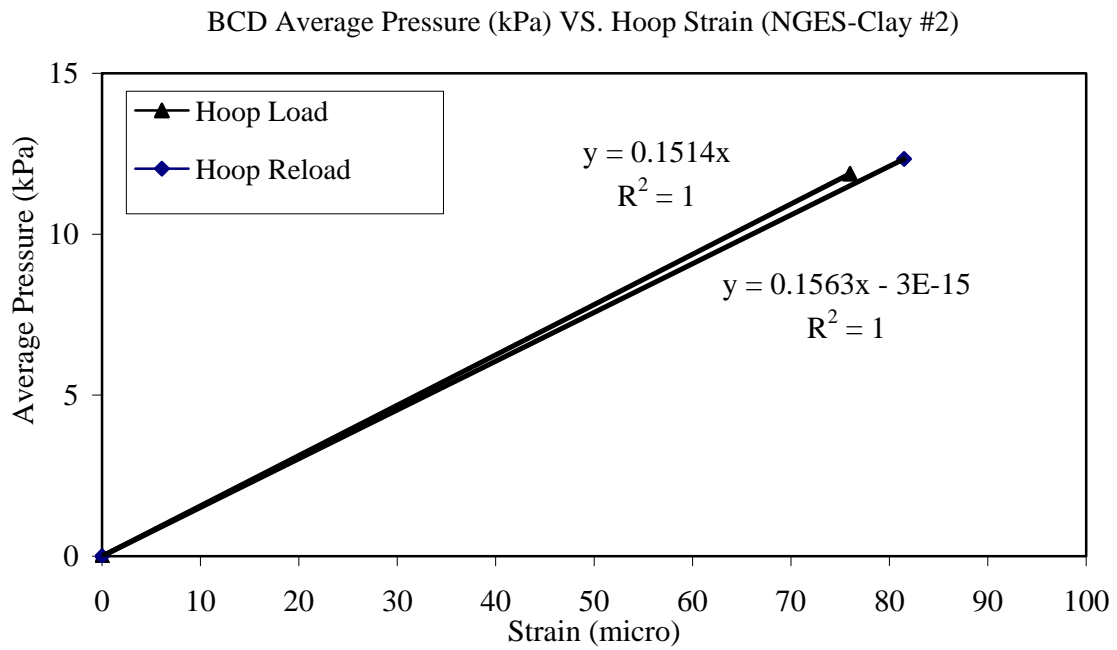
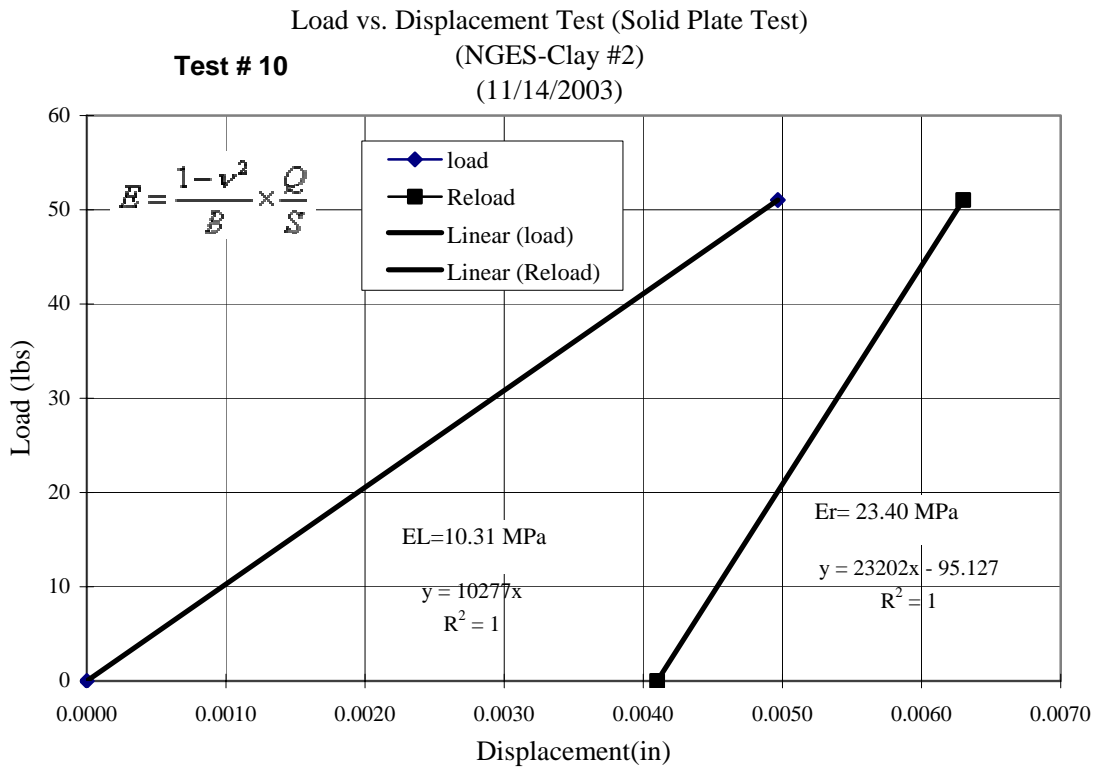
4. TAMU National Clay Site

**Test # 9** Load vs. Displacement Test (Solid Plate Test)  
(NGES-Clay#1)  
(11/14/2003)



BCD Average Pressure (kPa) VS. Hoop Strain (NGES-Clay #1)



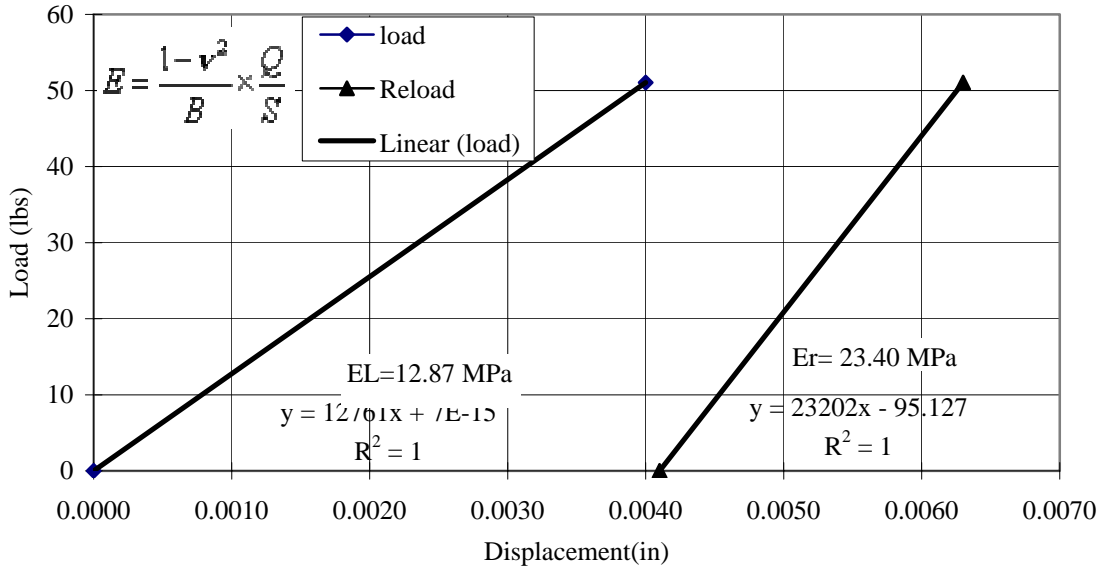


Load vs. Displacement Test (Solid Plate Test)

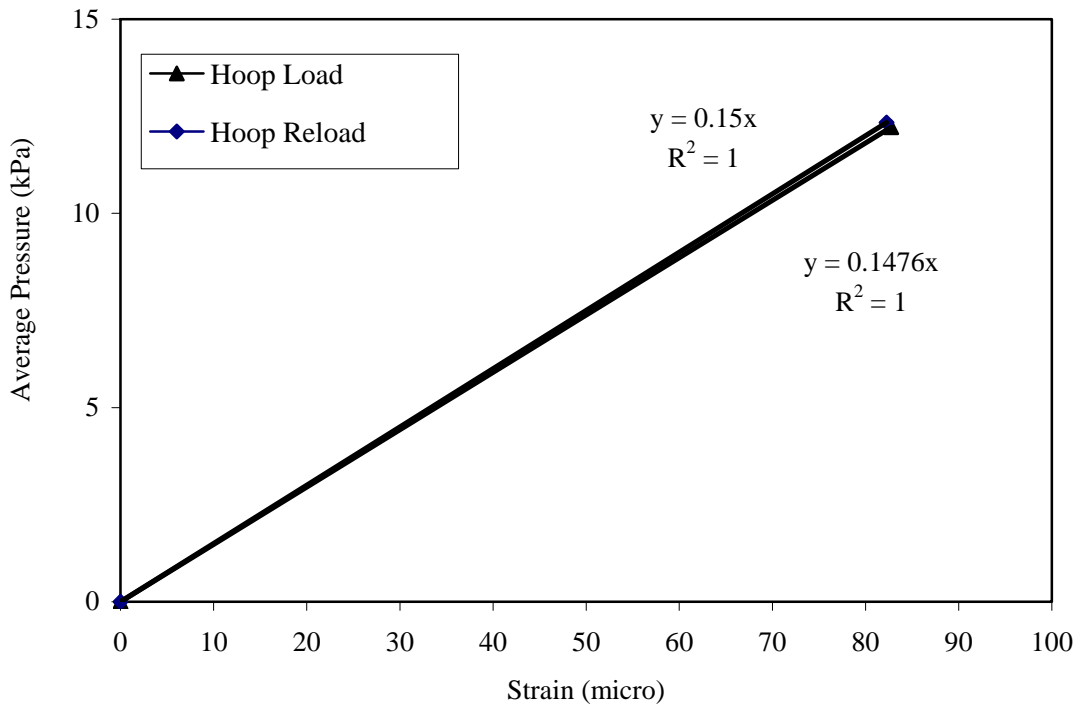
(NGES-Clay #3)

(11/14/2003)

Test # 11

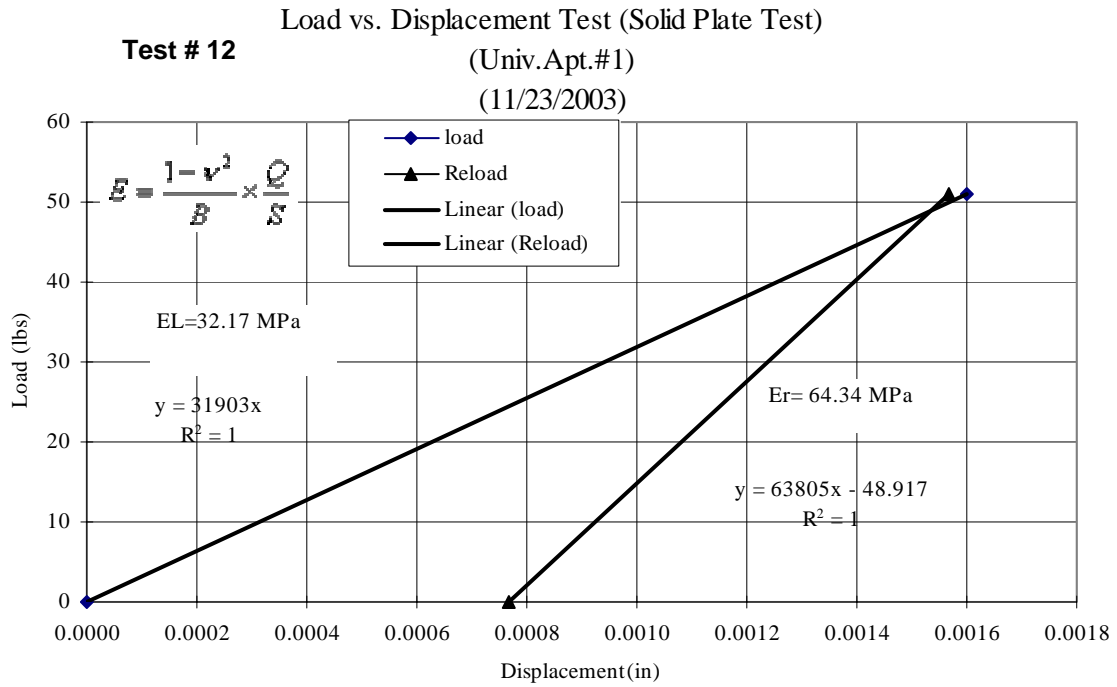


BCD Average Pressure (kPa) VS. Hoop Strain (NGES-Clay #3)

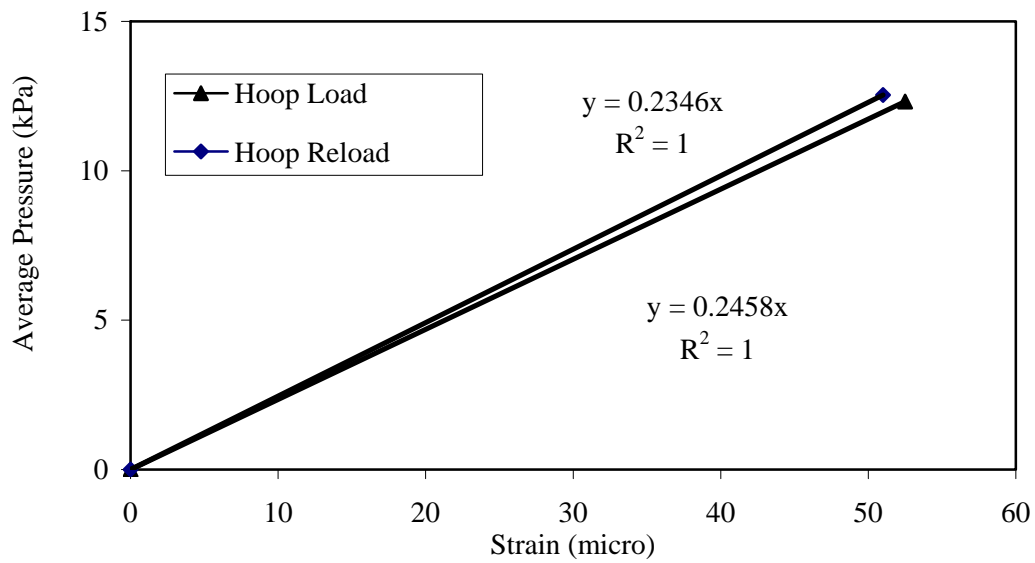




5. TAMU University Apt.



BCD Average Pressure (kPa) VS. Hoop Strain (Apt. #1)

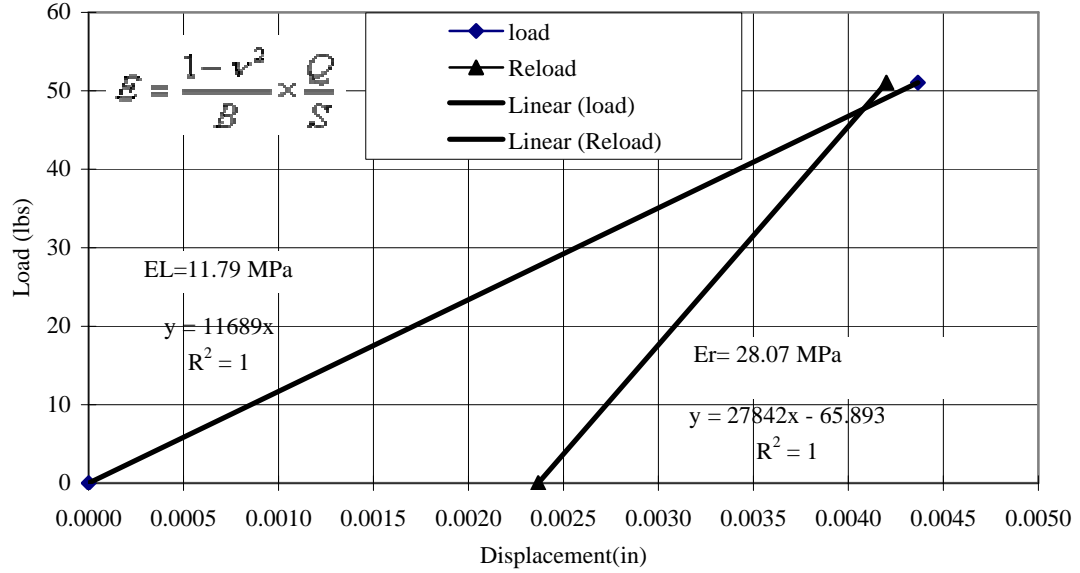


Load vs. Displacement Test (Solid Plate Test)

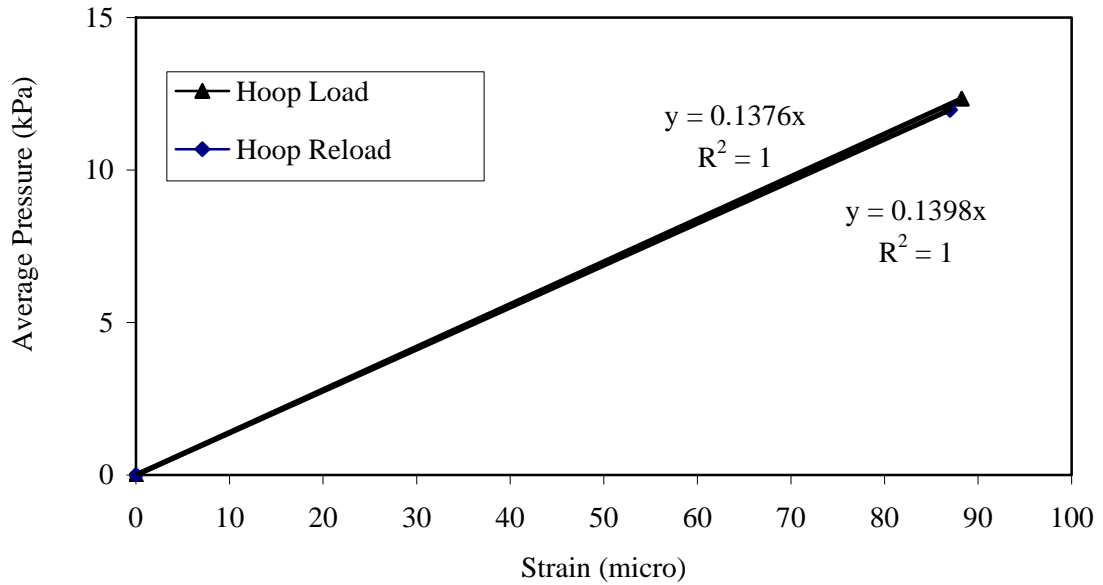
(Apt. #2)

(11/23/2003)

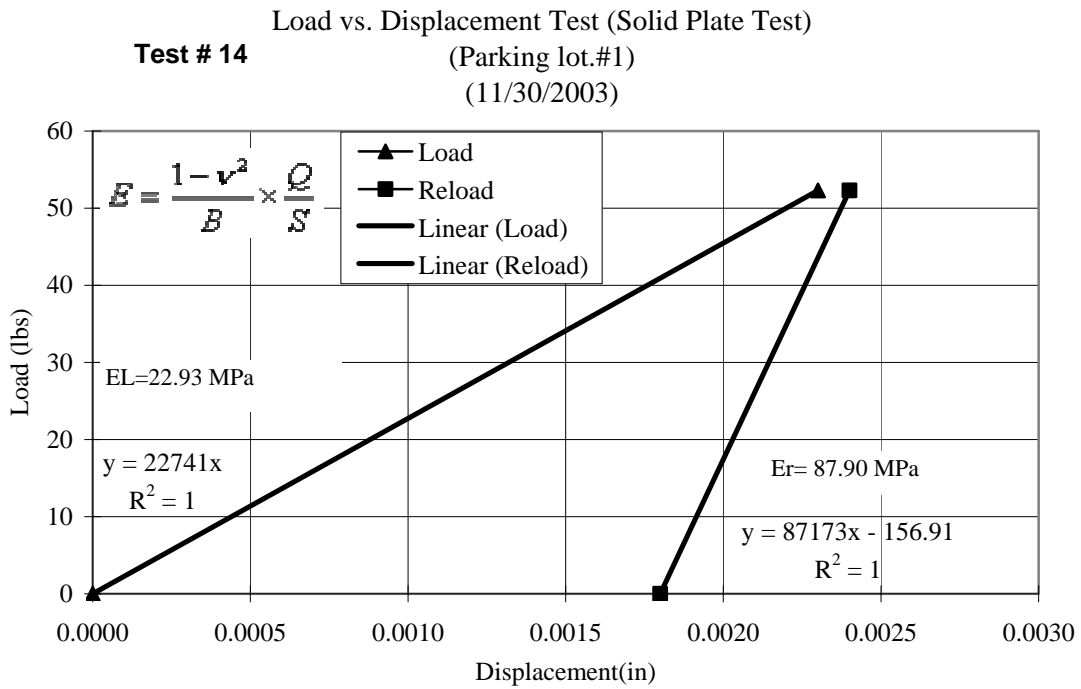
Test # 13



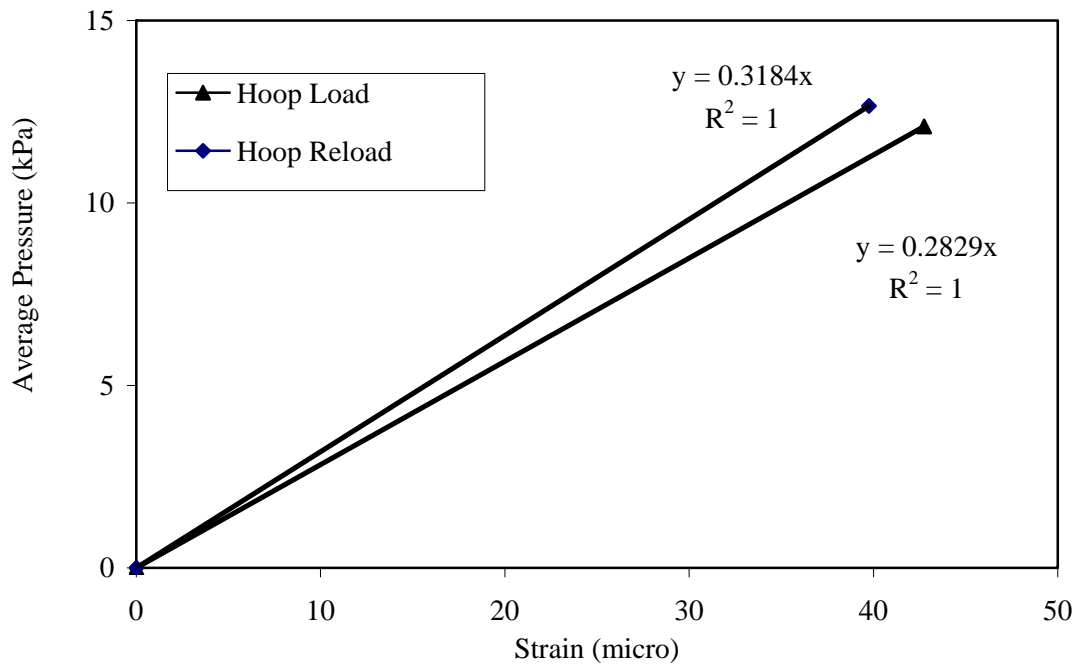
Average Pressure (kPa) VS. Hoop Strain (Univ.Apt. #2)



6. TAMU Parking Lot



BCD Average Pressure (kPa) VS. Hoop Strain (Parking Lot #1)

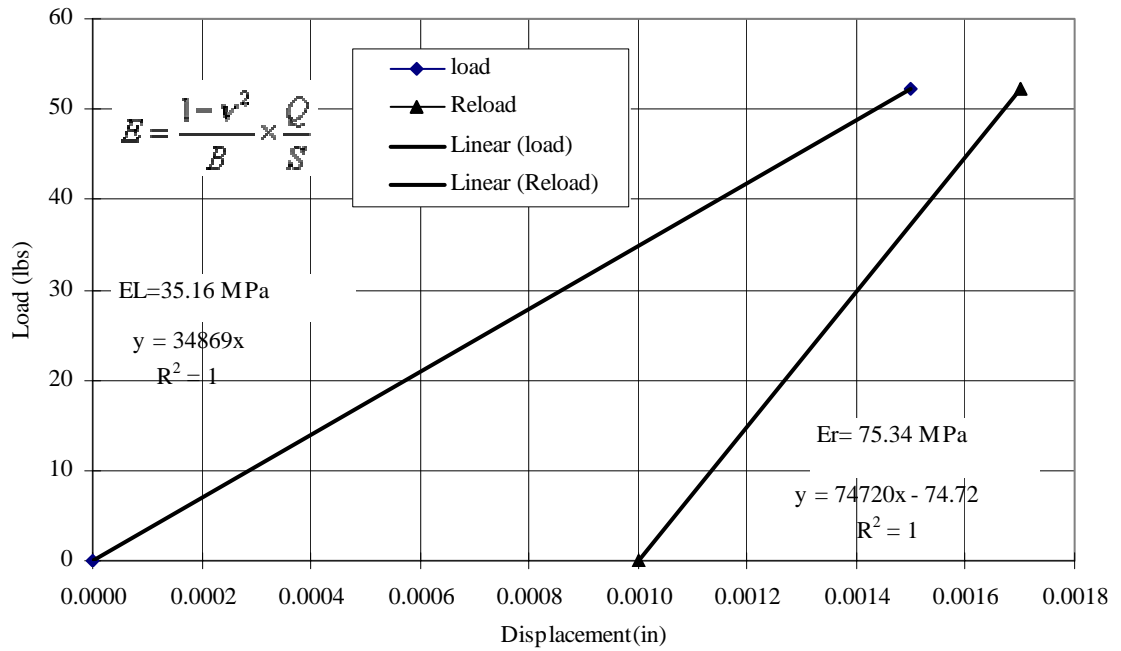


Load vs. Displacement Test (Solid Plate Test)

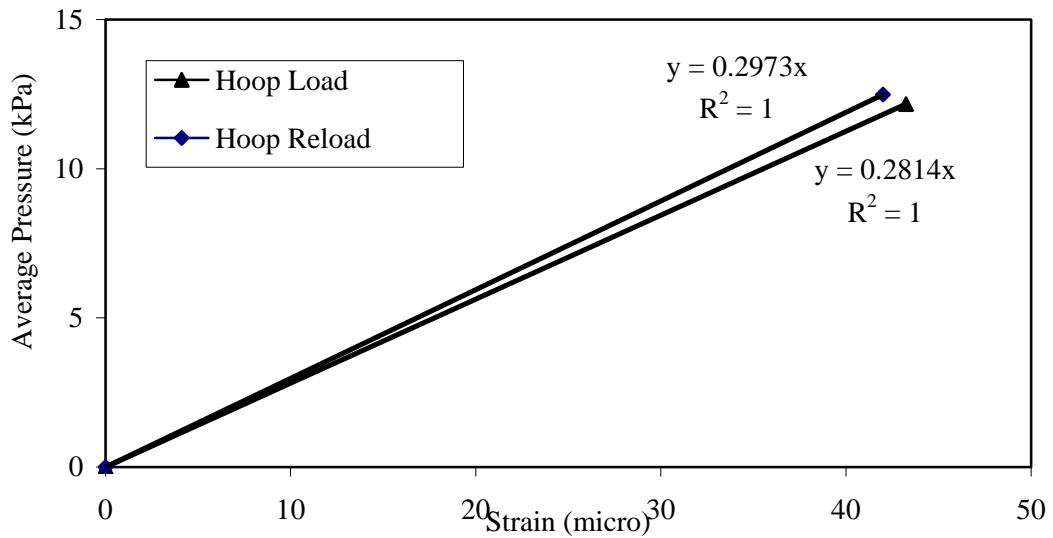
(Parking lot #2)

(11/30/2003)

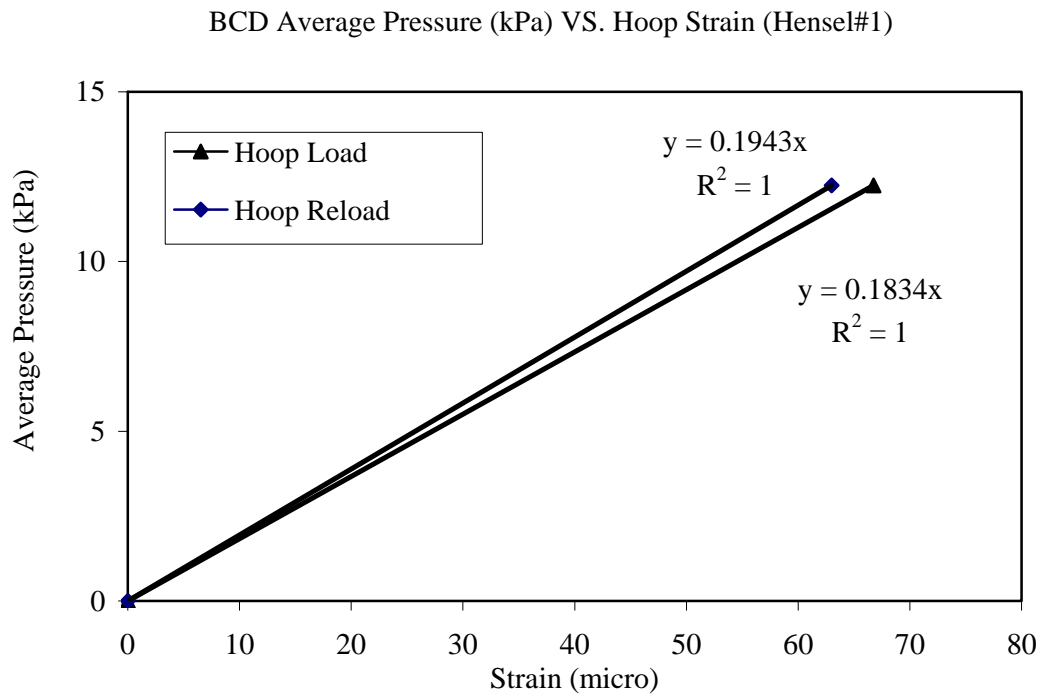
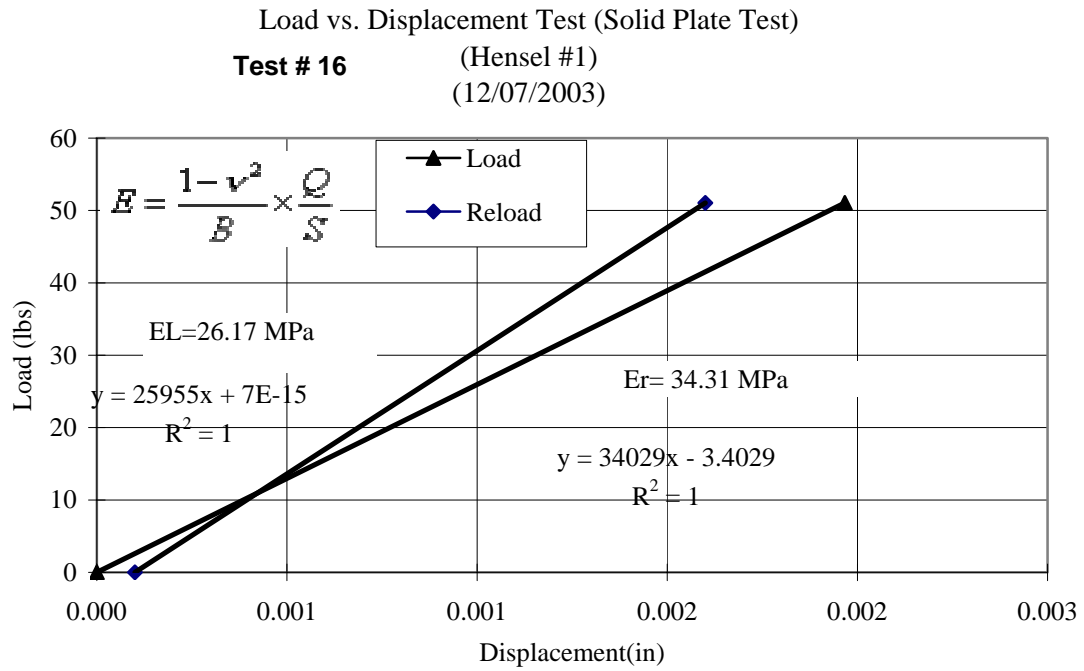
Test # 15



BCD Average Pressure (kPa) VS. Hoop Strain (Parking Lot #2)



7. Hensel Park

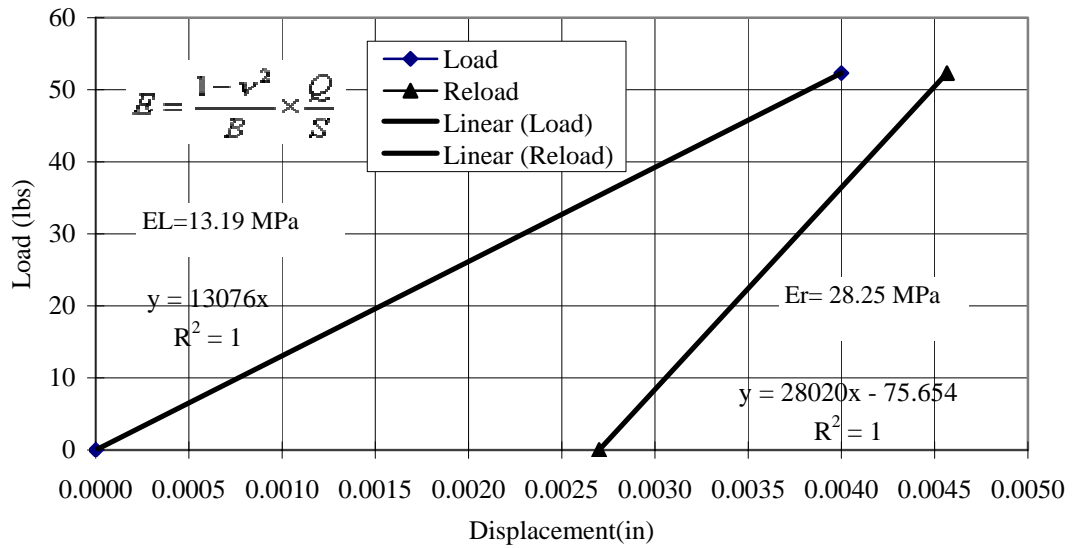


Load vs. Displacement Test (Solid Plate Test)

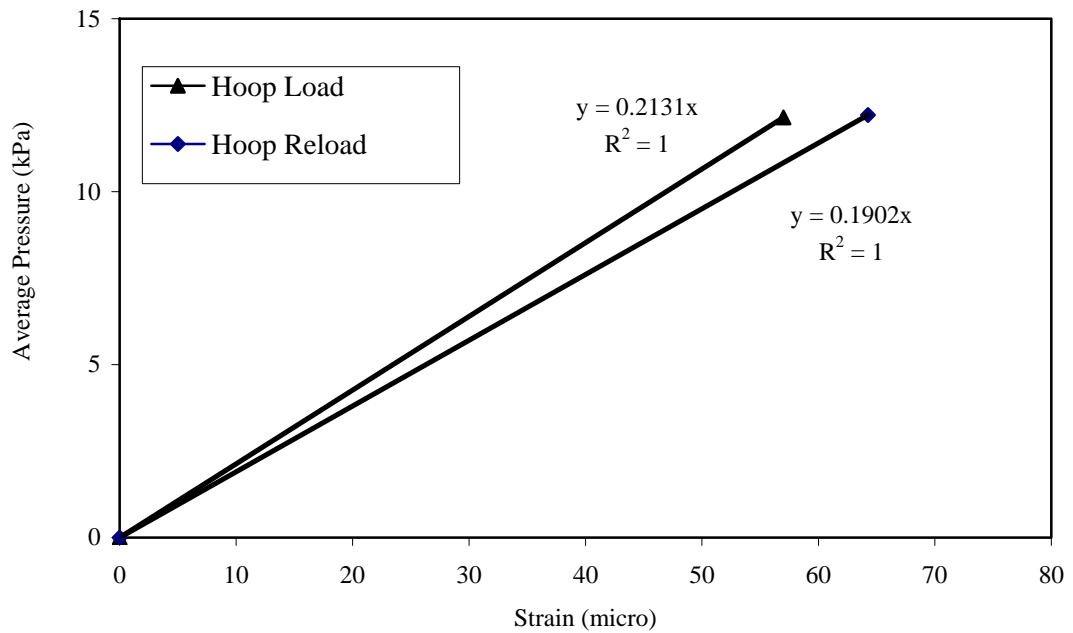
Test # 17

(Hensel.#2)

(12/07/2003)



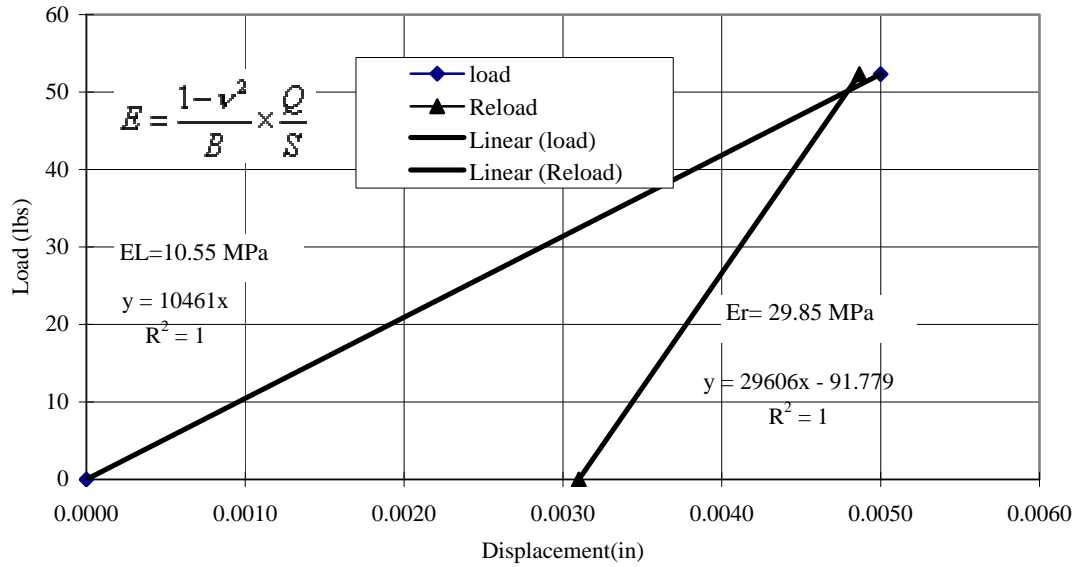
BCD Average Pressure (kPa) VS. Hoop Strain (Hensel #2)



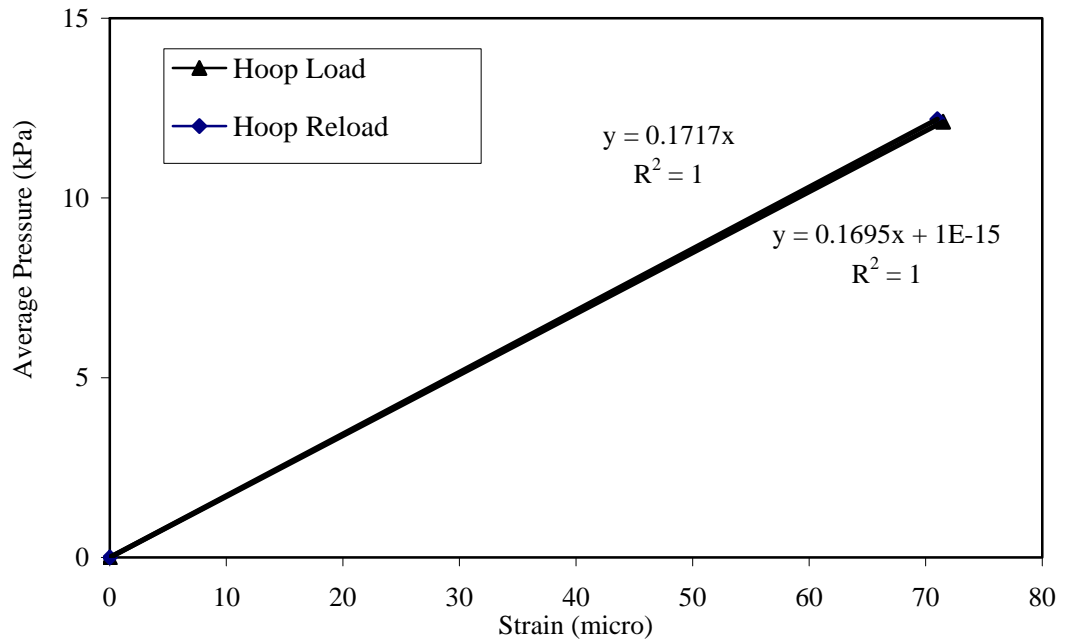
Load vs. Displacement Test (Solid Plate Test)

Test # 18

(Hensel #3)  
(12/07/2003)



BCD Average Pressure (kPa) VS. Hoop Strain (Hensel # 3)



## VITA

Yanfeng Li was born in Shanxi, China on February, 27, 1976. He entered Xi'an University of Architecture and Technology, China in 1993 and received his B.S. degree in civil engineering in July 1997. He continued his study at the same university and received his M.S. degree with the specialty in geotechnical engineering in May 2000.

The author's permanent address is:

Xi'an TieLu XinCun 95# 1503

Xi'an, P.R. China. 710054